

IR CAMERA

Document Title: Wavefront Sensors Subsystem Design

Document Number: VIS-DES-UOD-06042-0001

Issue: 3.0

Date: 8th March 2004

Document Prepared By:	Paul Clark WFS Work Package Manager	Signature and Date:	
Document Approved By:	Martin Caldwell IR Camera Systems Engineer	Signature and Date:	
Document Released By:	Kim Ward IR Camera Project Manager	Signature and Date:	<input type="text" value="PP"/>
Document Reviewed By:	Gavin Dalton IR Camera Project Scientist	Signature and Date:	<input type="text" value="PP"/>

The information contained in this document is strictly confidential and is intended for the addressee only. The unauthorised use, disclosure, copying, alteration or distribution of this document is strictly prohibited and may be unlawful.



Change Record

Issue	Date	Section(s) Affected	Description of Change/Change Request Reference/Remarks
0.1	18/10/02	Not Applicable	First Issue for comment
0.2	23/10/02	8 & 9	Sections updated toward first release status
0.3	25/10/02	All	Sections further updated toward first release status
0.4	30/10/02	All	Sections further updated toward first release status
0.5	8/11/02	7.5.3 & Conclusion	Referral to CIQ corrected
1.0	18/11/02		First Release
1.1	22/10/03	All	Major re-write to document systems aspects for IR Camera FDR
1.2	28/10/03	10	Further detail on synchronisation added
1.3	30/10/03	5	Updated details of software to be reviewed at IR Camera FDR
2.0	14/11/03	Acronyms, 7	Second Release for IR Camera FDR
2.1	3/3/04	All	Major re-write for WFS FDR
2.2	4/3/04	Most	Sections updated toward third release
2.3	5/3/04	Some	Final updates toward third release
3.0	8/3/04	A2 & A5	Third Release for WFS FDR

Notification List

The following people should be notified by email that a new version of this document has been issued and is available on the IR Camera Sharepoint database:

VPO: Will Sutherland
Simon Craig
Andy Born

RAL: Kim Ward
Martin Caldwell
Gavin Dalton

ATC: Andy Longmore
Mel Strachan

Durham: Paul Clark
Richard Myers
Peter Luke
Paul Berry
Nirmal Bissonauth



Doc. Number:	VIS-DES-UOD-06042-0001
Date:	8 th March 2004
Issue:	3.0
Page:	Page 3 of 3
Author:	Paul Clark

Acknowledgements

The author gratefully acknowledges the assistance of Paul Berry, Richard Bingham, Nirmal Bissonauth, Nigel Dipper, Peter Luke, Richard Myers and Richard Wilson in the preparation of this report and the associated software, optical, mechanical and electronic design effort.

The author also wishes to thank Kevin Burke, Martin Caldwell, Marc Ferlet, Tony Richards, Martin Whalley and Guy Woodhouse for their support and input into the design process. Scientific input from Gavin Dalton and Will Sutherland is also gratefully acknowledged.

Doc. Number:	VIS-DES-UOD-06042-0001
Date:	8 th March 2004
Issue:	3.0
Page:	Page 4 of 4
Author:	Paul Clark

TABLE OF CONTENTS

CHANGE RECORD.....2

NOTIFICATION LIST2

ACKNOWLEDGEMENTS.....3

1 INTRODUCTION7

1.1 TERMINOLOGY.....8

1.1.1 *LOWFS, LOCS, HOWFS, HOCS*8

1.1.2 *TCCD Controller, SDSU*.....8

2 ACRONYMS AND ABBREVIATIONS.....9

3 APPLICABLE DOCUMENTS11

4 REFERENCE DOCUMENTS.....13

5 SYSTEM OVERVIEW15

6 LOCS/AG UNIT DESIGN19

6.1 REQUIREMENTS19

6.2 CCD SELECTION19

6.2.1 *Validation of AG FOV*.....20

6.2.2 *Validation of LOCS FOV*.....20

6.2.3 *Operation after sunset*.....21

6.2.4 *Autoguider frame rate*.....21

6.3 OPTICAL DESIGN22

6.4 FILTER SELECTION.....24

6.5 SCIENCE BEAM CLEARANCE.....25

6.6 ALIGNMENT SENSITIVITY26

6.7 MECHANICAL DESIGN27

6.8 CCD MOUNTING & ALIGNMENT FEATURES.....32

6.9 THERMAL DESIGN33

6.10 LOCS/AG UNIT MASS.....35

6.11 CONTAMINATION CONTROL35

6.12 ELECTRICAL DESIGN36

6.12.1 *Clocks*.....36

6.12.2 *ESD and Over-Voltage Protection*36

6.12.3 *Filtering*.....36

6.12.4 *PCB Layer Stack-Up*37

6.12.5 *Grounding*37

6.12.6 *Separation of Analogue and Digital*.....37

6.12.7 *Outputs*37

6.12.8 *Cable Run*.....38

6.12.9 *Cryostat Connectors*.....39

7 HOCS OPTICAL DESIGN40

7.1 OVERVIEW40

7.2 OPTIONS40

7.3 DIMENSIONS41

Doc. Number:	VIS-DES-UOD-06042-0001
Date:	8 th March 2004
Issue:	3.0
Page:	Page 5 of 5
Author:	Paul Clark

7.4	VALIDATION OF HOCS STAR AVAILABILITY	41
8	ABERRATION MEASUREMENT ACCURACY	42
8.1	LOCS PREDICTED ACCURACY	42
8.2	HOCS PREDICTED ACCURACY	42
8.3	REQUIRED INTEGRATION TIME	42
9	PROCESSOR REQUIREMENTS	44
10	SOFTWARE	45
11	EMI & DETECTOR SYNCHRONISATION	47
12	DECLARED MATERIALS LIST	48
13	CONCLUSION	48
14	APPENDIX 1: COMPLIANCE MATRICES	49
14.1	OVERALL WFS COMPLIANCE MATRIX	49
14.2	SOFTWARE COMPLIANCE MATRIX	52
14.2.1	<i>Guide Sensor Compliance</i>	52
14.2.2	<i>Low Order Wavefront Sensor Requirements</i>	54
14.2.3	<i>High Order Wavefront Sensor Requirements</i>	55
15	APPENDIX 2: DECLARED MATERIALS LIST	56
16	APPENDIX 3: MECHANICAL DRAWINGS (PETER LUKE).....	57
17	APPENDIX 4: ELECTRICAL SCHEMATICS AND BOARD LAYOUT (PAUL BERRY).....	70
17.1	OVERALL EMC GROUNDING DIAGRAM	71
17.2	CABLE HARNESSES	72
17.3	BOARD SCHEMATICS	74
17.4	BOARD LAYOUT	77
17.5	PARTS LIST	78
18	APPENDIX 5: TEST PLAN	79
18.1	WFS VERIFICATION MATRIX	79
18.2	SUMMARY AND DESCRIPTION OF TEST PROCEDURES	80
18.2.1	<i>Verification Procedure 0.1: LOCS/AG CCD Properties</i>	80
18.2.2	<i>Verification Procedure 0.2: LOCS/AG Filter Properties</i>	80
18.2.3	<i>Verification Procedure 0.3: LOCS/AG Beamsplitter Properties</i>	80
18.2.4	<i>Verification Procedure 0.4: HOCS Beamsplitter Properties</i>	80
18.2.5	<i>Test Procedure 1: LOCS/AG Alignment Setting (Best Focus Position)</i>	81
18.2.6	<i>Test Procedure 2: LOCS/AG Internal Stability (Thermal & Flexure)</i>	81
18.2.7	<i>Test Procedure 3: AG Centroid Accuracy</i>	82
18.2.8	<i>Test Procedure 4: LOWFS Zernike Coefficient Determination Accuracy</i>	82
18.2.9	<i>Test Procedure 5: HOWFS Zernike Coefficient Determination Accuracy</i>	83
18.3	VERIFICATION AND TEST PROCEDURES	83
18.3.1	<i>Verification Test 0.1</i>	84
18.3.2	<i>Verification Test 0.2</i>	85
18.3.3	<i>Verification Test 0.3</i>	86
18.3.4	<i>Verification Test 0.4</i>	87
18.3.5	<i>Test Procedure 1</i>	88

Doc. Number:	VIS-DES-UOD-06042-0001
Date:	8 th March 2004
Issue:	3.0
Page:	Page 6 of 6
Author:	Paul Clark

18.3.6	Test Procedure 2	89
18.3.7	Test Procedure 3	90
18.3.8	Test Procedure 4	91
18.3.9	Test Procedure 5	92
19	APPENDIX 6: LOCS/AG OPTICAL DESIGN REPORT (RICHARD BINGHAM).....	93
20	APPENDIX 7: ALTERNATIVE NON-CEMENTED LOCS DESIGN (R BINGHAM)	101
21	APPENDIX 8: HOCS OPTICAL DESIGN REPORT (RICHARD BINGHAM).....	102
21.1	INTRODUCTION AND SUMMARY	102
21.2	MATERIALS	103
21.3	BEAMSPLITTER COATINGS	103
21.4	OPTICAL DIAGRAMS FOR TYPE A, ON AXIS	103
21.4.1	Dimensions and tolerances for Type A.....	107
21.4.2	Sample Images.....	109
21.4.3	A Trial Aberration in the Telescope	112
21.4.4	Aberrations in the beamsplitters	115
21.4.5	The Curvature Sensor placed Off-Axis.....	117
21.5	CURVATURE SENSOR TYPE B	119
21.6	CURVATURE SENSOR TYPE C	121
21.7	DIMENSIONS OF DEVICES TYPES B AND C.....	122
22	APPENDIX 9: STRAY LIGHT ANALYSIS (MARC FERLET).....	123
22.1	INTRODUCTION	123
22.2	MODEL FOR GHOST EQUIVALENT BRIGHTNESS	123
22.3	OPTICAL MODEL DESCRIPTION AND RESULTS.....	125
22.3.1	Model assumptions	125
22.3.2	Ghost images at IRCAM focal plane.....	126
22.3.3	Field positions	130
22.3.4	Case of real (absorbing) WFS filter substrate.....	132
22.4	CONCLUSION	133
23	APPENDIX 10: SCIENCE BEAM CLEARANCE (TONY RICHARDS).....	134
23.1	CLEARANCE BETWEEN PICK-OFF MIRROR AND NEAREST DETECTOR BEAM.....	135
24	APPENDIX 11: CUBE BEAMSPLITTER QUALIFICATION TEST	137
25	APPENDIX 12: LOCS/AG ALIGNMENT ANALYSIS (RICHARD BINGHAM).....	139
26	APPENDIX 13: SKY COVERAGE CALCULATIONS.....	142
26.1	AUTOGUIDER FIELD OF VIEW VALIDATION	143
26.2	LOCS FIELD OF VIEW VALIDATION	146
26.3	AUTOGUIDER OPERATION AFTER SUNSET.....	149
26.4	HOCS STAR AVAILABILITY	152
27	APPENDIX 14: LOCS ABERRATIONS (RICHARD BINGHAM).....	155

Doc. Number:	VIS-DES-UOD-06042-0001
Date:	8 th March 2004
Issue:	3.0
Page:	Page 7 of 7
Author:	Paul Clark

1 Introduction

This report contains the subsystem design of the VISTA IR Camera Wavefront Sensors, presented for final design review on March 31st 2004.

The Wavefront Sensors work package comprises three key components: autoguider (or guide sensor), low order curvature sensors (or low order wavefront sensors) and a high order curvature sensor (or high order wavefront sensor). Together these systems fulfil the VISTA project requirements for guiding and open and closed loop wavefront sensing. The design has developed over the preliminary and final design phases to fulfil the requirements in the most cost effective manner within the constraints imposed by the design of the IR Camera and Telescope themselves.

The Wavefront Sensors successfully passed Delta-PDR on 2nd June 2003, six months after the initial IR Camera PDR (10th & 11th December 2002). At the time of the PDR, difficulties associated with the modelling of the performance of the sensors prevented compliance with their requirements from being demonstrated. Over the following months intensive work allowed these difficulties to be resolved and compliance was demonstrated at the Delta-PDR. Steps have been taken to minimise the impact of the delayed (Delta) PDR on the detailed design of the Wavefront Sensors and the design is currently trailing that of the rest of the IR Camera by only three months.

The design of the VISTA IR Camera Wavefront Sensors has evolved from the Conceptual Design, presented in RD01, through the design for PDR, presented in AD01, to the final design presented herein. AD02 presents the additional work required to allow the work package to pass delta-PDR. AD02 contains in particular the results of the extensive modelling work undertaken to predict the aberration measurement accuracy of the curvature sensing technique. AD15 is an additional design document presented at the IR Camera FDR to demonstrate that there are no issues associated with the design of the wavefront sensors that could prevent the Camera itself from passing FDR.

The following sections of this report present the optical, mechanical, electronics and software design of the Wavefront sensors allowing it to be assessed against the requirements and the terms of reference for the review:

“The FDR is a scrutiny to the detailed drawings, lists etc of the Final Design of a development item. The Camera Team has been advised to interpret this as the provision of detailed assembly drawings for each subsystem plus manufacturing drawings of any critical components. The objective is to verify the conformance of the design with the technical specification by review of the Final Design, the accompanying analyses, results of development and qualification tests.”

The compliance matrix summarising the design requirements is presented in Appendix 1. The requirements are derived from three key documents: the Camera Technical Specification



Doc. Number:	VIS-DES-UOD-06042-0001
Date:	8 th March 2004
Issue:	3.0
Page:	Page 8 of 8
Author:	Paul Clark

AD03, the Cryostat-to-Sensors ICD AD04 and associated drawings AD05, and the Sensors Subsystem Requirements AD06.

1.1 Terminology

1.1.1 LOWFS, LOCS, HOWFS, HOCS

Throughout this and the other FDR documents the reader will find reference to both Low Order Curvature Sensors (LOCS) and Low Order Wavefront Sensors (LOWFS). The IR Camera Technical Specification [AD03] specifies the requirements that the Low Order Wavefront Sensor must fulfil but without specifying what type of sensor should be used. In the VISTA IR Camera Wavefront Sensor Work Package, the Low Order Sensors have been implemented as Curvature Sensors. The term LOCS is therefore the name of the sensor that fulfils the LOWFS requirements. The two names in effect both refer to the same pieces of equipment.

The same is true for the High Order Wavefront Sensor (HOWFS) which is also implemented as a Curvature Sensor (HOCS) utilising optics placed in the Camera filter wheel. So again the two names, HOWFS and HOCS, both refer to the same system.

In general, the project software documentation refers to LOWFS and HOWFS, whereas the sub-system design documentation refers to LOCS and HOCS.

1.1.2 TCCD Controller, SDSU

Within this and the other IR Camera documents, reference is made to both Technical CCD Controllers (TCCD Controllers) and SDSUs. The ESO TCCD Controller comprises: a control electronics box; CCD head connection cables; fibre optic cables; and a PMC (PCI Mezzanine) interface card. Following their recent tender exercise, ESO will be procuring these systems from Astronomical Research Cameras Inc. The controllers are commonly known as SDSU (San Diego State University) controllers throughout the astronomical community and are currently in their third generation (SDSU III). The term "SDSU" is used therefore to refer to the control electronics box alone, four of which will be mounted on the rear of the IR camera to control the WFS CCDs.

Some IR Camera software documentation also makes reference to the term ACE (Array Control Electronics). This is the name of ESO's older generation of controllers which the TCCD Controller supersedes.

Doc. Number:	VIS-DES-UOD-06042-0001
Date:	8 th March 2004
Issue:	3.0
Page:	Page 9 of 9
Author:	Paul Clark

2 Acronyms and Abbreviations

ACE	Array Control Electronics
AG	Auto Guider
AIT	Acceptance, Integration & Test
BI	Back Illuminated
CCD	Charge Coupled Device
CIQ	Camera Image Quality
CS	Curvature Sensor / Sensing
CTE	Coefficient of Thermal Expansion
DML	Declared Materials List
EF	(Curvature Sensing Image Analysis Software Package)
EMC	Electro-Magnetic Compatibility
EMI	Electro-Magnetic Interference
ESO	European Southern Observatory
FDR	Final Design Review
FEA	Finite Element Analysis
FET	Field Effect Transistor
FOV	Field Of View
FPA	Focal Plane Array
FT	Frame Transfer
HOCS	High Order Curvature Sensor
HOWFS	High Order Wavefront Sensor
ICD	Interface Control Document
IR	Infrared
IRACE	Infrared Array Control Electronics
LCU	Local Control Unit (VME Processor Card)
LOCS	Low Order Curvature Sensor
LOWFS	Low Order Wavefront Sensor
NIMO	Non-Inverted Mode Operation (CCD)
PCB	Printed Circuit Board
PCI	Peripheral Component Interconnect (Computer Data Bus Standard)
PDR	Preliminary Design Review
PMC	PCI Mezzanine Card
QE	Quantum efficiency
RC	Resistor Capacitor (Electronic Load)
RMS	Root Mean Square
SDSU	San Diego State University CCD Controller
SH	Shack-Hartmann
TCCD	Technical CCD
TCS	Telescope Control System
TIM	Time Interface Module
VISTA	Visible and Infrared Survey Telescope for Astronomy

Doc. Number:	VIS-DES-UOD-06042-0001
Date:	8 th March 2004
Issue:	3.0
Page:	Page 10 of 10
Author:	Paul Clark

VLT	Very Large Telescope (ESO Paranal Observatory)
VME	Versa Module Europa (19" Rack Data Bus Standard)
WFCAM	Wide Field Camera
WFS	Wavefront Sensor
WP	Work Package
ZEMAX	(Optical Design Software Package)



3 Applicable Documents

AD01	Wavefront Sensors Subsystem Design (<i>Status At PDR</i>)	VIS-DES-UOD-06042-0001 1.0, 18 th November 2002
AD02	Wavefront Sensors Subsystem Design (Delta PDR)	VIS-TRE-UOD-06042-0004 2.0, 22 nd May 2003
AD03	VISTA Infrared Camera Technical Specification	VIS-SPE-ATC-06000-0004 2.0, 20 th November 2003
AD04	Cryostat-to-Sensors Interface Control Document	VIS-ICD-RAL-06061-5001 3.0
AD05	Cryostat-to-Sensors ICD Drawings	VIS-ICD-RAL-06061-5101 1.0, 21 st November 2003
AD06	IR Camera Sensors Subsystem Requirements Specification	VIS-SPE-RAL-06040-0001 2.0, 16 th November 2003
AD07	Statement of Work for the VISTA IR Camera	VIS-SOW-ATC-06000-0007 1.0, 20 th November 2003
AD08	IR Camera Mass and Balance Budget	VIS-BDG-RAL-06013-1004 2.0, 23 rd October 2003
AD09	IR Camera Power Budget	VIS-BDG-RAL-06013-1005 2.0, 15 th November 2003
AD11	IR Camera System Integration & Test Plan	VIS-PLA-RAL-06091-0001 1.0, 18 th November 2003
AD12	VLT Electronic Design Specification	VLT-SPE-ESO-10000-0015 5, 6 th March 2001
AD13	Electromagnetic Compatibility and Power Quality Specification (Part 1)	VLT-SPE-ESO-10000-0002 2, 11 th March 1992
AD14	Electromagnetic Compatibility and Power Quality Specification (Part 2)	VLT-SPE-ESO-10000-0003 1, 5 th February 1992

Wavefront Sensors Subsystem Design

Doc. Number:	VIS-DES-UOD-06042-0001
Date:	8 th March 2004
Issue:	3.0
Page:	Page 12 of 12
Author:	Paul Clark

AD15	Wavefront Sensors Subsystem Design (<i>Status At Camera FDR</i>)	VIS-DES-UOD-06042-0001 2.0, 14 th November 2003
AD16	Wavefront Sensors CCD Technical Specification	VIS-SPE-UOD-06042-0006 1.0, 10 th December 2003



4 Reference Documents

RD01	Conceptual Design for Guiding, Focussing and Wavefront Sensing	VIS-TRE-ATC-00180-0005 1.0, 5 th October 2001
RD02	IR Camera Image Quality Budget	VIS-BDG-RAL-06013-1001 2.0, 17 th November 2003
RD03	Low Order Wavefront Sensors Software Design Description	VIS-DES-UOD-06048-0001 1.0, 4 th March 2004
RD04	High Order Wavefront Sensors Software Design Description (LCU Part)	VIS-DES-UOD-06048-0002 2.0, 4 th March 2004
RD05	Autoguider Software Design Description (LCU Part)	VIS-DES-UOD-06048-0003 1.0, 4 th March 2004
RD06	Image Analysis Algorithms for VISTA Wavefront Sensing	VIS-TRE-UOD-06042-0005 1.0, 12 th November 2003
RD07	VISTA IR Camera Software Requirements	VIS-DES-ATC-06080-0010 2.0, 12 th November 2003
RD08	VISTA IR Camera Structural Analysis	VIS-ANA-RAL-06063-0001 2.0, 14 th November 2003
RD09	IR Camera Thermal Design & Analysis	VIS-ANA-RAL-06072-0001 2.0, 13 th November 2003
RD10	Connector Configuration List	VIS-LST-RAL-06013-0006 1.0, 18 th November 2003
RD11	Routed Systems Diagram	VIS-DES-RAL-06013-9002 1.0, 19 th November 2003
RD12	IR Camera Declared Materials List	VIS-LST-RAL-06013-0003 2.0, 13 th November 2003
RD13	IR Camera EMC Interference Prevention Plan	VIS-PLA-RAL-06018-0001 2.0, 8 th March 2004

Doc. Number:	VIS-DES-UOD-06042-0001
Date:	8 th March 2004
Issue:	3.0
Page:	Page 14 of 14
Author:	Paul Clark

RD14	System Block Diagram	VIS-DES-RAL-06013-9001 1.0, 18 th Nov 2003
RD15	Optical Models for VISTA IRCAM	VIS-DES-ATC-06021-0002 1.0, 13 th May 2003
RD16	Active Optics and Guiding Workstation Software Design Description	VIS-SPE-RAL-13030-0003 2.0, 3 rd March 2004
RD17	VISTA IR Camera Software Functional Specification	VIS-DES-ATC-06081-0001 2.0, 12 th November 2003

Doc. Number:	VIS-DES-UOD-06042-0001
Date:	8 th March 2004
Issue:	3.0
Page:	Page 15 of 15
Author:	Paul Clark

5 System Overview

The key components of the Wavefront Sensor system, within the Camera cryostat, are:

- Two identical combined Low Order Curvature Sensor (LOCS) / Autoguider (AG) Units, subsequently referred to as LOCS/AG Units, positioned on the IR Camera WFS Plate, above the Filter Wheel, on opposite sides of the field of view, each containing:
 - A pickoff mirror, to divert light into the unit
 - A filter to limit the wavelengths used by the unit to 720-920nm (I-band) and also attenuate any science band wavelengths reflected back out into the IR Camera
 - A cube beamsplitter to divide light between the pair of curvature sensor CCDs and reflect light to the autoguider CCD
 - Two 2Kx2K curvature sensor CCDs
 - One 2Kx1K frame-transfer autoguider CCD
 - A PCB containing CCD buffer and protection circuitry
 - A Mechanical assembly
 - CCD heating resistors
 - Temperature sensing diodes
- Two flexible circuit wiring harnesses to connect the LOCS/AG units to hermetic connectors on a cryostat port
- The beam-splitting optic components of the High Order Curvature Sensor (HOCS), housed in the intermediate positions of the filter wheel, placing pre- and post-focus images of a single star simultaneously on one (or more) of the science detectors

External to the Camera cryostat are:

- Four ESO Technical CCD Controllers (mounted on the camera)
- 24V Power Supply (mounted on the camera)
- Fibre optic cables
- A split-backplane VME Rack containing four LCU processor cards with PMC fibre interface cards and ESO TIM cards (elsewhere in the telescope enclosure)
- A guide workstation (in the VLT control room)
- A wealth of purpose-written, ESO compliant software

Figure 5.1 shows a cross section of the complete VISTA IR Camera. Figure 5.2 is an extract from the Camera System Block Diagram [RD14] showing the electrical components outlined above. Figure 5.3 shows the location of the two LOCS/AG units within the camera cryostat. Figure 5.4 shows one HOCS optical component in relation to the camera window and lenses.

Doc. Number:	VIS-DES-UOD-06042-0001
Date:	8 th March 2004
Issue:	3.0
Page:	Page 16 of 16
Author:	Paul Clark

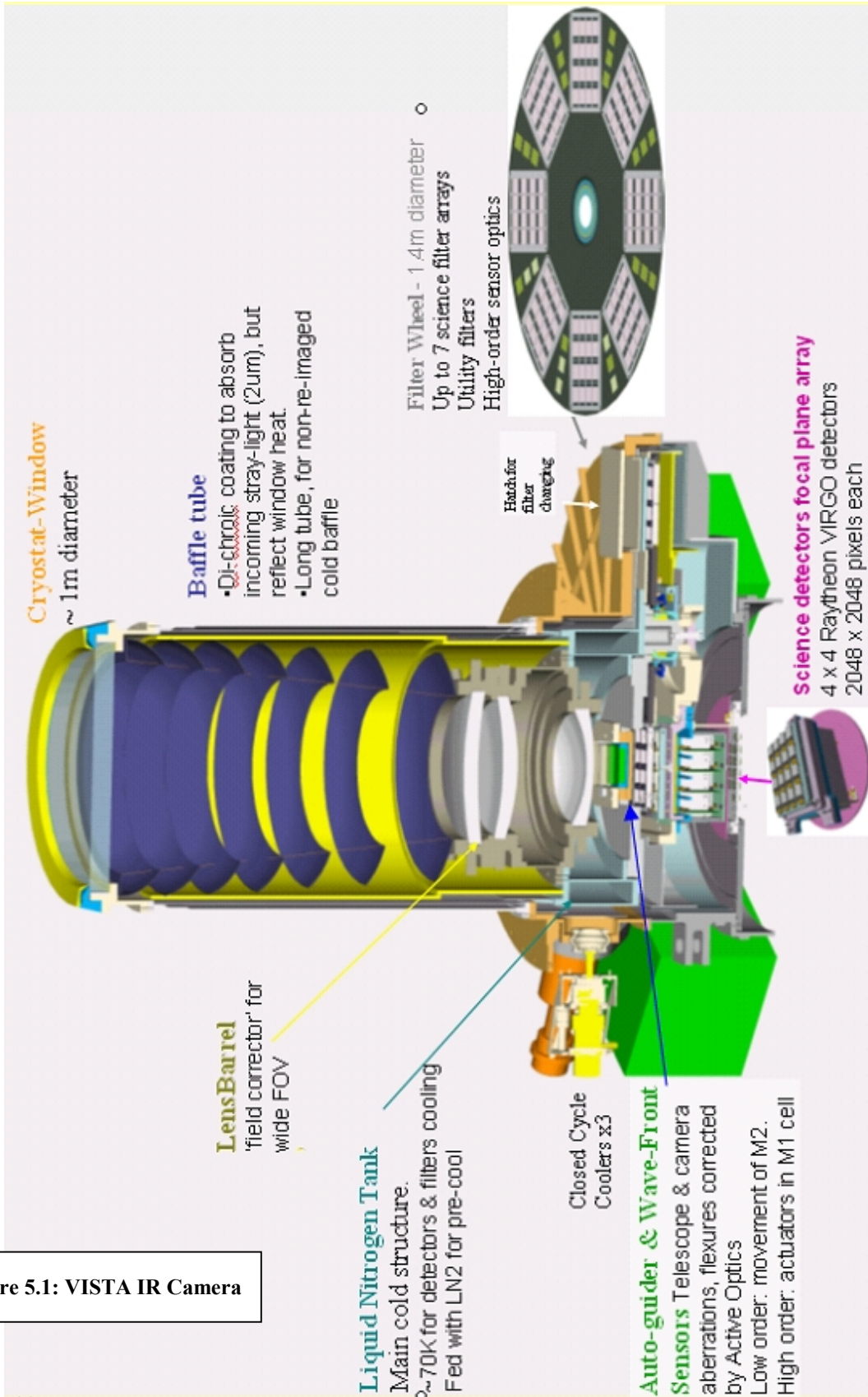


Figure 5.1: VISTA IR Camera

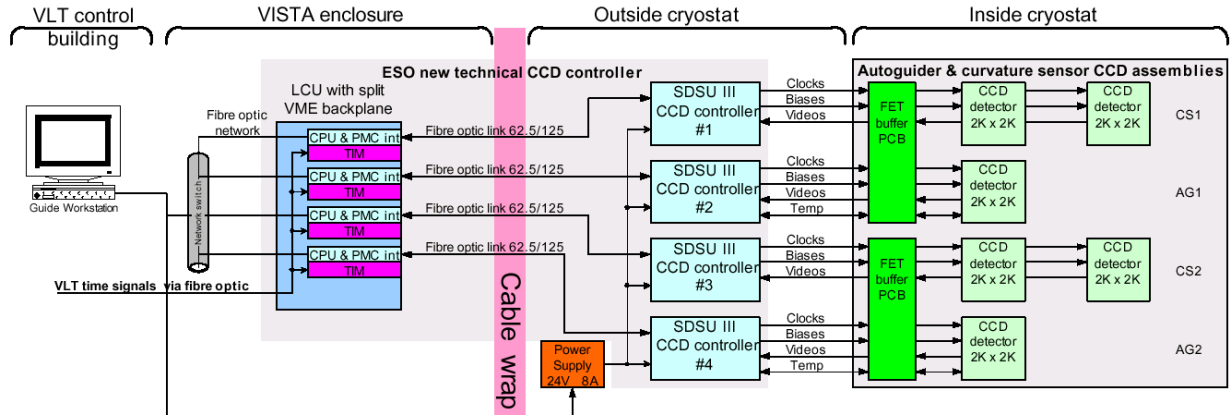


Figure 5.2: WFS Electrical Block Diagram

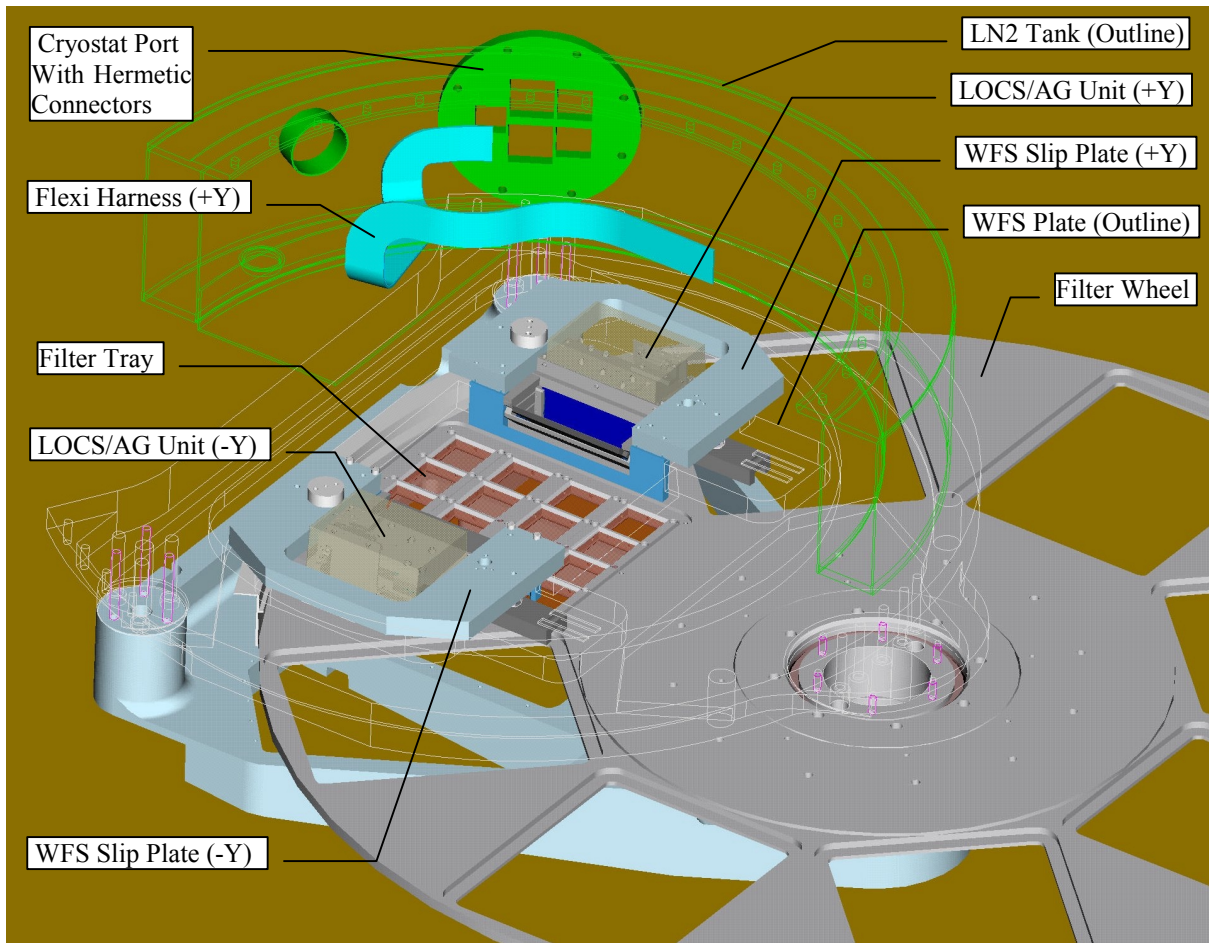


Figure 5.3: Location of the Two LOCS/AG Units

Doc. Number:	VIS-DES-UOD-06042-0001
Date:	8 th March 2004
Issue:	3.0
Page:	Page 18 of 18
Author:	Paul Clark

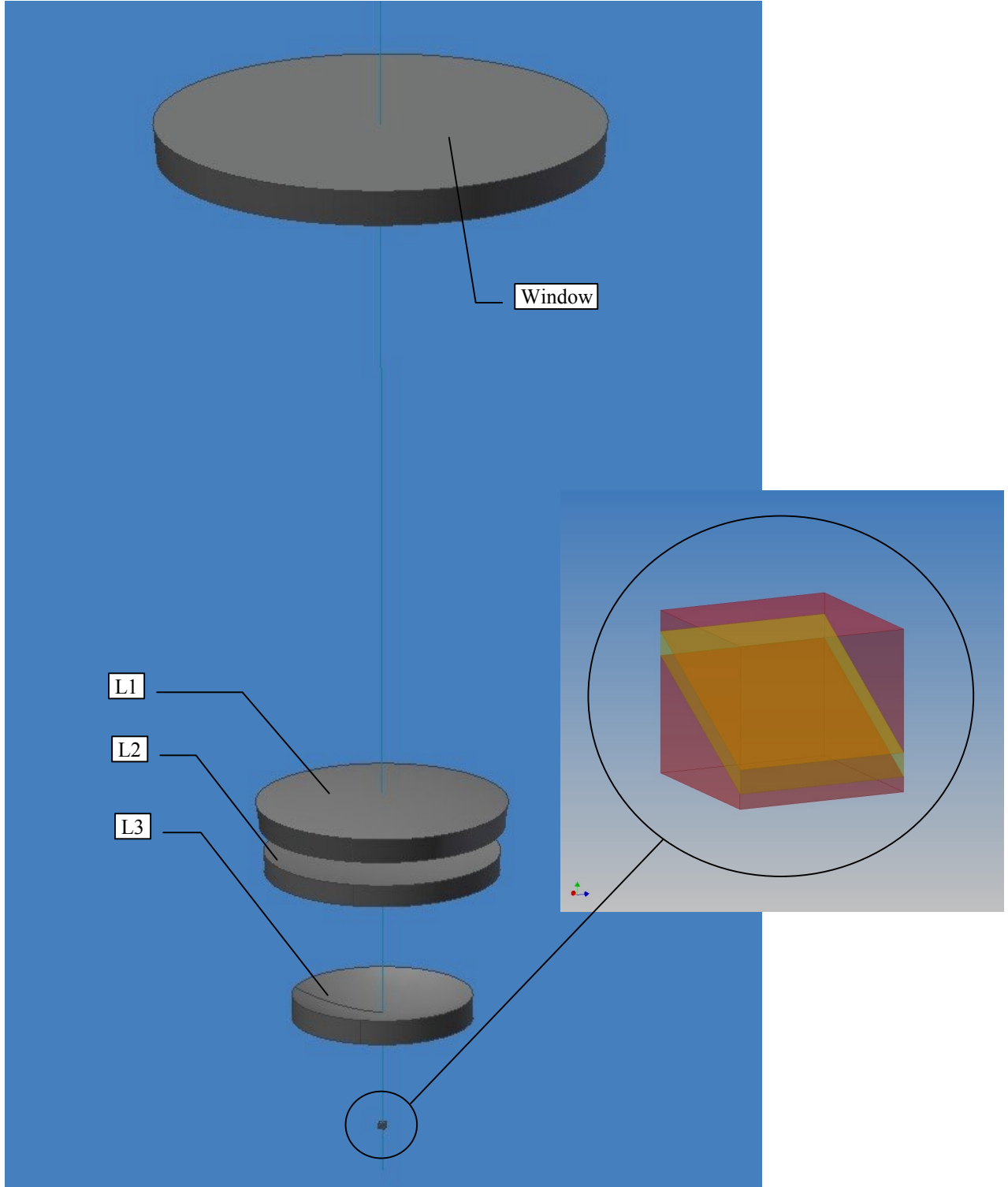


Figure 5.4: HOCS Optical Component

Doc. Number:	VIS-DES-UOD-06042-0001
Date:	8 th March 2004
Issue:	3.0
Page:	Page 19 of 19
Author:	Paul Clark

6 LOCS/AG Unit Design

This section describes the design of the LOCS/AG unit including optical, mechanical, electronic and thermal aspects of the design. The software associated with these systems is described in a later section.

6.1 Requirements

The requirements for the LOCS/AG units, including individual requirements for the LOCS and AG, are summarised in Appendix 1.

The main constraints on the optical and mechanical design of the LOCS/AG units come from:

- Requirements 2,3,22 and 23 which govern the location of the sensors within the field of view
- Requirements 21 and 24 which make the provision of two LOCS sensors necessary, one on either side of the FOV
- Requirements 57-60 which specify optical clearances between the sensors and the science beams, mechanical constraints (e.g. clearance above the FPA and hence filter wheel) and mounting details

6.2 CCD Selection

As described in AD01 sections 5.4 and 5.5, the required footprint of the LOCS and AG are both equivalent to 2Kx2K 13.5 μ m pixels. The calculation of this footprint is re-validated in sections 6.2.1 and 6.2.2 below. In order to make the LOCS/AG unit design symmetrical, to avoid detector vignetting and to provide the required frame rate, the combined AG footprint is provided by two 2Kx1K frame transfer CCDs, one mounted alongside the LOCS in each of the two identical LOCS/AG units.

The CCDs themselves are custom-packaged (Invar) deep-depletion frame-transfer-wired variants of E2V's CCD4240 (BI, NIMO) as described in AD02 section 8. To maximise cost effectiveness and minimise the need for spares, a single detector type will be procured but with two different mask options. The autoguider CCD in each unit will be equipped with a mask that covers half the chip allowing it to be used in frame transfer mode. The curvature sensor CCDs will have masks that cover the 40 columns nearest the readout register providing a storage area for the defocused star image during readout. AD16 provides the technical specification for the devices. CCD procurement is underway and the delivery schedule is in line with the Camera project plan.

6.2.1 Validation of AG FOV

The requirement for the autoguider field of view is defined in AD03 4.5.3 e) and specifies that the field must be big enough for there to be a 99% probability of a suitably bright guide star being visible for any desired exposure on sky at full moon (requirement 5). In the conceptual design [RD01] the required autoguider field was calculated backwards through a guide star R-band magnitude of 15.6 from a desired signal to noise ratio of 20. In Appendix 13 section 1 this calculation is re-validated but, rather than working backwards from a desired signal to noise ratio, the delivered signal to noise ratio is calculated using the chosen 2Kx2K combined AG footprint with an I-band star magnitude of 15.2. This 99% guide star brightness is calculated from the Gemini (D. Simons) model of R-band star availabilities at the galactic pole for the equivalent autoguider field radius and is adjusted for I-band.

The signal to noise ratio is calculated as:

$$\frac{\sum f_{obj} t}{\sqrt{(\sum (f_{obj} + f_{bg} + f_{dark}) t + Num_{pix} \sigma_{rd}^2)}}$$

where:

Num_{pix} is the number of pixels the object image is spread over

f_{obj} is the flux rate for the object (e⁻/sec)

f_{bg} is the flux rate for the sky background (e⁻/pixel/sec * Num_{pix})

f_{dark} is the dark current rate (e⁻/pixel/sec * Num_{pix})

t is the exposure time

σ_{rd} is the detector read noise (e⁻)

As shown in Appendix 13 section 1, the autoguider will deliver a signal to noise ratio of 25 using an exposure time of 90ms (made possible by the CCD frame transfer architecture).

6.2.2 Validation of LOCS FOV

The low order curvature sensor signal to noise ratio is calculated in the same way as that for the autoguider but using an exposure of 30s and spreading the signal over a larger number of pixels due to the 1mm defocus distance. Appendix 13 section 2 contains the result of this calculation showing that the sensor signal to noise ratio will be 150 hence meeting requirement 30 with ample margin.

A magnitude 16 star observed with the same 30-second exposure would still deliver a signal to noise ratio of 87.

Doc. Number:	VIS-DES-UOD-06042-0001
Date:	8 th March 2004
Issue:	3.0
Page:	Page 21 of 21
Author:	Paul Clark

6.2.3 Operation after sunset

Requirement 8 specifies that the autoguider should be operable 30 minutes after sunset using a suitably bright guide star. In order to calculate if this is achievable, the same spreadsheet was used and adjusted as follows:

- A minimum exposure time of 10ms was selected
- The guide star magnitude was adjusted to provide a signal of $60,000e^-$ in this same exposure time
- The sky brightness was then adjusted until the resulting signal to noise ratio was close to 7 (the minimum for reliable operation of the guider)

The calculation shown in Appendix 13 section 3 concludes that a guide star magnitude of 9.2 provides a signal to noise ratio of 7.8 with a sky brightness of 3 mag/arcsec^2 . This calculation is somewhat nonsensical since 3 mag/arcsec^2 is roughly equivalent to daylight and the camera itself would saturate almost immediately.

Using a more realistic sky brightness of 13 mag/arcsec^2 and an exposure of 50ms, it would be possible to guide on a magnitude 14 star with a signal to noise ratio of 19.3.

6.2.4 Autoguider frame rate

As discussed in AD02 section 7, the 10Hz autoguider frame rate requirement has already been demonstrated with the CCD4240, fulfilling requirement 6.

6.3 Optical Design

The optical design of the LOCS/AG units was undertaken by Richard Bingham. His design report is included as Appendix 6. Further detail on the LOCS aberrations is given in Appendix 14.

The chosen LOCS design is based upon the use of a cube beamsplitter to divide light between the two CCDs. A cross-section of the design is shown in figure 6.3.1, reproduced from Appendix 6.

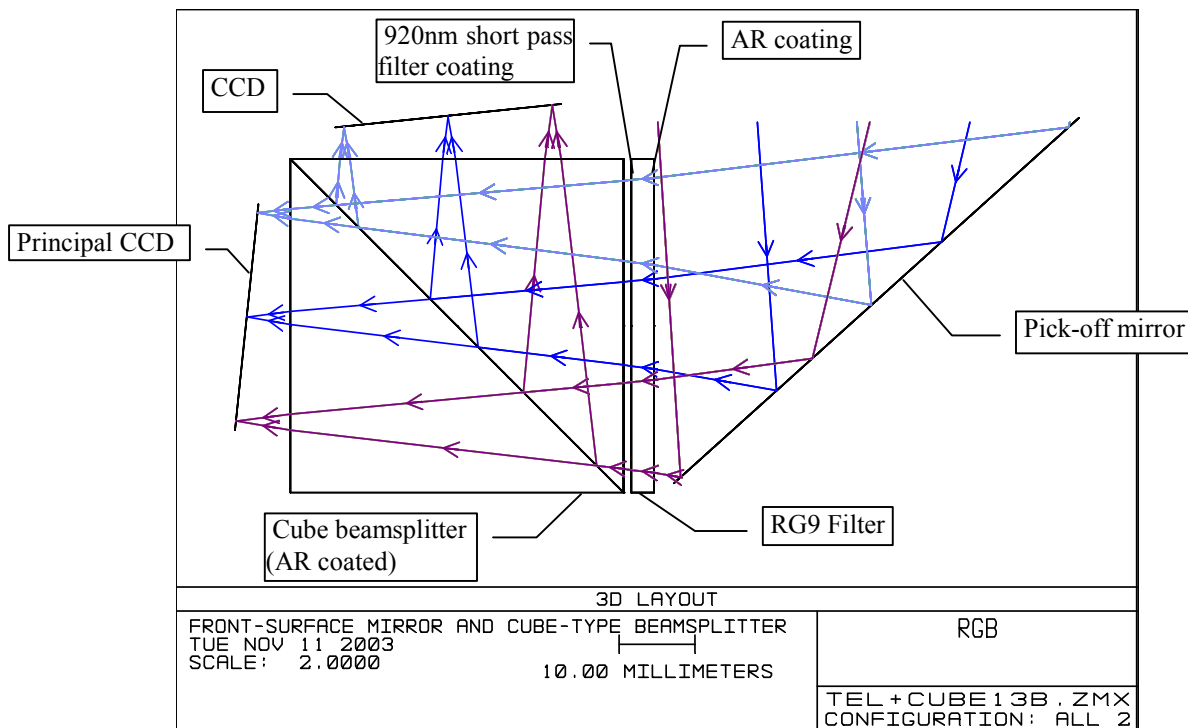


Figure 6.3.1: Cross-section of the LOCS/AG optical path

During the detailed design phase, it became clear that it would not be possible to continue to use the single plate beamsplitter design proposed at CoDR and PDR. The plate beamsplitter would have introduced significant aberrations in the transmissive path to the principal CCD due to the optical path difference across the converging beam as it passes through the tilted plate. Correct operation of the LOCS would have been prevented by the different aberrations 'seen' by each CCD. The cube design overcomes this problem. The cube beamsplitter design has been tested successfully in a cryogenic qualification test, the results of which are included in Appendix 11. An alternative non-cemented beamsplitter design is available as a fall-back (Appendix 7) but this is not considered necessary.

Doc. Number:	VIS-DES-UOD-06042-0001
Date:	8 th March 2004
Issue:	3.0
Page:	Page 23 of 23
Author:	Paul Clark

A 3D view of the optical components, including rays to the corners of the detectors is shown in figure 6.3.2. It is important to note that Appendix 6 was written and figure 6.3.2 produced before a decision was taken to rotate the autoguider CCD through 90 degrees. This was necessary to prevent the CCD package from violating the sensor space envelope. Figure 6.3.3 shows the correct equivalent footprint of the LOCS and (rotated) AG CCDs superimposed on the camera FOV.

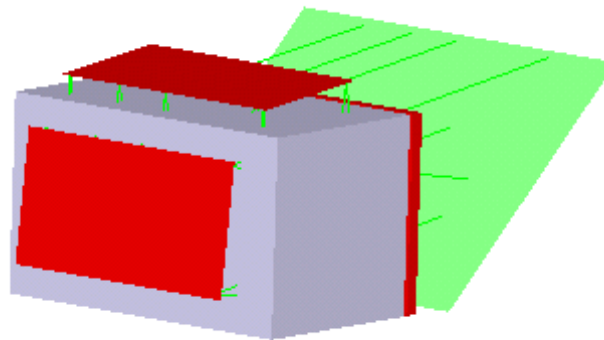


Figure 6.3.2: 3D Optical Representation of the LOCS/AG Components

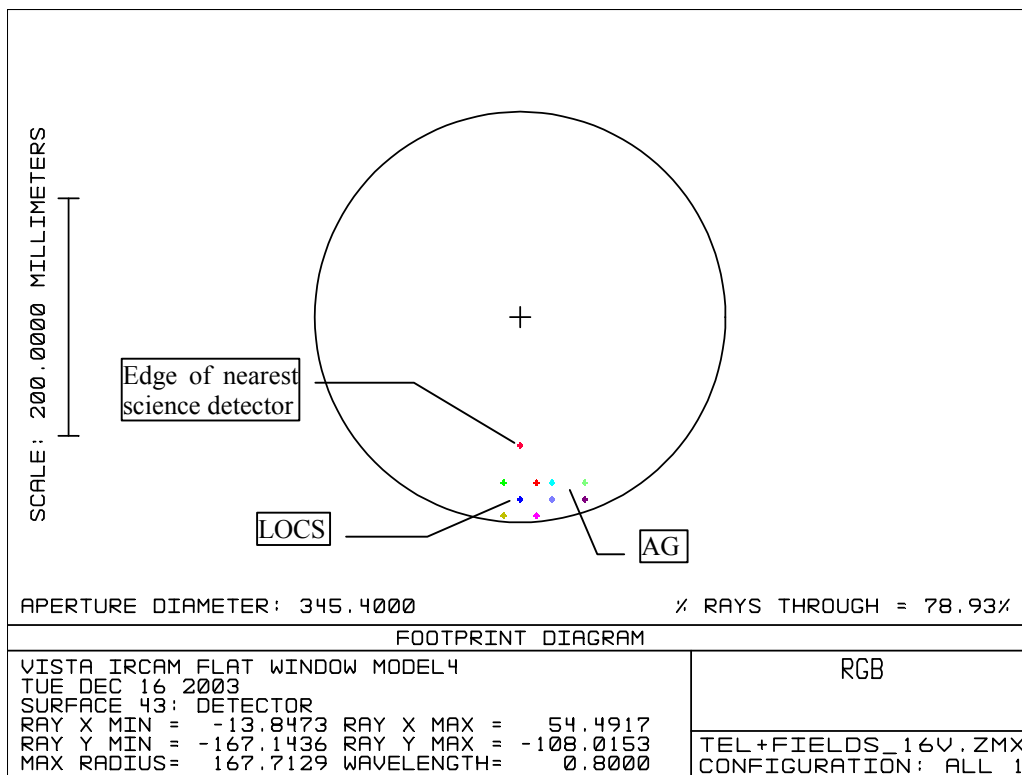


Figure 6.3.3: Footprint of the LOCS/AG CCDs on Camera FOV

6.4 Filter Selection

The LOCS/AG unit is required to utilise a wavelength pass-band which:

- is as close as possible to the science wavelengths
- is within the capabilities of CCDs
- avoids worsening sky OH lines beyond 920nm

The chosen pass-band has therefore been selected as 720nm to 920nm, pseudo-I band.

As described in AD02 section 8, the chosen CCDs will utilise deep-depletion (high-resistivity) silicon to maximise QE at these long wavelengths and to minimise the fringing normally experienced by thinned CCDs at these same wavelengths.

The LOCS/AG filter could be implemented using a normal interference filter coating on glass. However the filter also needs to be able to suppress the rejected science wavelength light that would otherwise be reflected back out into the camera cryostat.

As described in AD01 section 5.8, the filter will be implemented using 3mm-thick Schott RG9 filter glass which absorbs light below 700nm and above 1100nm. A 920nm short pass coating will be applied to the rear of the RG9 and a broad band AR coating to the front. The throughput to the CCDs will therefore be as shown in Figure 6.4.1.

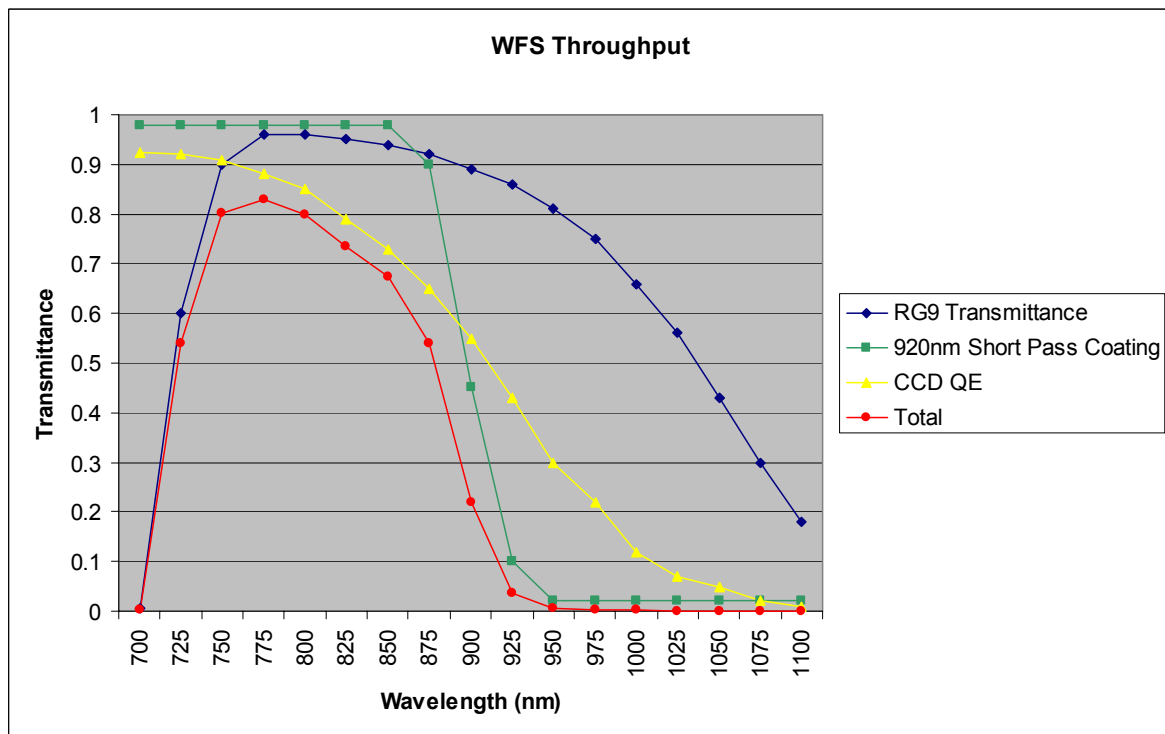


Figure 6.4.1: WFS Throughput

RG9 has an unfortunate second pass-band centred on 2500nm as shown in figure 6.4.2. A stray light analysis has been performed to demonstrate that the science wavelength light reflected off the 920nm filter coating and which exits the RG9 after a second pass (6mm) does not cause unwanted ghosting on the science array. The analysis is presented in Appendix 9 and concludes that a magnitude 1 star image reflected back from the filter will cause ghosting equivalent to 1% of the sky background in Y and Zsloan. The ghosting is therefore considered acceptable and the RG9-based design valid. If the RG9 were to be replaced by standard glass then the same level of ghosting would occur from a magnitude 5 star.

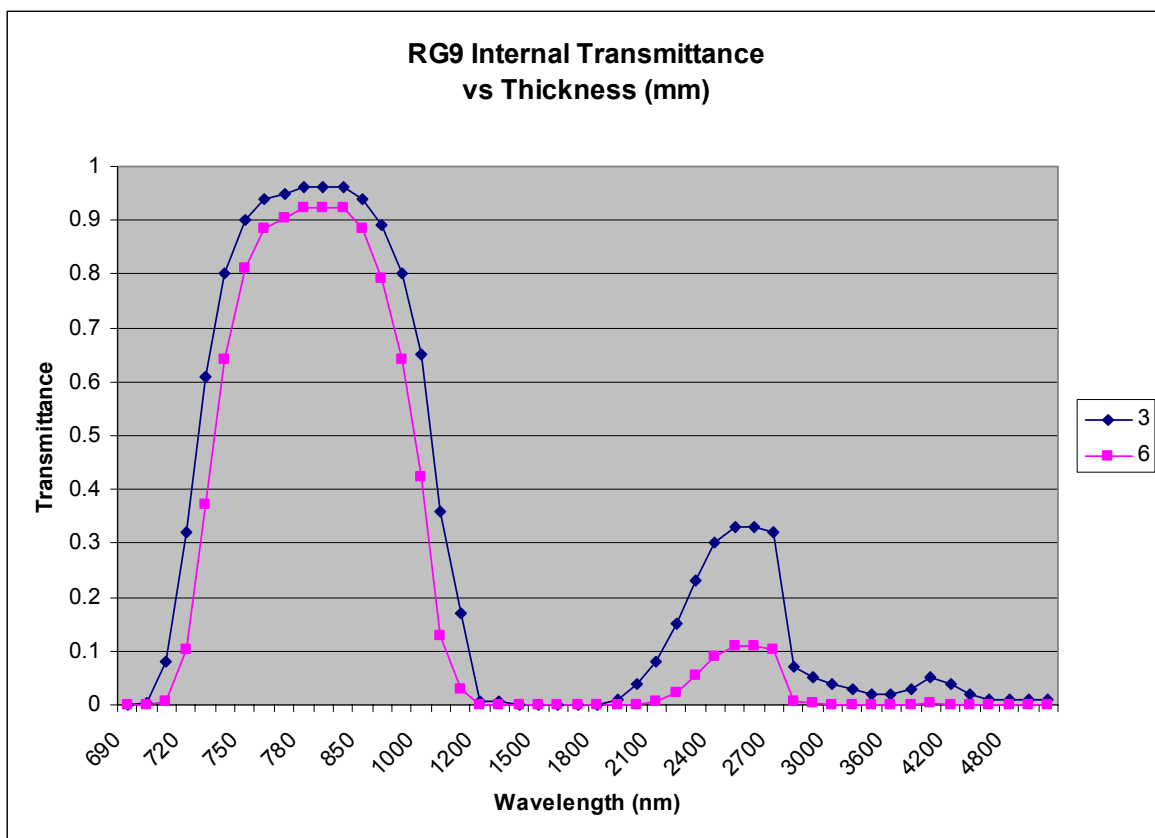


Figure 6.4.2: RG9 Transmittance

6.5 Science Beam Clearance

The optical design of the LOCS/AG units allows the CCDs' view to sky to be unvignetted and the equivalent detector footprint to be positioned several millimetres away from the edge of the Camera FOV (see figure 6.3.3). The lowest surface of the cube beamsplitter has been positioned 46mm above the focal plane (Requirement 58) and the extreme edge of the pick-off mirror is positioned the required 1mm away from the nearest science beam (Requirement 59) while also allowing a 0.5mm gap between the WFS beam and the edge of the mirror such

Doc. Number:	VIS-DES-UOD-06042-0001
Date:	8 th March 2004
Issue:	3.0
Page:	Page 26 of 26
Author:	Paul Clark

that the mirror does not have to be polished to its extreme edge. Appendix 10 illustrates these details.

6.6 Alignment Sensitivity

The optical design of the LOCS/AG unit utilises the angle of the pick-off mirror to desensitise the system to misalignment in Y relative to the optical axis. Lines extended from the surfaces of the mirror and principal CCD would meet on the focal plane (without WFS or science filters present). Figure 6.6.1 illustrates this. In this way, any misalignment in Y (or X) only results in a shift of the part of the Camera FOV seen by the CCDs and not a change in focus.

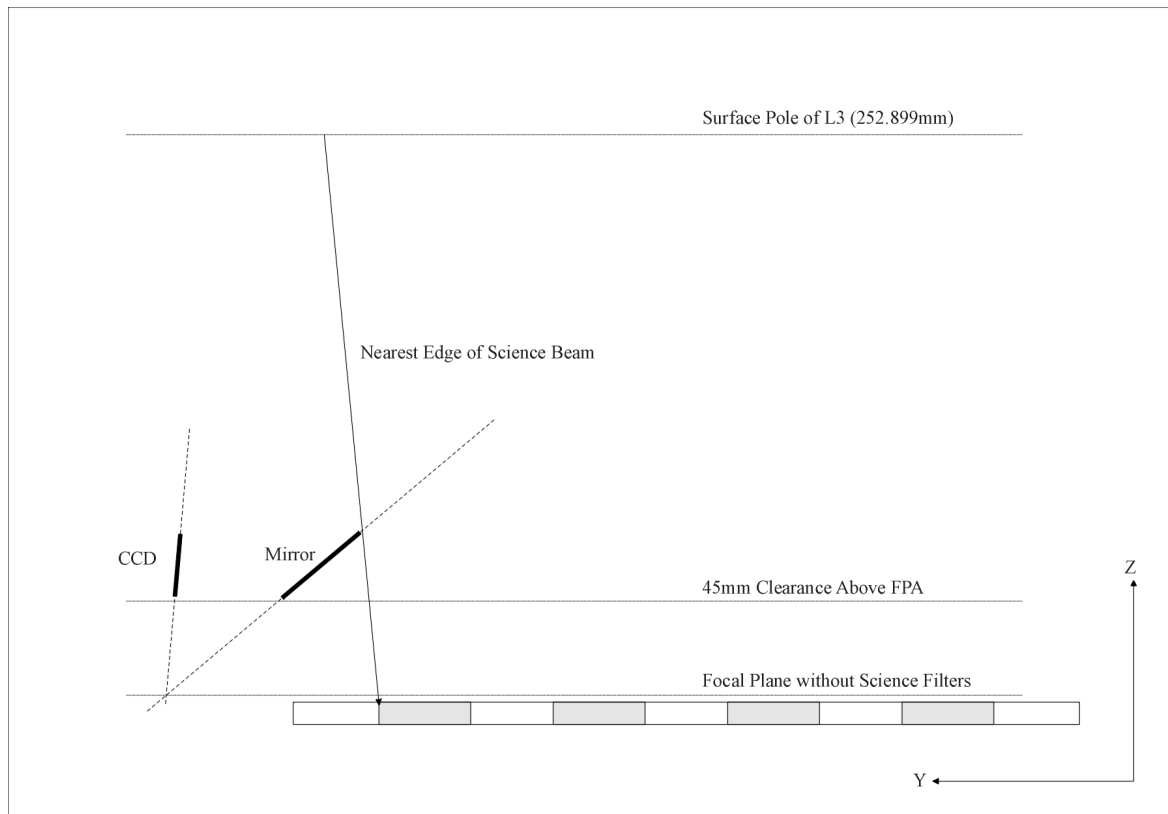


Figure 6.6.1: Positioning of the WFS Pick-off Mirror and Principal CCD

An analysis of the (mis-) alignment sensitivity has taken place and is included in Appendix 12. A movement of the unit by up to 5mm in either X or Y will introduce a maximum P-V change in the image aberrations of less than 0.3 waves, much less than the static aberrations always seen by the sensors (see also RD15 section 10 and AD01 section 7.4). This insensitivity lessens the impact of the unit focus requirement (69 & 70).

The LOCS/AG unit will be accurately internally aligned, relative to the external reference marks and alignment surfaces specified in the ICD [AD04], by precision shimming of the

Doc. Number:	VIS-DES-UOD-06042-0001
Date:	8 th March 2004
Issue:	3.0
Page:	Page 27 of 27
Author:	Paul Clark

optics and detectors (if required). The WFS shuffle plates on the WFS frame will be positioned accurately during Camera AIT. The philosophy behind the alignment of the LOCS/AG units is that each of the two units (or three if the manufacture of a spare is requested) will be internally aligned such that the units are fully interchangeable. The metal parts of the units will be machined accurately such that internal shimming should not be necessary but this remains an option if required.

The insensitivity to misalignment has an additional benefit in that changes in the WFS plate temperature and hence radial contraction/expansion due to ambient temperature changes will not introduce significant aberrations either (see RD09 section 6.2).

6.7 Mechanical Design

The mechanical design of the LOCS/AG units is governed by the physical location of the optics and detector surfaces from the optical design plus the mechanical and mounting constraints imposed by the Sensors to Cryostat ICD [AD04]. As can be seen from the mechanical drawings of the LOCS/AG unit in Appendix 3, the design complies with the requirements of the ICD (58-61). The internal construction of the LOCS/AG units is as shown in the following figures. The mechanical components of the LOCS/AG units will be made from the same Aluminium alloy as the WFS plate.

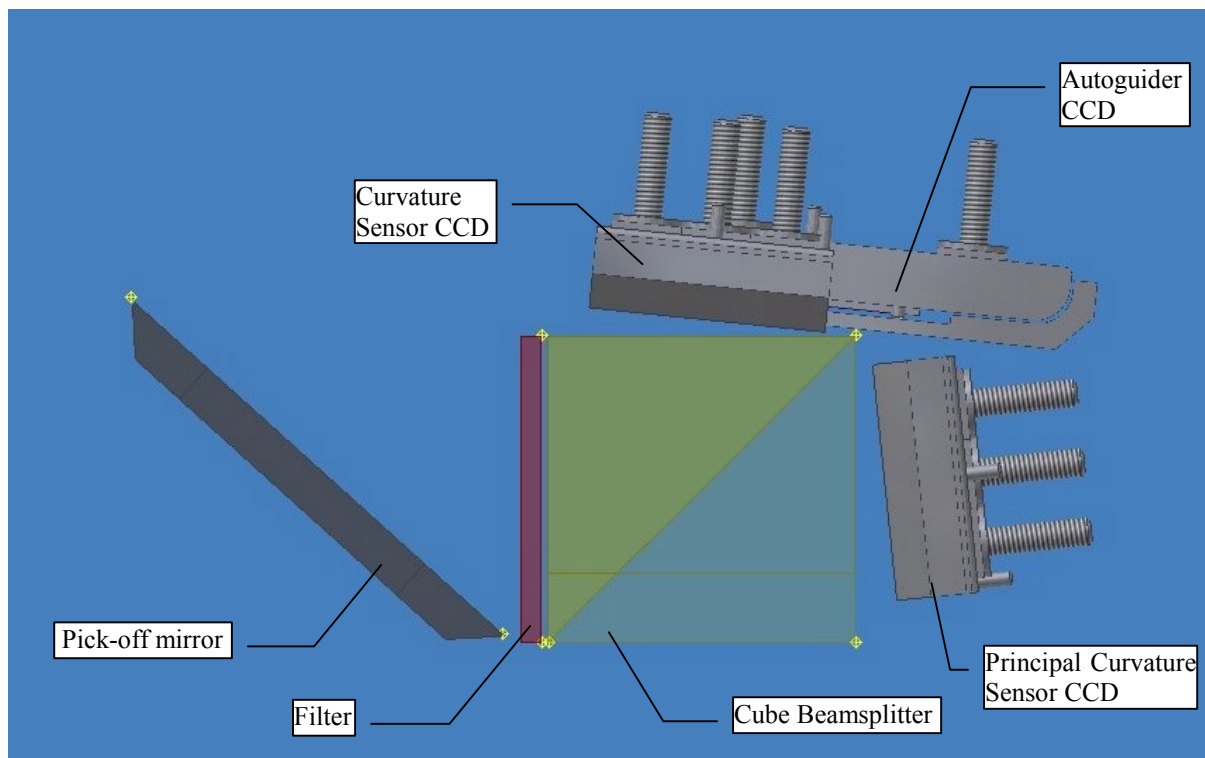


Figure 6.7.1: LOCS/AG Optics and Detectors, Side View

Doc. Number:	VIS-DES-UOD-06042-0001
Date:	8 th March 2004
Issue:	3.0
Page:	Page 28 of 28
Author:	Paul Clark

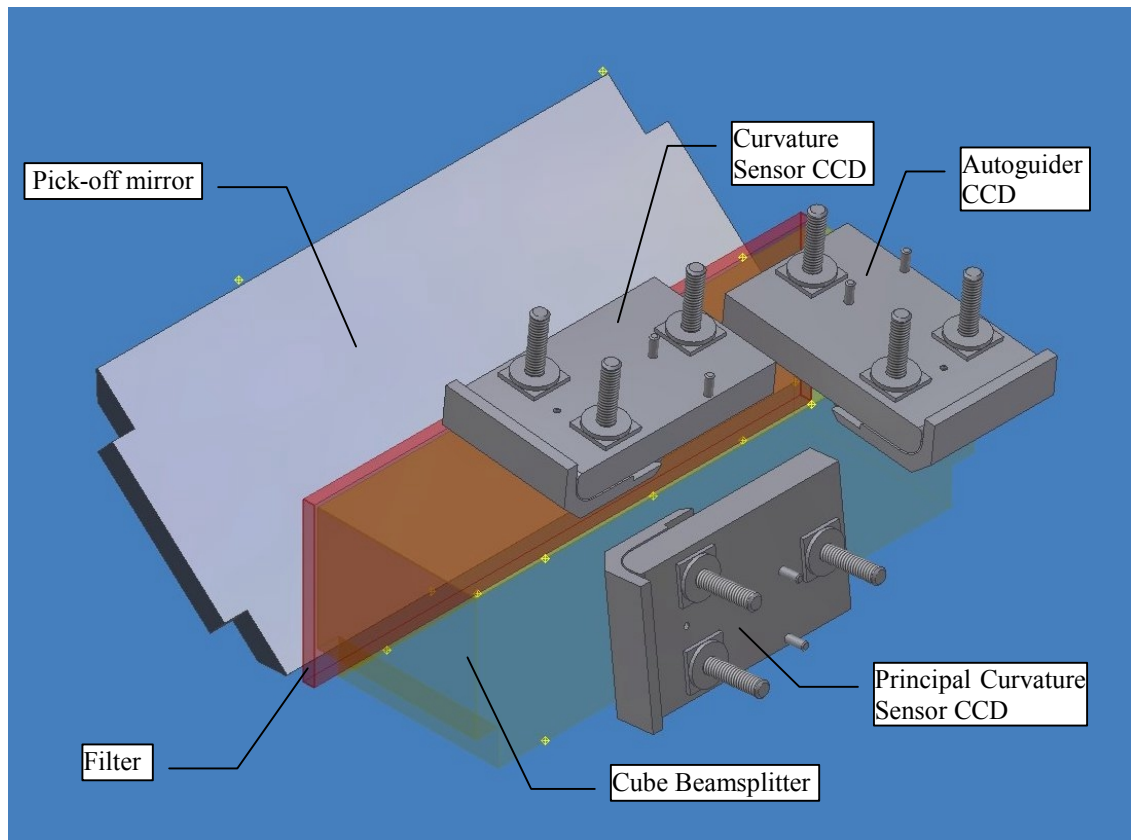


Figure 6.7.2: LOCS/AG Optics and Detectors

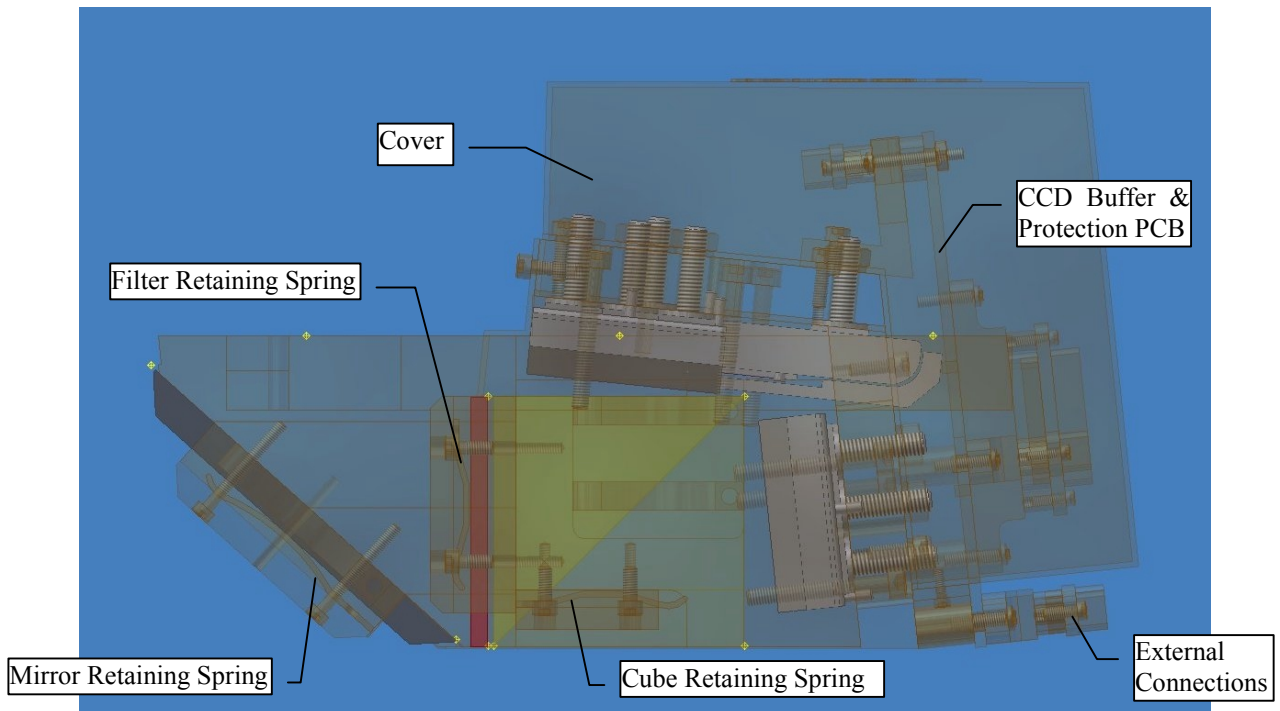


Figure 6.7.3: LOCS/AG Unit Transparent Side View

Doc. Number:	VIS-DES-UOD-06042-0001
Date:	8 th March 2004
Issue:	3.0
Page:	Page 29 of 29
Author:	Paul Clark

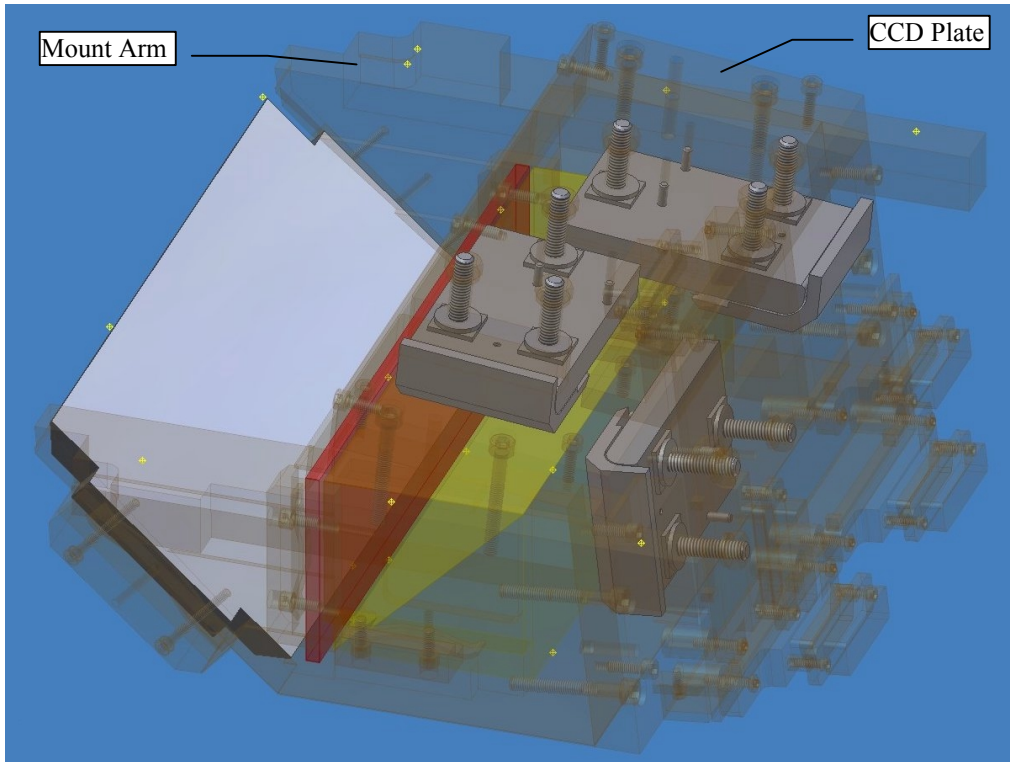


Figure 6.7.4: LOCS/AG Unit Transparent View (Cover Removed)

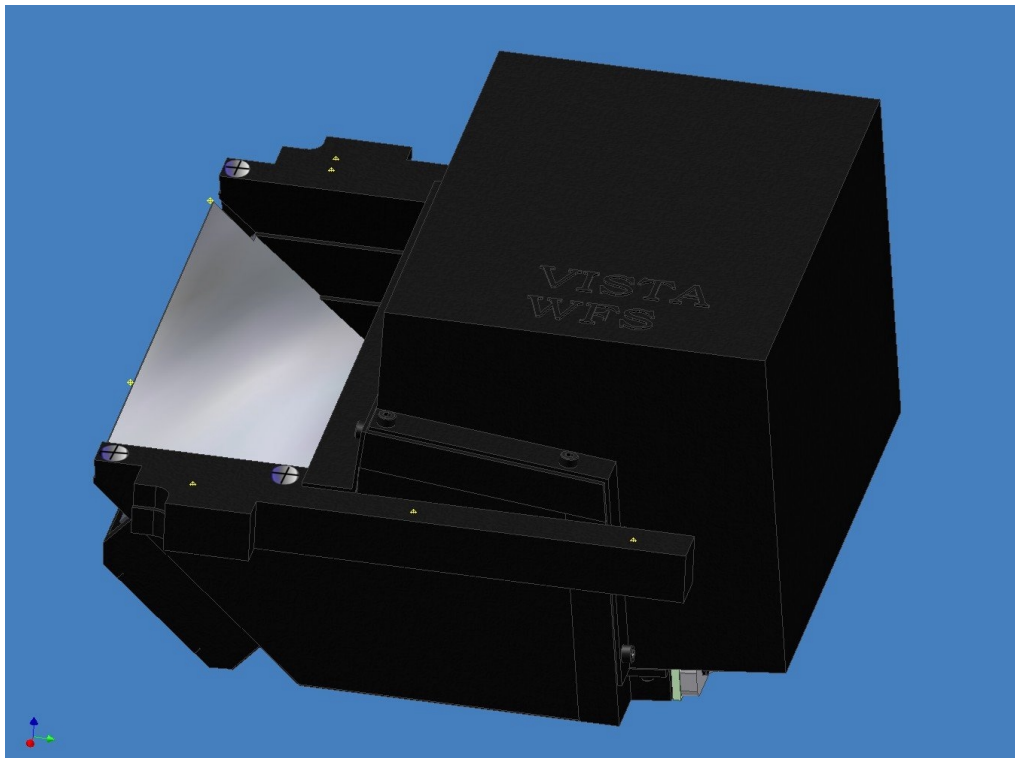


Figure 6.7.5: LOCS/AG Unit External View

Doc. Number:	VIS-DES-UOD-06042-0001
Date:	8 th March 2004
Issue:	3.0
Page:	Page 30 of 30
Author:	Paul Clark

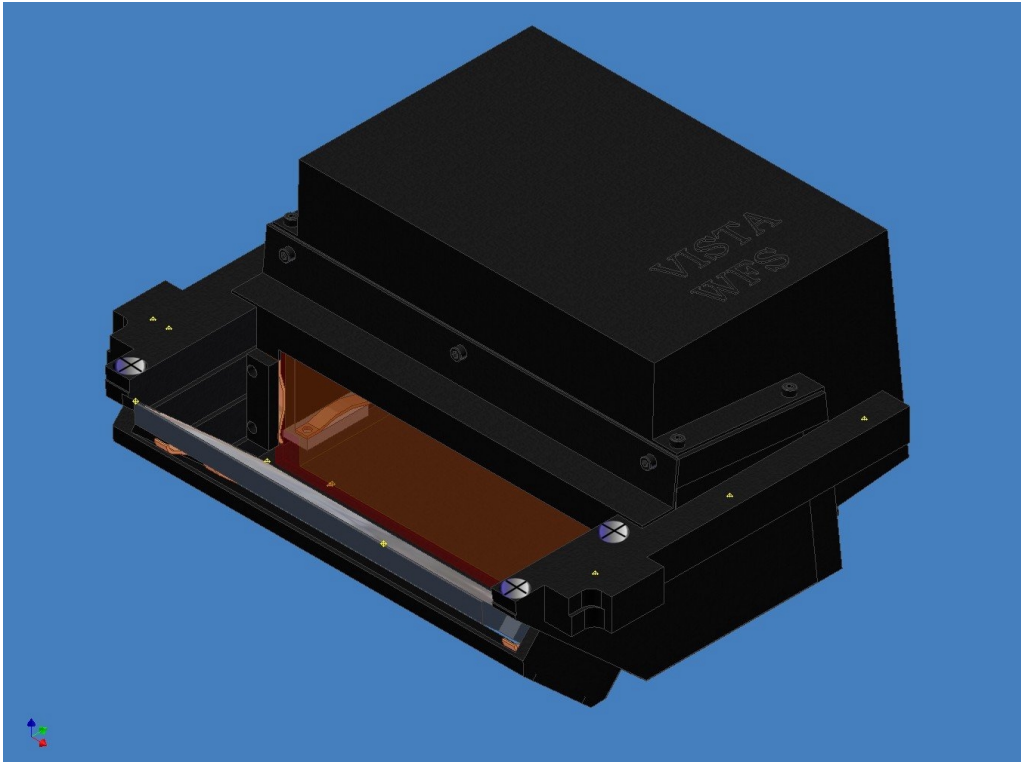


Figure 6.7.6: LOCS/AG Unit External View

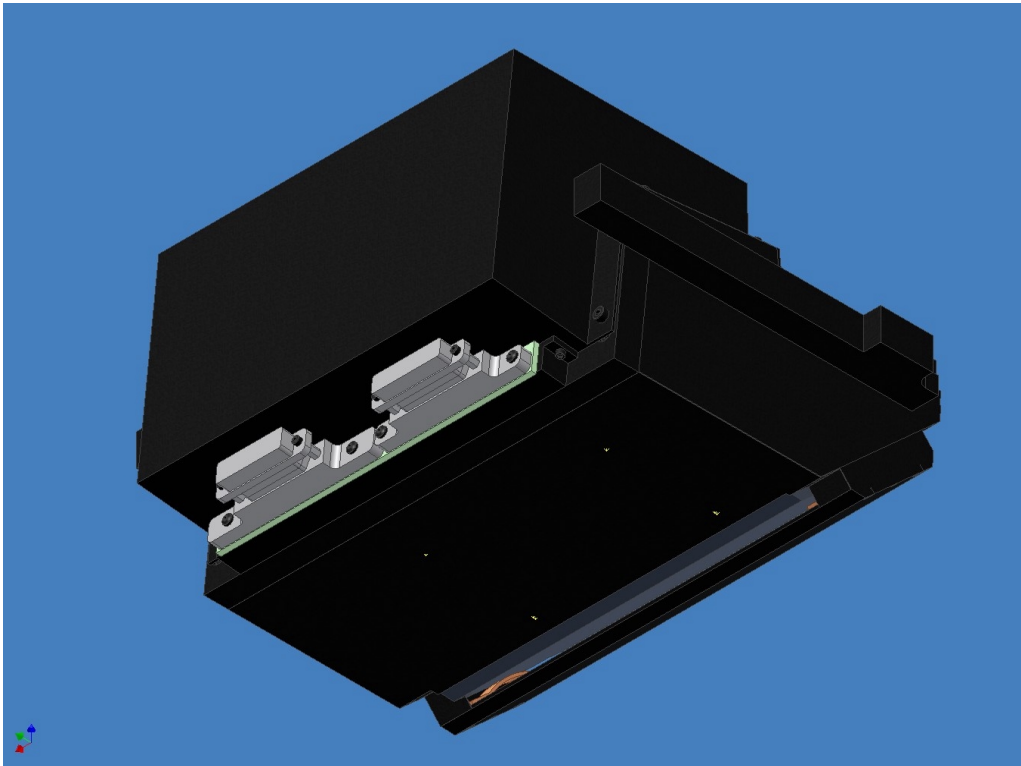


Figure 6.7.7: LOCS/AG Unit External View

Doc. Number:	VIS-DES-UOD-06042-0001
Date:	8 th March 2004
Issue:	3.0
Page:	Page 31 of 31
Author:	Paul Clark

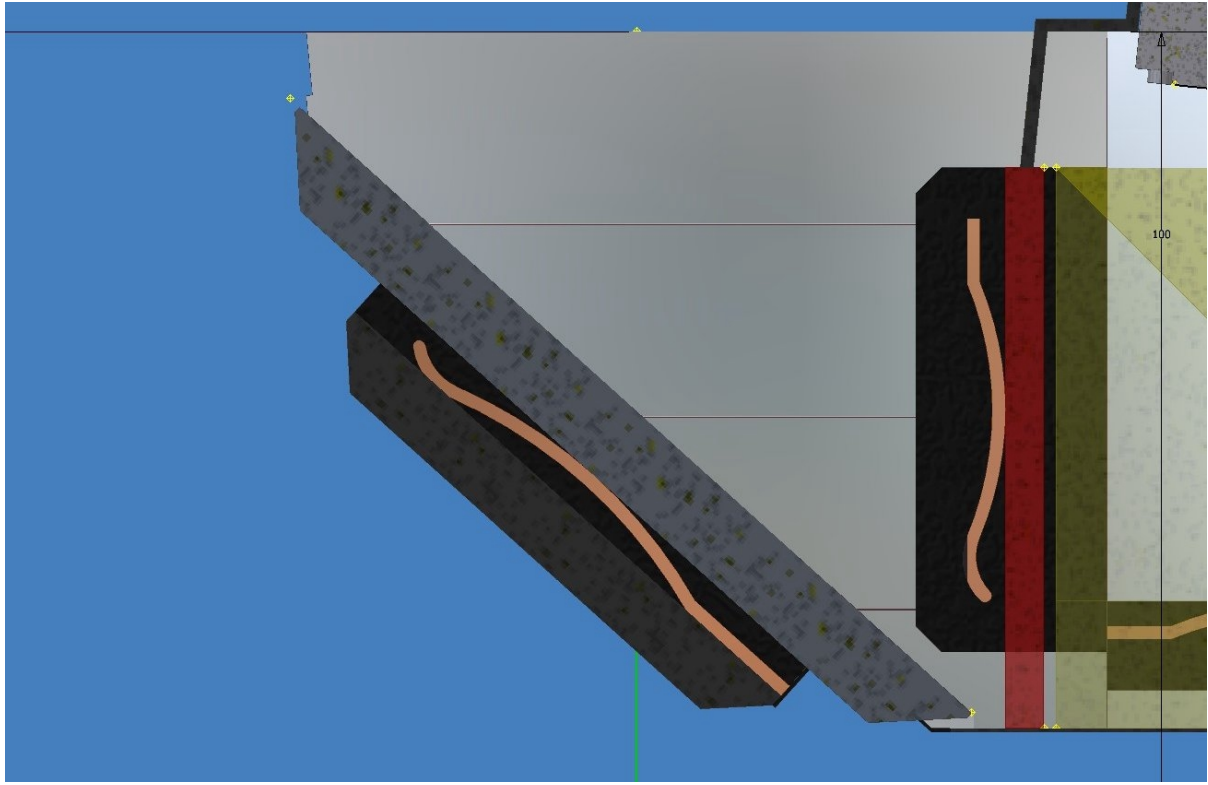


Figure 6.7.8: LOCS/AG Optics Retaining Springs

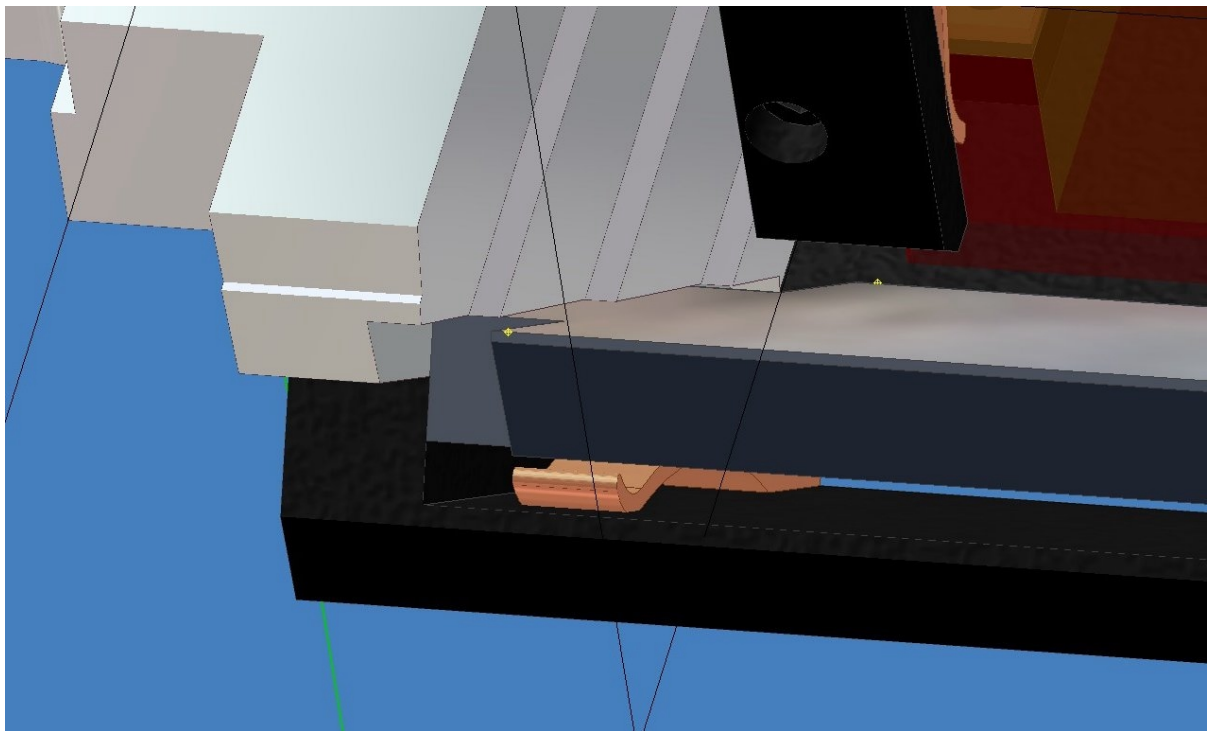


Figure 6.7.9: LOCS/AG Optics Retaining Springs

6.8 CCD Mounting & Alignment Features

Full drawings of the CCD package are contained in Appendix 3, although these may later be modified by E2V during the design phase of the CCD procurement. Figure 6.8.1 illustrates the mounting and alignment features on the rear of the package. Kinematic location pins on the front surface of the package allow the detector substrate to be accurately positioned during manufacture relative to the rear central and rotation-constraining pins.

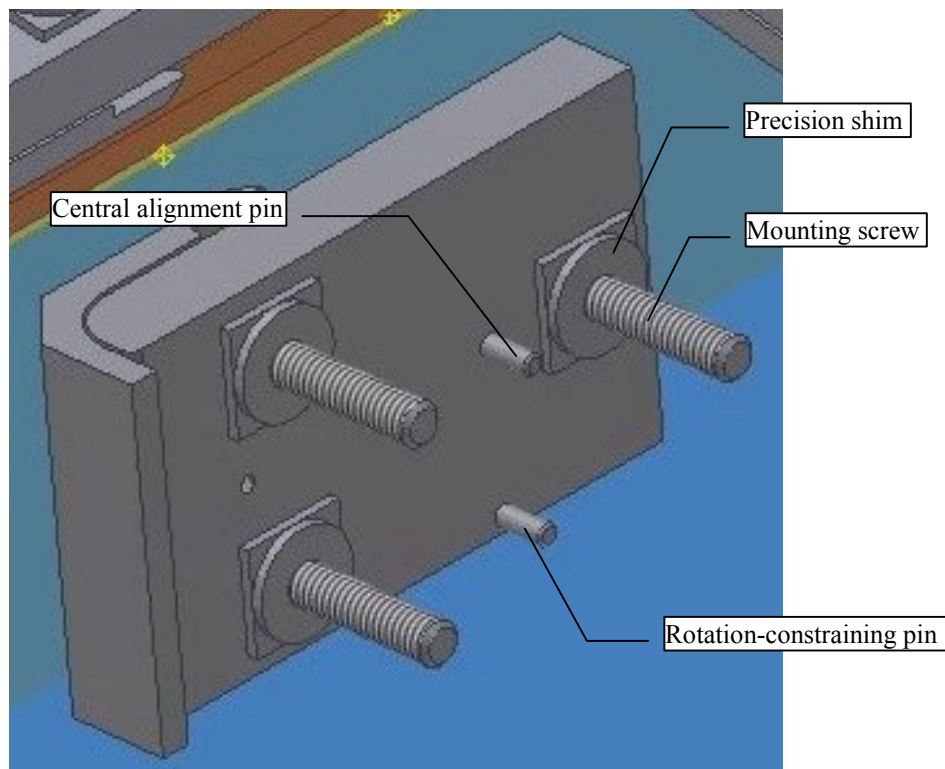


Figure 6.8.1: CCD Mounting & Alignment Detail

Three mounting pads are provided on the rear of the CCD package. The CCD manufacturer will fit precision shims to these pads to position the detector surface to a tolerance of $\pm 20\mu\text{m}$.

A central alignment pin is provided to allow the active centre of the detector to be positioned accurately. A second pin is provided to constrain detector rotation. The central pin fits into a round hole in the appropriate CCD plate, the rotation constraining pin fits into a corresponding slotted hole.

The three mounting screws will pass through clearance holes in the CCD plate, to allow for the difference in thermal expansion between the Invar detector package and the Aluminium plate, before being secured with insulating washers.

6.9 Thermal Design

The thermal design of the LOCS/AG units is summarised in figure 6.9.1.

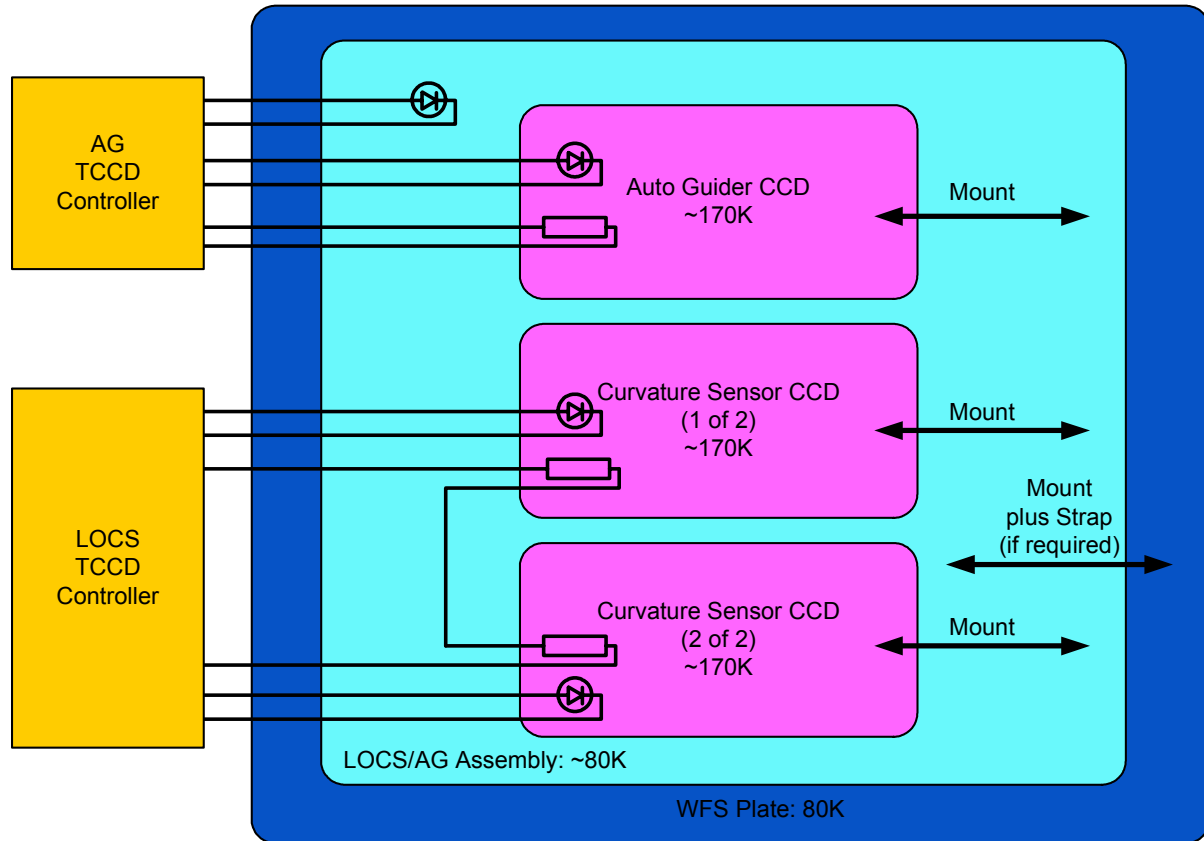


Figure 6.9.1: LOCS/AG Unit Thermal Design

The LOCS/AG CCDs are to be maintained at a constant temperature of approximately 170K. The temperature needs to be above 150K for correct operation and below 210K to reduce the dark current to acceptable levels [AD15 9.1]. The WFS plate temperature will be maintained at approximately 80K by the camera cold head system [RD09, Tables 6.2-1 and 6.1-2]. The CCDs will be slightly over-cooled by thermal conduction into the CCD plates, through the remainder of the LOCS/AG unit assembly and into the surrounding WFS plate. Provision has been made to include additional cooling straps between the LOCS/AG units and the WFS plate should the thermal path through the intermediate mounting surfaces not be sufficient. CCD temperatures will be servo-controlled by the ESO TCCD Controllers via heating resistors and temperature sensing diodes. Each Controller has two temperature-sensing channels and one heating channel. For the LOCS, each CCD will have its temperature monitored by a single diode and heating power shared between each pair. For the AG, the

Doc. Number:	VIS-DES-UOD-06042-0001
Date:	8 th March 2004
Issue:	3.0
Page:	Page 34 of 34
Author:	Paul Clark

temperature of the CCD will be monitored by one diode, the other being used to monitor the temperature of the surrounding metalwork.

The power dissipated by each LOCS CCD will be of the order 250mW while the AG CCD will dissipate of the order 760mW due to its almost constant clocking. The total power dissipation of the two LOCS/AG units is presented in AD15 section 9.1.

At the time of writing, it has not been possible to fully detail the interface between the individual detectors and the CCD plates due to difficulties with accurately modelling the heat flow between the two. A qualification test will take place post-FDR to establish if the chosen metal-to-metal mounting design, which is preferable from a manufacture and alignment perspective, is fully viable in terms of the required thermal insulation. It may be necessary to revise the mounting detail to include additional insulation if the qualification test indicates this is necessary. This is regarded as fine detailing of the design and is not considered a significant risk item but will be entered into the IR Camera Risk Register. The CCD pad mount detail currently being investigated is shown in figure 6.9.2. Currently the approximate heat flow through this design is 0.4W per pad, which would require the servo heating load to be increased to ~1W per detector. An allowance of 10W is made for the two LOCS/AG units within the IR Camera Thermal Analysis [RD09] and so this additional heat load would still be within budget but attempts will be made to minimise this.

Doc. Number:	VIS-DES-UOD-06042-0001
Date:	8 th March 2004
Issue:	3.0
Page:	Page 35 of 35
Author:	Paul Clark

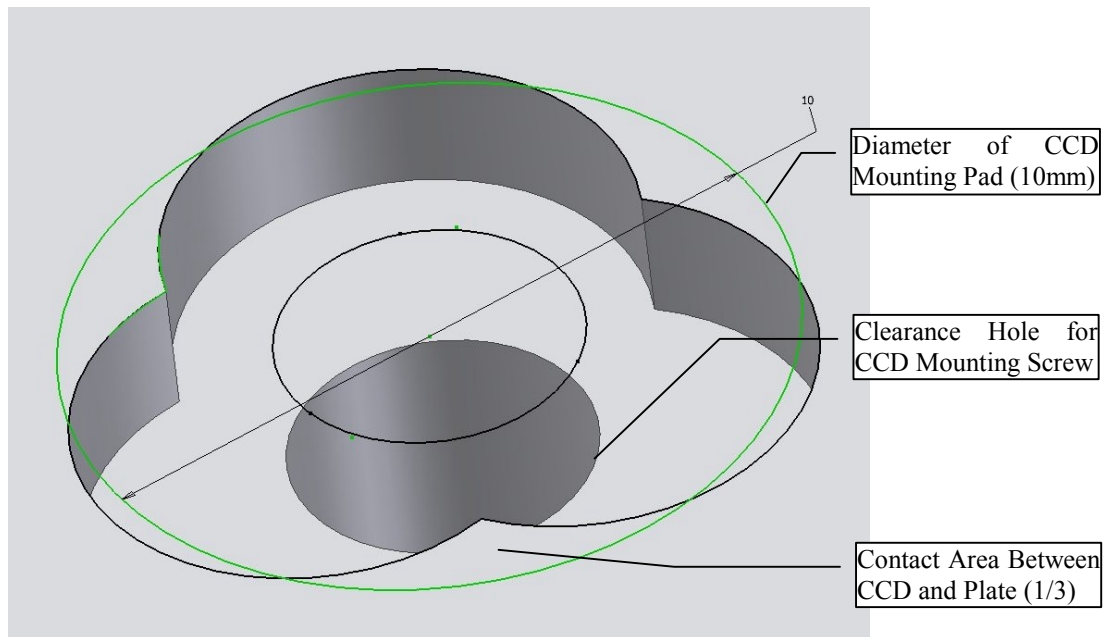


Figure 6.9.2: CCD Plate Detector Pad Mounting Detail

6.10 LOCS/AG Unit Mass

The predicted mass of each complete LOCS/AG unit has been confirmed as 2.25kg, matching the value that was presented at Camera FDR [AD15 section 7] and used in the FEA analysis [RD08].

6.11 Contamination Control

The LOCS/AG units will be assembled and stored in a class 100 clean area and only brought out into a class 10,000 clean area for optical and electrical testing. The CCDs will be delivered in suitable packaging by the manufacturer [AD16 section 7.18]. All other components will be cleaned prior to assembly. The complete units will be suitably packaged prior to shipping to RAL for integration.

6.12 Electrical Design

The electrical design of the LOCS/AG unit buffer and protection PCB plus harness is described in the following sub-sections. Appendix 4 contains the: grounding diagram; harness diagram; board schematics; board layout and parts list for the LOCS/AG units.

6.12.1 Clocks

The TCCD Controller clock board ground has been chosen as the point of reference for V_{ss} , meaning that the clock signals will swing between -9 and +1V.

6.12.2 ESD and Over-Voltage Protection

To protect against ESD damage, all signals connected to the CCD are also connected to a transient voltage suppressor chip from the SP72x series: the 16 pin SP720 or 8 pin SP721. These chips have been used extensively and successfully in other astronomical instruments including WFCAM.

The chips are silicon-controlled rectifiers and contain active circuitry that will clamp the input signal to the power rail if it exceeds the power rail voltage by a forward diode drop ($\sim 0.7V$). By connecting a Zener diode to act as a reference to the power rails, it is possible to control the cut-off voltage. Diodes with a Zener voltage of 30V have been chosen for this board.

Over-voltage protection is provided by Zener diodes on the SDSU boards.

6.12.3 Filtering

A standard filtering system has been used to remove high frequency noise and provide decoupling and bypassing for the bias and the power signals. It is shown below.

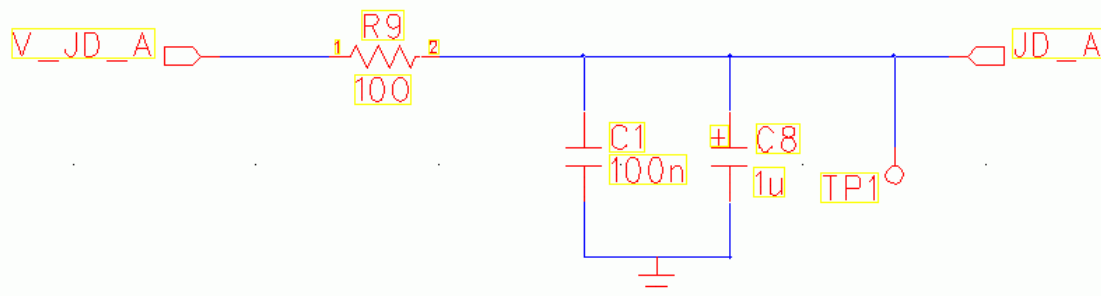


Figure 6.11.3.1: Diagram showing filtering used on bias line V_{JD_A}

6.12.4 PCB Layer Stack-Up

The following layer stack-up was chosen to allow easy routing and adequate separation of traces.

Layer	Type	Signals Allowed
Top	Primary Component Layer, Routing	Bias, Outputs
Inner Layer 2	Ground Split/Mixed Plane Layer	GND, AGND
Inner Layer 3	Routing	Bias Outputs
Inner Layer 4	Plane	JD_A, JD_B, AG_JD
Inner Layer 5	Ground Split/Mixed Plane Layer	GND, AGND
Inner Layer 6	Routing	Clocks
Inner Layer 7	Ground Split/Mixed Plane Layer	Vss, AGVss
Bottom	Secondary Component Layer, Routing	Clocks

Table 6.11.4.1: PCB Layer Stack-Up

6.12.5 Grounding

6.12.5.1 Vss

The CCD uses Vss as substrate and, upon recommendation from Guy Woodhouse (who quoted Jamey Ericsson), this should be provided by the ground on the clock board.

6.12.5.2 SDSU tricks

Previous experience has shown that for optimum performance the video board ground should be connected to the clock board ground at the output connector. These in turn, should both be connected to the chassis of the SDSU, which acts as the star point of the system.

6.12.6 Separation of Analogue and Digital

Bias and outputs are kept on the upper layers of the board, clock signals on the lower half with a power and ground core.

Flexibility in the design has been provided by the use of jumpers *JP4*, *JP10*, *JP11* and *JP13*. The analogue plane layers can be connected to either Vss or to the GND signal from the SDSU video board, which is brought in as a bias.

6.12.7 Outputs

Although we are planning to read out each CCD through one channel, both amplifiers are connected to buffer amplifiers. Selection of the output channel is provided by zero ohm resistors, fitted as required. This will allow us to choose the best readout channel should there be a difference, and also provide an element of redundancy should a problem arise with one of the on-chip outputs. There are software implications here and it will be necessary to liaise with the project software engineers before making such a decision.

In order to reduce noise in the long cable run, we will use a pseudo differential wiring scheme. This involves the use of an identical trace to run alongside the actual output, thereby picking up the same noise. This common-mode noise is then rejected at the differential amplifier in the SDSU due to its inherent design. To maintain similar characteristics for both signal traces, a matched-pair JFET is used, where the transistors are specifically manufactured to be as close in performance as possible. To simulate the CCD output, a resistor equal to the CCD output resistance is connected to the substrate voltage.

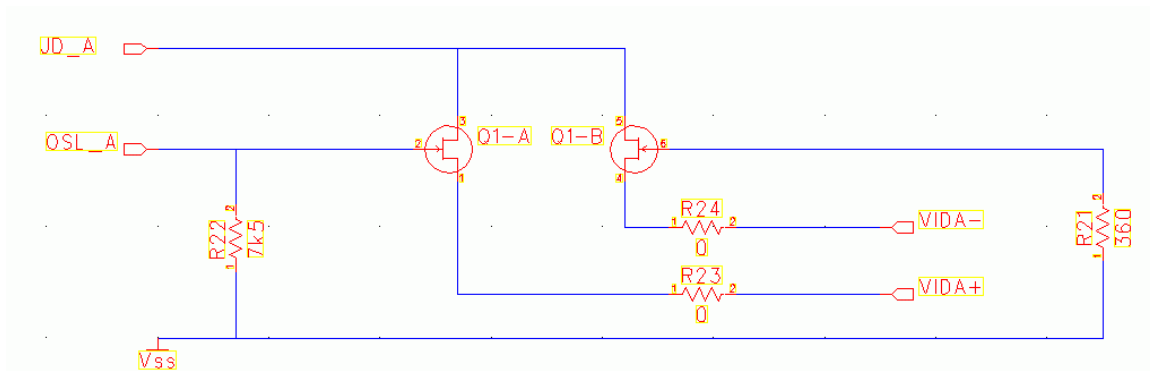


Figure 6.11.7.1: Diagram showing circuit configuration for output *OSL_A*

6.12.8 Cable Run

The CCD cable harnesses will be implemented as flexible circuits. Due to the curved path that the LOCS/AG cables must follow through the cryostat (see ICD AD04) it is envisaged that each cable will be made as a single piece since the overall dimensions are within the capabilities of standard flexible circuit manufacturers.

6.12.8.1 Cable harness

There will be 5 virtual cables inside the curvature sensors' overall wrap: temperature measurement and control; Output from CCDA; Output from CCDB; Bias Signals; Clock Signals. The autoguider cable follows the same principle, but as there is only one CCD, there will thus be only 4 virtual cables.

Each of the 9 virtual cables has their own cable screen connected at the SDSU end to the indicated ground. The option of continuing the screen onto the circuit board is provided, but it is envisioned that this will not be necessary.

6.12.8.2 Flexible Circuit

As stated above, it is anticipated that the flexible circuits will be manufactured as single items due to their limited overall dimensions. Should this not prove possible, we will adopt the U-bend technique already used by ESO to manufacture longer straight circuits.

Doc. Number:	VIS-DES-UOD-06042-0001
Date:	8 th March 2004
Issue:	3.0
Page:	Page 39 of 39
Author:	Paul Clark

6.12.9 Cryostat Connectors

The LOCS/AG unit cryostat connectors are as shown in the following table and comply with those specified in the ICD [see: AD04 section 9, requirement 62 and AD15 section 10].

Signals	Connector
AG Clock/Bias/Temperature	MIL-C-26482, Size 22, 55 Pins
AG Video	MIL-C-26482, Size 16, 26 Pins
CS Clock/Bias/Temperature	MIL-C-26482, Size 22, 55 Pins
CS Video	MIL-C-26482, Size 16, 26 Pins
Thermal Protection Heating Circuit	MIL-C-26482, Size 14, 12 Pins

Table 6.11.9.1: LOCS/AG Cryostat Connections

7 HOCS Optical Design

The design of the HOCS optics was undertaken by Richard Bingham. His design report is included as Appendix 8.

7.1 Overview

The HOCS optical design is based on the use of a two-layer cube beamsplitter. Based on an original idea by Martin Caldwell, this optical element delivers pre- and post-focus images from a single star simultaneously. The optic and its ray-trace are reproduced in figure 7.1.

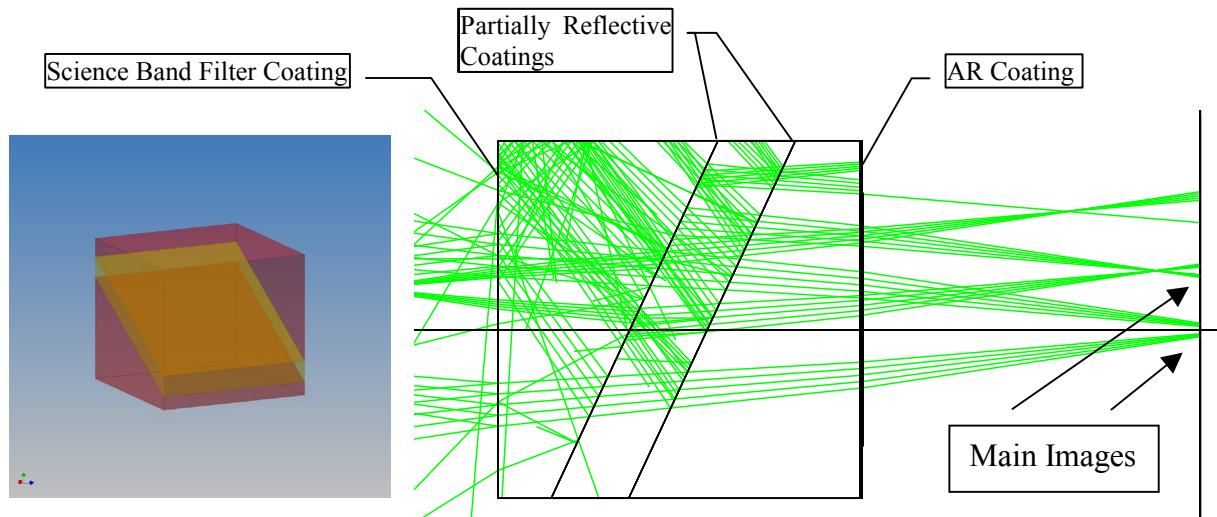


Figure 7.1: HOCS Optical Element and Ray Trace

A qualification test of the use of cemented cube beamsplitters in a cryogenic environment has been performed and documented in Appendix 11.

7.2 Options

One or more HOCS optical elements will be installed in the mini-filter intermediate filter wheel positions.

There are a number of possible permutations:

- Three versions of the HOCS optical element are shown in Appendix 8 providing defocus distances of 1mm, 1.5mm and 2.1mm respectively. The analysis of curvature

Doc. Number:	VIS-DES-UOD-06042-0001
Date:	8 th March 2004
Issue:	3.0
Page:	Page 41 of 41
Author:	Paul Clark

sensing aberration measurement [section 9 and AD02 section 6.2] has shown that larger defocus distances provide better measurement accuracy on high order aberrations. Smaller defocus distances provide better accuracy on low order aberrations. Currently the modelling indicates that the optimum defocus distance is 1mm. However, since the three designs are available, multiple optical elements could be procured and installed if required.

- The optical element can be coated with any desired science wavelength filter coating, J and Ks being the most popular choices. The coating performance does not need to match that of the actual science filters since throughput is far less of an issue since an arbitrarily bright star can be selected.
- The optical elements can be installed in multiple mini-filter positions to allow sensing: as close to on-axis as possible; at extreme -X, near-zero Y; and at extreme Y, near-zero X.

The final combination of HOCS elements will be selected by the project scientists within the available budget.

7.3 Dimensions

The HOCS optical element dimensions are shown in Appendix 8 Table 1. These dimensions have been distributed within the IR Camera Team allowing the design of the filter wheel mini-filter holders to be detailed in due course.

7.4 Validation of HOCS Star Availability

In the same way that the LOCS field of view is re-validated in section 6.2.2, Appendix 13 section 4 contains a calculation of the delivered signal to noise ratio for the J-band HOCS. There is a 99% probability of finding a J-band magnitude 8.4 star within 0.5° of the pole. At a full moon sky brightness of 15.9 mag/arcsec² and an exposure time of 60 seconds, a signal to noise ratio of over 2000 is delivered. This adequately fulfils requirement 44.

Using a magnitude 8.4 star may cause saturation problems on the brighter extra-focal image. The spreadsheet calculation therefore predicts that a magnitude 12 star observed with a 10 second exposure would still deliver a signal to noise ratio of 72.6.

Doc. Number:	VIS-DES-UOD-06042-0001
Date:	8 th March 2004
Issue:	3.0
Page:	Page 42 of 42
Author:	Paul Clark

8 Aberration Measurement Accuracy

AD02, reviewed at the WFS delta-PDR, contains detailed information on the curvature sensor technique and the intensive work that was carried out to predict the aberration measurement accuracy of both the LOCS and HOCS.

The analysis has concluded that both the LOCS and HOCS will deliver the required accuracy.

8.1 LOCS Predicted Accuracy

Sections 5.2 and 5.3 of AD02 predict that the LOCS will achieve the required accuracy of 30nm RMS per term from Z4 to Z10 (defocus, astigmatism, coma and trefoil) in the presence of aberrations up to ± 120 nm from their nominal value in 0.75" seeing (requirement 27 & 28).

Closed loop performance of the LOCS is described in section 7.5.2 of AD01 (requirement 29).

8.2 HOCS Predicted Accuracy

Section 6.2 of AD02 predicts that the HOCS will achieve the required Root-Sum-Square accuracy of <50nm from Z4 to Z25 in the presence of a spectrum of aberrations up to 200nm from their nominal value (requirement 46). It should be noted that the HOCS requirement was changed in issue 2 of the IR Camera Technical Specification from an across-the-board required accuracy of 10nm RMS per term to the Root-Sum-Square figure quoted above.

8.3 Required Integration Time

Requirement 45 specifies that the HOCS must be able to deliver the required aberration measurement accuracy within a total exposure time of <180s. To investigate if this is indeed achievable, a simulation of the variance of atmospheric aberrations against exposure time was carried out. The results of the simulation are shown in figures 8.3.1 and 8.3.2 below and illustrate that atmospheric aberrations achieve a Root-Sum-Square variance of 50nm in an exposure time of 64 seconds (including tip and tilt).

The simulation parameters were:

- Fried Turbulence Parameter (r_0) = 20 cm
- Telescope Diameter (D) = 4m
- Wind speed for turbulent layer = 10ms^{-1}
- The Standard Deviation is proportional to $(D/r_0)^{(5/6)}$

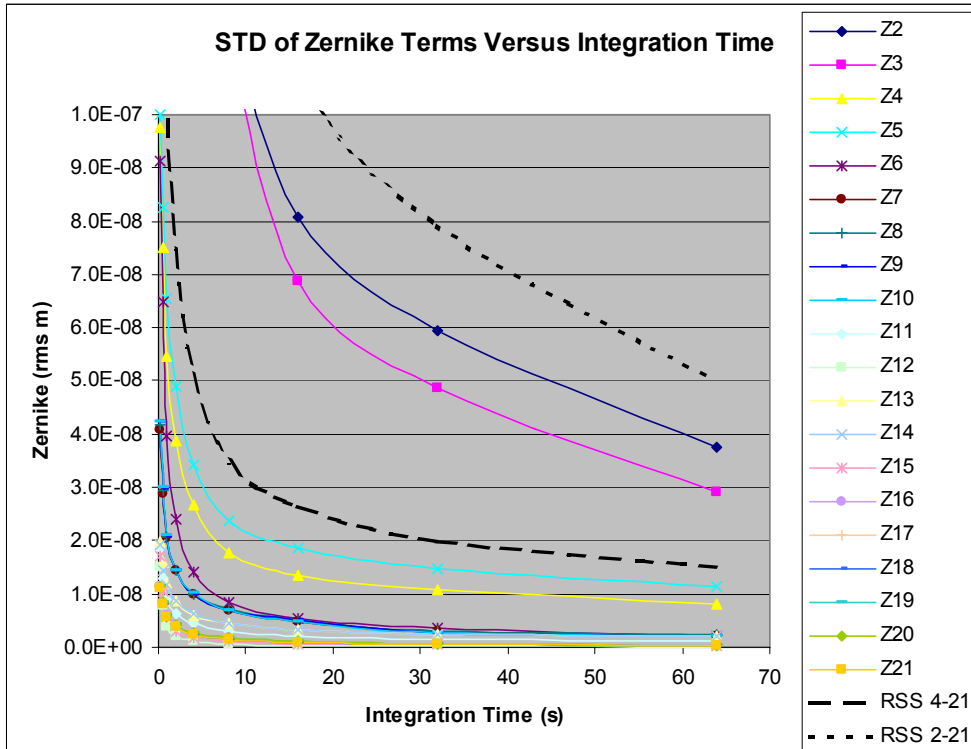


Figure 8.2.1: Variation of Zernike Terms vs Integration Time (Linear)

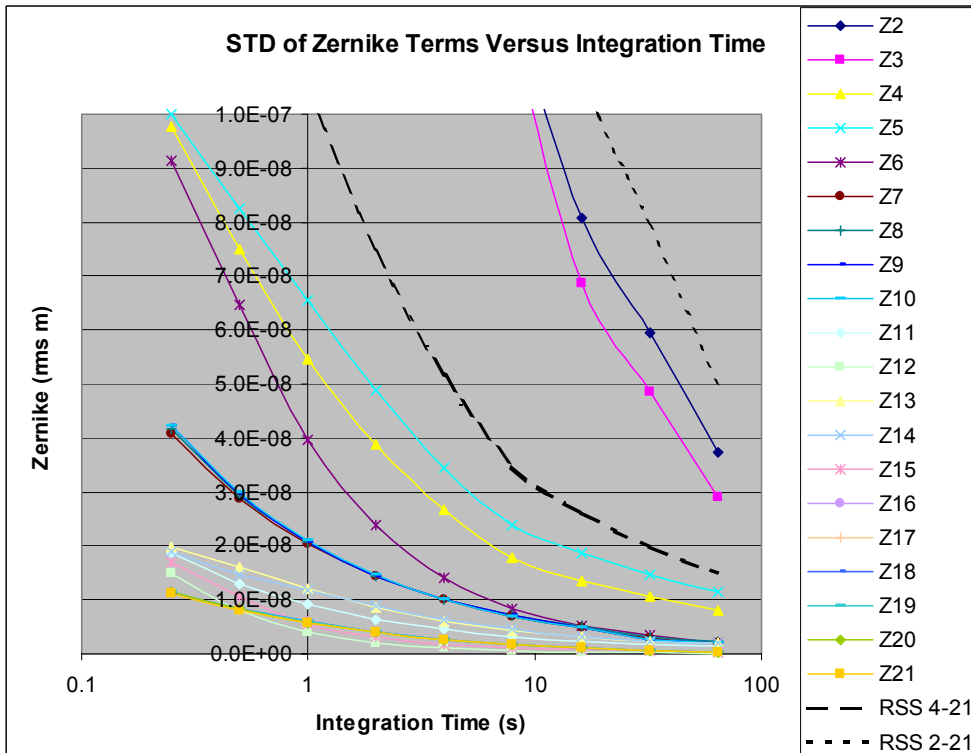


Figure 8.2.2: Variation of Zernike Terms vs Integration Time (Log)

Doc. Number:	VIS-DES-UOD-06042-0001
Date:	8 th March 2004
Issue:	3.0
Page:	Page 44 of 44
Author:	Paul Clark

9 Processor Requirements

In order to achieve the 15-second (previously 5-second) LOCS coefficient processing time requirement (33), AD02 section 5.3 indicates that a 1GHz-class processor is likely to be required. The LOCS coefficient processing will be performed on an ESO VME LCU processor card. Currently only the Motorola MVME5500 offers a 1GHz (Power-PC) processor and this card is not currently supported by ESO. We propose therefore, rather than requesting ESO to support the 5500 now, to delay the purchase of the LCU cards until the LOCS software development is progressed and the true execution time measured on a current ESO LCU processor. The 15-second processing time will not be required until VISTA becomes operational on sky. By delaying the purchase of the final LCU cards until nearer then, we benefit from Moore's law and provide ESO with a longer timescale to provide support for the 5500. The 5500 is very competitively priced (~£2K) especially since it is Motorola's flagship product. Many of Motorola's older processor cards are no longer being manufactured. Obviously the request to provide support for the 5500, if definitely required, will be made in good time but it is sensible to delay this request until the full processing requirements are established.

10 Software

The software associated with the wavefront sensor systems is described in detail in the following documents. These documents are to be reviewed as an integral part of the WFS FDR.

Low Order Wavefront Sensors Software Design Description (LCU Part)	VIS-DES-UOD-06048-0001 1.0, 4 th March 2004
Autoguider Software Design Description (LCU Part)	VIS-DES-UOD-06048-0003 1.0, 4 th March 2004
Image Analysis Algorithms for VISTA Wavefront Sensing	VIS-TRE-UOD-06042-0005 1.0, 12 th November 2003

Table 10.1: WFS Software Documents

The high order wavefront sensor software design description was reviewed as part of the IR Camera FDR.

High Order Wavefront Sensors Software Design Description	VIS-DES-UOD-06048-0002 2.0, 4 th March 2004
--	---

Table 10.2: High Order Wavefront Sensor Software Design Description

The following document, which recently passed its own FDR, provides an essential overview of the whole of the VISTA active optics and guiding software. This document should be read in conjunction with the above four wavefront sensor software documents.

Active Optics and Guiding Workstation Software Design Description	VIS-SPE-RAL-13030-0003 2.0, 3 rd March 2004
---	---

Table 10.3: Active Optics and Guiding Software Design Description

Doc. Number:	VIS-DES-UOD-06042-0001
Date:	8 th March 2004
Issue:	3.0
Page:	Page 46 of 46
Author:	Paul Clark

The following document contains the complete software requirements for the IR Camera and is the document against which the wavefront sensor documents should be reviewed. Section 2.7 refers to the wavefront sensors.

VISTA IR Camera Software Requirements	VIS-DES-ATC-06080-0010 2.0, 12 th November 2003
---------------------------------------	---

Table 10.3: IR Camera Software Requirements

The following document is the software functional specification derived from the above requirements. Section 5.6 refers to the wavefront sensors.

VISTA IR Camera Software Functional Specification	VIS-DES-ATC-06081-0001 2.0, 12 th November 2003
---	---

Table 10.4: IR Camera Software Functional Specification

The WFS software compliance matrix is tabulated in Appendix 1 section 2.

Doc. Number:	VIS-DES-UOD-06042-0001
Date:	8 th March 2004
Issue:	3.0
Page:	Page 47 of 47
Author:	Paul Clark

11 EMI & Detector Synchronisation

Section 11 of AD15 describe the electrical design measures that will be implemented to ensure the lowest probability of interference occurring between the different detector systems within the IR Camera. RD13 also describes these same measures.

Should interference between the detector systems still prove to be a problem despite the implementation of the measures outlined above, there is a final fall-back strategy which is to synchronise the different detector systems such that they cannot interfere (ie. no other detector system is clocking while another is reading out).

After further discussion with ESO staff at the IR Camera FDR, it is evident that there a a number of synchronisation techniques that could be implemented if absolutely necessary:

- The technique of interleaving curvature sensor readout between 10Hz autoguider readouts is possible and could be implemented either through software time synchronisation (made possible by the use of ESO's TIM time synchronisation system) or by providing inhibit/enable signals between the TCCD controllers. Such a technique would still allow requirement 17 to be met. See AD15 section 11.2.2.
- The curvature sensor and autoguider TCCD controllers could receive inhibit/enable signals via a fibre-optic link from the science array controller (IRACE) system. See AD15 section 11.2.3.

However, since it is not known at this time that such measures are necessary, there is no gain to be had in implementing them now. Early EMC testing is planned for the first phase of Camera AIT so EMI problems will be highlighted as early in the program as possible. If then required the most appropriate synchronisation technique could be implemented to solve the problems without impact to the project schedule.

Currently the WFCAM project have encountered no EMI problems between the CCD autoguider and the four Hawaii IR arrays despite their very close proximity – much closer than the systems will be in VISTA. This information is indeed encouraging and indicates that it would be foolish to invest a great deal of effort in producing a solution to a problem that might not exist.

Doc. Number:	VIS-DES-UOD-06042-0001
Date:	8 th March 2004
Issue:	3.0
Page:	Page 48 of 48
Author:	Paul Clark

12 Declared Materials List

The list of materials to be included within the Camera cryostat as part of the Wavefront Sensors is presented in Appendix 2. This list will be incorporated into the next release of the DML for the Camera as a whole [RD12].

13 Conclusion

This document contains the final design of the VISTA IR Camera Wavefront Sensors for the purposes of the FDR, 31st March 2004. Compliance with the project requirements is demonstrated. The optical, mechanical, electronic and software design is presented as are the requirements compliance matrix and the test plan.



Doc. Number:	VIS-DES-UOD-06042-0001
Date:	8 th March 2004
Issue:	3.0
Page:	Page 49 of 49
Author:	Paul Clark

14 Appendix 1: Compliance Matrices

14.1 Overall WFS Compliance Matrix



Wavefront Sensor Compliance Matrix						
Req#	Document Reference	Item	Specification Value	Estimated Value	Compliance	Comment
1	AD03 4.5.2	a) Provide a guide sensor, controller and software			Comply	Two sensors and two controllers plus software will be provided
2		b) Position to exploit peripheral sectors of focal plane			Comply	See section 6.3
3		c) Sensor shall not vignette science detectors			Comply	See section 6.5
4		d) Sensor shall operate concurrently with observations			Comply	Addressed by R007 SWR 2.7.1.07 & EMI Mitigation Plan
5		e) Probability of finding usable star	99%	99%	Comply	See section 6.2.1 for calculation of signal/noise ratio
6		f) Sample rate	≥10Hz	10Hz	Comply	See section 6.2.4 for evidence of readout rate
7		g) Centroid accuracy	±0.04 arcsec rms		TBC	~ 1/6th pixel. Determined by ESO ccdcon software
8		h) Operation 30 mins after sunset			Comply	Suitably bright guide star required. See section 6.2.3
9		i) Operational latency	1s		TBC	Determined by AgServer software latency
10	AD03 4.5.3	Guide detector controller: ESO compliance			Comply	Next Generation TCCD Controller will be used
11	AD03 4.5.4	a) Definable read out parameters			Comply	See SWR 2.7.1.01
12		b) Guide star metrics			Comply	See SWR 2.7.1.01
13		c) Guide star metric logging			Comply	See SWR 2.7.1.01
14		d) Plot guide star metrics on a workstation			Comply	See SWR 2.7.1.01
15		e) Send guide signal to TCS	10Hz	10Hz	Comply	See SWR 2.7.1.01
16		f) Software host			Comply	See SWR 2.7.1.02 & System Architecture
17		g) Guide sensor beat skipping	1 max in any 0.5s		Comply	See section 11
18		h) VLT software re-use			Comply	See SWR 2.7.1.05
19		i) Operational latency	1s		TBC	See SWR 2.7.1.06
20		j) Non-sidereal guiding			Comply	See SWR 2.7.1.08
21	AD03 4.6.2	a) Provide two sensors, a controller and software			Comply	Two sensors and two controllers plus software will be provided
22		b) Position to exploit peripheral sectors of focal plane			Comply	See section 6.3
23		c) Sensor shall not vignette science detectors			Comply	See section 6.5
24		d) Diametrically opposite positioning			Comply	See section 6.3
25		e) Sensors shall operate concurrently with observations			Comply	See SWR 2.7.2.04 & EMI Mitigation Plan
26		f) Frame rate	40s	30s	Comply	See section 6.2.2
27		g) Aberration measurement accuracy	±30nm rms in 40s	28nm rms	Comply	See section 8.1
28		h) Performance in the presence of seeing	±30nm rms at 0.75"		Comply	See section 8.1
29		i) Closed loop convergence	2-3 iterations		Comply	See section 8.1
30		j) Probability of finding usable star	99%	99%	Comply	See section 6.2.2 for calculation of signal/noise ratio
31		k) Exposure coincidence	1s	0	Comply	The two CCDs are connected as one
32		l) Exposure coincidence on two sensors	3s		TBC	See SWR 2.7.2.06
33		m) Coefficient processing time	15s	15s	Comply	See SWR 2.7.2.05 & Section 9
34		n) Science observation overhead	0.5s		TBC	See SWR
35	AD03 4.6.3	Sensor detector controller: ESO compliance			Comply	Next Generation TCCD Controller will be used
36	AD03 4.6.4	a) Definable read out parameters			Comply	See SWR 2.7.2.01
37		b) Wavefront coefficients			Comply	See SWR 2.7.2.01
38		c) Wavefront coefficient logging			Comply	See SWR 2.7.2.01
39		d) Plot wavefront coefficients on a workstation			Comply	See SWR 2.7.2.01
40		e) Send coefficients to TCS			Comply	See SWR 2.7.2.01
41		f) Software host			Comply	See SWR 2.7.2.02 & System Architecture
42		g) VLT software re-use			Comply	See SWR 2.7.2.03
43		h) Non-sidereal tracking			Comply	See SWR

44	AD03 4.7.2	a) Probability of finding suitable star b) Required integration time c) Aberration measurement accuracy d) Curvature sensor design e) Sensor detector controller: ESO compliance	99% within 1° ≤180s ≤50nm RSS	99% 64s 48nm RSS	Comply Comply Comply Comply Comply	See section 7.4 for calculation of signal/noise ratio See section 8.3 See section 8.2 See section 7 Next Generation TCCD Controller will be used
45	AD03 4.7.3	a) Sensor read out			Comply	See SWR 2.7.3.01
46	AD03 4.7.4	b) Data storage			Comply	See SWR 2.7.3.01
47		c) Calibration source control			N/A	Calibration source only required for Shack Hartmann system
48		d) Aberration analysis			Comply	See SWR 2.7.3.01
49		e) Raw data display			Comply	See SWR 2.7.3.01
50		f) Wavefront display			Comply	See SWR 2.7.3.01
51		g) VLT software re-use			Comply	See SWR 2.7.3.02
52		h) Software host			Comply	See SWR 2.7.3.02 & System Architecture
53	AD04 7	Geometry parameters and beam envelope definition			Comply	
54	AD04 8 and A	Clearance above FPA	45mm	45mm	Comply	See section 6.5, 6.7 and Appendix 3
55		Clearance to nearest edge of science beam	1mm	1mm	Comply	See section 6.5
56		Connector accommodation volume	See AD05		Comply	See Appendix 3
57		Interface surfaces dimensions	See AD05		Comply	See Appendix 3
58	AD04 9	Electrical & Data Interfaces			Comply	See section 6.11.9
59		Cryostat connectors & identification			Comply	
60		Cryostat harness cross sectional area			Comply	
61	AD06 5.1	Auto-guider system requirements - same as AD03 4.5.2	45mmx15mm		Comply	See AD03 4.5.2 above
62	AD06 5.2	LOWFS system requirements - same as AD03 4.6.2			Comply	See AD03 4.6.2 above
63	AD06 5.3	HOWFS system requirements - same as AD03 4.7.2			Comply	See AD03 4.7.2 above
64	AD06 7	Optical, mechanical & electrical interfaces			Comply	See AD04 requirements above
65	AD06 8.1	Sensor reference axes and reference marks			Comply	See section 6.7
66	AD06 8.2	Sensor positional tolerances			Comply	
67		Focus	25µm		Comply	By design and confirmed by measurement - see test plan
68		Detector centring	200µm		Comply	By design and confirmed by measurement - see test plan
69		Stability	0.01 arcsec		TBC	Compliance is anticipated but depends on flexure test results
70	AD06 9.1	Optical characterisation				See test plan
71	AD06 9.2	Functional performance tests				See test plan
72	AD06 10	Physical properties				
73		Space envelope			Comply	See AD04 8 above
74		Surface finishes and power dissipation			Comply	See section 6.7 and 6.9
75		Materials			Comply	See Appendix 2
76		Mass			Comply	See section 6.10
77		Contamination control			Comply	See section 6.11
78	AD06 11	Deliverables			Comply	
79		Key				
		AG Requirement				
		LOCS Requirement				
		HOCS Requirement				
		LOCS/AG Requirement				
		WFS Requirement				

14.2 Software Compliance Matrix

Software Requirements from VIS-SPE-ATC-06080-0010 [RD07]

[RD03] VIS-DES-UOD-06048-0001

LOWFS Software Design Description

[RD04] VIS-DES-UOD-06048-0002

HOWFS Software Design Description

[RD05] VIS-DES-UOD-06048-0003

AG Software Design Description

[RD13] VIS-DES-RAL-13030-0003

Active Optics and Guiding Workstation Software Design Description

14.2.1 Guide Sensor Compliance

ID	Software Requirement	Compliance	Reference
SWR 2.7.1.01	Software and hardware on which to run it shall be provided to: (a) read out the CCD using definable parameters, including frame rate, pixel rate, area of interest. (b) measure metrics (value and error) of the guide star, including (x,y) centroid, integrated flux above background, FWHM, eccentricity, seeing estimate. (c) log the guide star metrics. (d) plot the guide star metrics on a workstation. (e) send a guide correction signal to the telescope control software at a rate of 10 Hz or greater.	Ok	Reusing VLT software. Standard CCS logging facilities will provide (c),(d). Standard TCCD software will meet (a), (b) See section 8 of [RD05]
SWR 2.7.1.02	The software shall run on the Telescope Control Workstation(s) and Guide Sensor TCCD detector controller.	Ok	Section 6 of [RD05]
SWR 2.7.1.04	The guide sensor may skip a single 'beat' during readout of a wavefront sensor. This shall cause the guide signal to remain static and shall not cause discontinuity. The guide sensor shall not cause a discontinuity. The guide sensor shall not miss more than one beat in any 0.5 second	Ok	Section 3 of [RD05]

	interval.		
SWR 2.7.1.05	ESO-VLT software shall be used wherever appropriate.	Ok	All of [RD05]
SWR 2.7.1.06	The guide sensor shall be operational within 1 second of receiving the guide star position, assuming the guide star is within 3 arcseconds of its predicted location.	TBC	Reusing VLT software.
SWR 2.7.1.07	The guide sensor shall operate concurrently with science observations.	Ok	
SWR 2.7.1.08	<p>(a) It is a requirement for the IR Camera software to allow the VISTA telescope to track a non-sidereal object using open-loop tracking. The Observation Software must provide a non-sidereal drift rate to the telescope control software.</p> <p>(b) The autoguider software must also correct the guide signal for any small drifts in the position of the guide star caused by atmospheric refraction.</p> <p>(c) It is a goal for the IR Camera software to support closed-loop tracking of a non-sidereal object by allowing the position of the guide star to move across the surface of the autoguider detector. The software should achieve as high a frame rate as possible, but is not constrained by the 10 Hz requirement in this case.</p>	Ok	(a) and (b) can be met by probeServer. Section 4 of [RD05] software. (c) is not a requirement.
SWR 2.7.1.09	The autoguider software must report an error if the guide star metrics (signal to noise, image shape, FWHM, etc.) indicate that the guide star is unsuitable, so the operator may be given the opportunity to select a new star.		Section 3 of [RD05]. agServer will fail guiding loop. It's up to high level software [RD13] to decide what to do next.
SWR 2.7.1.10	The autoguider software must be able to operate with fewer than a full set of autoguider chips, or with a faulty autoguider chip. The software shall have the ability to disregard data from faulty or missing chips.		High Level Software responsibility, [RD13] to turn off auto guiders.

14.2.2 Low Order Wavefront Sensor Requirements

ID	Software Requirement	Compliance	Comments
SWR 2.7.2.01	Software and hardware on which to run it shall be provided to: (a) read out the CCDs using definable parameters, including frame rate, pixel rate, area of interest. (b) determine the wavefront incident at each sensor (defocus, astigmatism, coma and trefoil) using appropriate coefficients, e.g. Zernike or quasi-Zernike. (c) log the wavefront coefficients. (d) plot the wavefront coefficients on a workstation as a function of time. (e) transmit the wavefront coefficients to the telescope control software at a rate of up to once every 40 seconds.	Ok	Reusing VLT software. Standard CCS logging facilities will provide (c), (d). Standard TCCD software will meet (a). [RD03] is all about (b).
SWR 2.7.2.02	The software shall run on the Telescope Control Workstation(s) and LOWFS TCCD detector controller hardware.	Ok	Section 7 of [RD03].
SWR 2.7.2.03	VLT software shall be used wherever appropriate.	Ok	Reuse of LCU server framework. Section 6 of [RD03].
SWR 2.7.2.04	The LOWFS shall operate concurrently with science observations.	TBD	EMI Implications rather than software
SWR 2.7.2.05	The wavefront coefficients shall be available to the TCS within 15 seconds of completion of each exposure. It is a goal to make the coefficients available within 5 seconds.	TBC	May require faster (1GHz) LCU but compliance is anticipated
SWR 2.7.2.06	The start and end of exposure on the two CCDs of one sensor shall be coincident within 1 second. Exposures on the two different sensors shall be coincident within 3 seconds.	Ok	Hardware Issue. Two CCDs are wired together.
SWR 2.7.2.07	The LOWFS software must be able to operate with only one operational detector. In this case the software should only provide the subset of wavefront coefficients which can be derived unambiguously with one detector.	Ok	Responsibility of [RD13]

14.2.3 High Order Wavefront Sensor Requirements

ID	Software Requirement		Comments
SWR 2.7.3.01	Software and hardware on which to run it shall be provided to: (a) read out the high order Wavefront Sensor data using definable parameters. (b) store the data in the same manner as a science exposure. (c) analyse the stellar and calibration data generating wavefront coefficients (low order Zernike coefficients and high order mirror mode coefficients) and transmit these to the TCS. (d) display the raw data. (e) display the wavefront. The system must have the ability trigger the analysis automatically by the arrival of new data, i.e. to run the analysis on-line.	Ok	DCS (IRACE) satisfies (a), (b). (c) met by [RD04] (d) and (e) will be implemented also but they are not described anywhere.
SWR 2.7.3.02	The HOWFS data will be obtained using the science detector controller hardware, and the HOWFS image analysis software shall run on the Instrument Workstation.	Ok	OS, ICS, IRACE and [RD04]
SWR 2.7.3.03	VLT software shall be used wherever appropriate.	Ok	Section 6 of [RD04]
SWR 2.7.3.05	The HOWFS is not required to operate concurrently with science observations.	Ok	
SWR 2.7.3.06	The HOWFS software must be able to cope with broken or missing science detectors.	Ok	OS, ICS, IRACE determine this.
SWR 2.7.3.07	The HOWFS image analysis shall correct the wavefront information it generates to on axis.	Ok	HOWFS provides the option for subtracting off axis coefficients. Null aberrations File must be provided. Section 4.2 and 9 of [RD04]

15 Appendix 2: Declared Materials List

WFS Declared Material List			
Unit	Part	Material	
LOCS/AG Units	WFS Housing Arms	Aluminium Alloy	
	CCD Plates	Aluminium Alloy	
	Cover	Aluminium Alloy	
	Retaining Clamps	Aluminium Alloy	
	Retaining Springs	Beryllium Copper	
	Fasteners	Stainless Steel	
	Paint Finish	Nextel	
	Pick Off Mirror	BK7	
	Filter	Schott RG9	
	Cube Beamsplitter	Fused Silica	
	CCDs (Custom E2V CCD4240)	Invar 36	
		Silicon Substrate	
		Kapton & Copper Flex Circuit	
		Micro-D Connector	
	Buffer & Protection PCB (See Appendix 4 section 5)	PCB (Copper, Epoxy, Glass Laminate)	
		Micro-D Connectors	
		Resistors (Surface Mount)	
		Capacitors Tantalum (Surface Mount)	
		Capacitors Ceramic (Surface Mount)	
Zener Diodes (Surface Mount)			
Transient Suppression Packages			
2N5564 Dual FET			
Solder			
Cooling Straps		Braided Copper	
Cryostat Harness		Kapton & Copper Flex Circuit	
		Micro-D Connectors	
		MIL-C-26482 Hermetic Connectors	
HOCS Optics		Fused Silica	

Table 1: Wavefront Sensors Declared Materials List

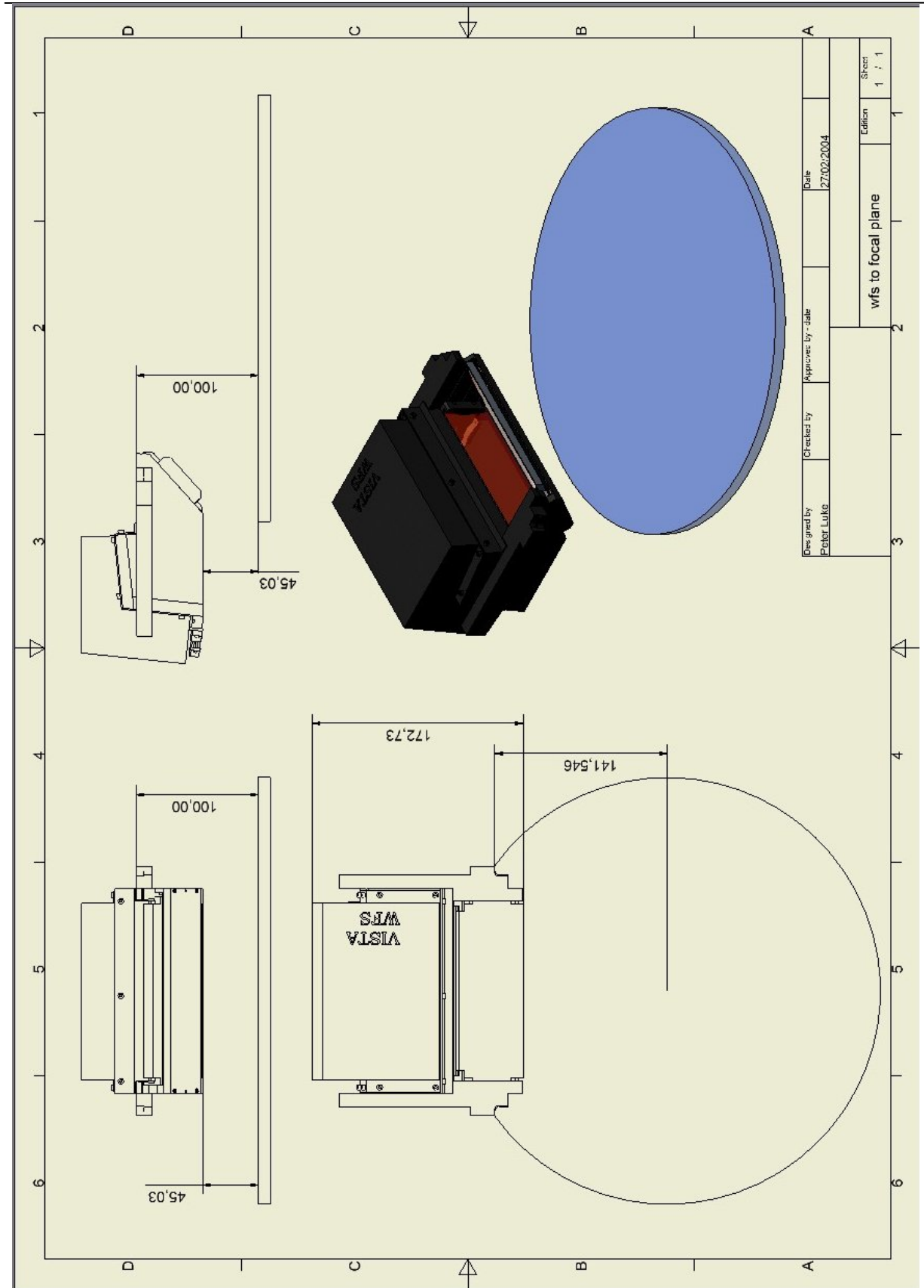
Doc. Number:	VIS-DES-UOD-06042-0001
Date:	8 th March 2004
Issue:	3.0
Page:	Page 57 of 57
Author:	Paul Clark

16 Appendix 3: Mechanical Drawings (Peter Luke)

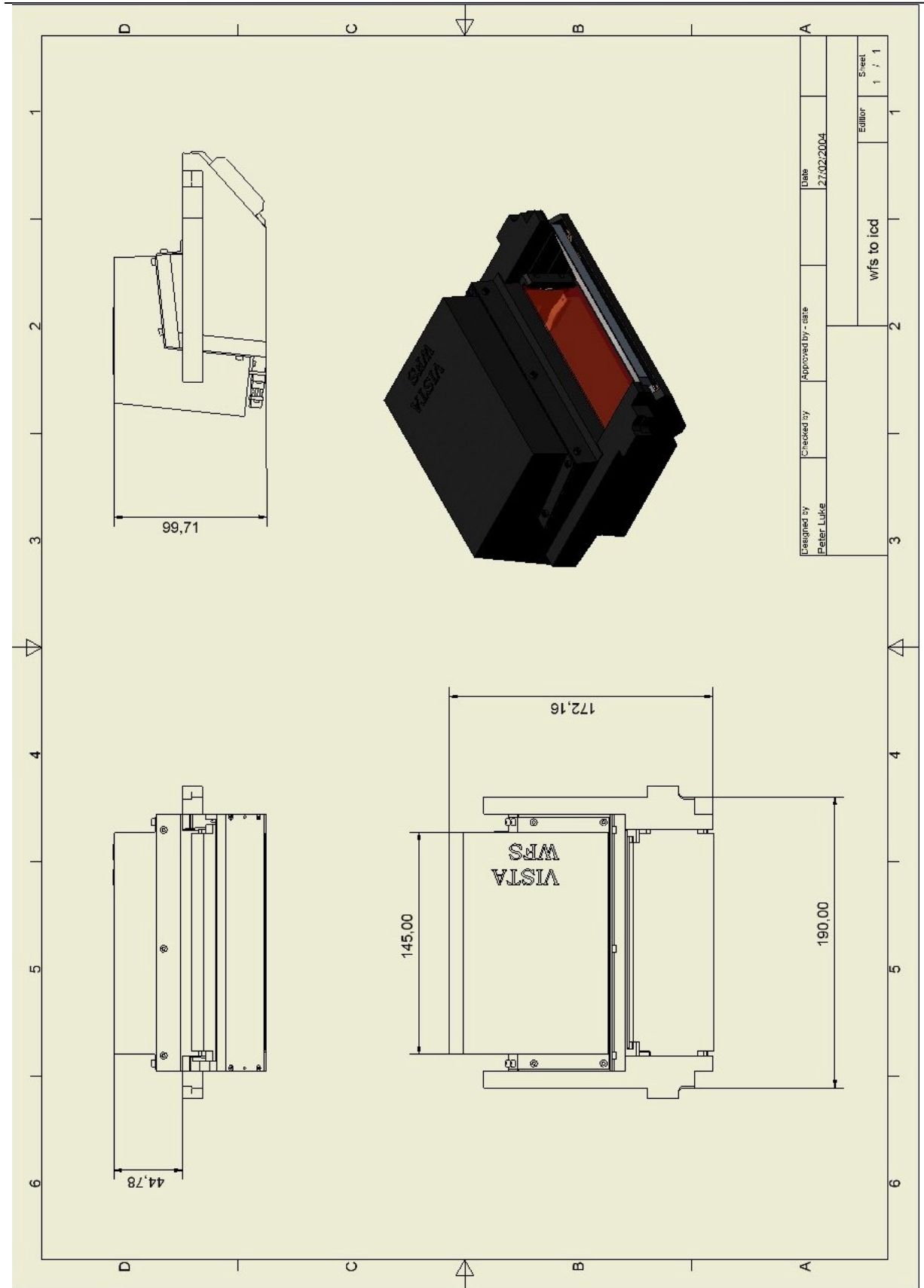
The following pages contain the mechanical drawings for the LOCS/AG unit.



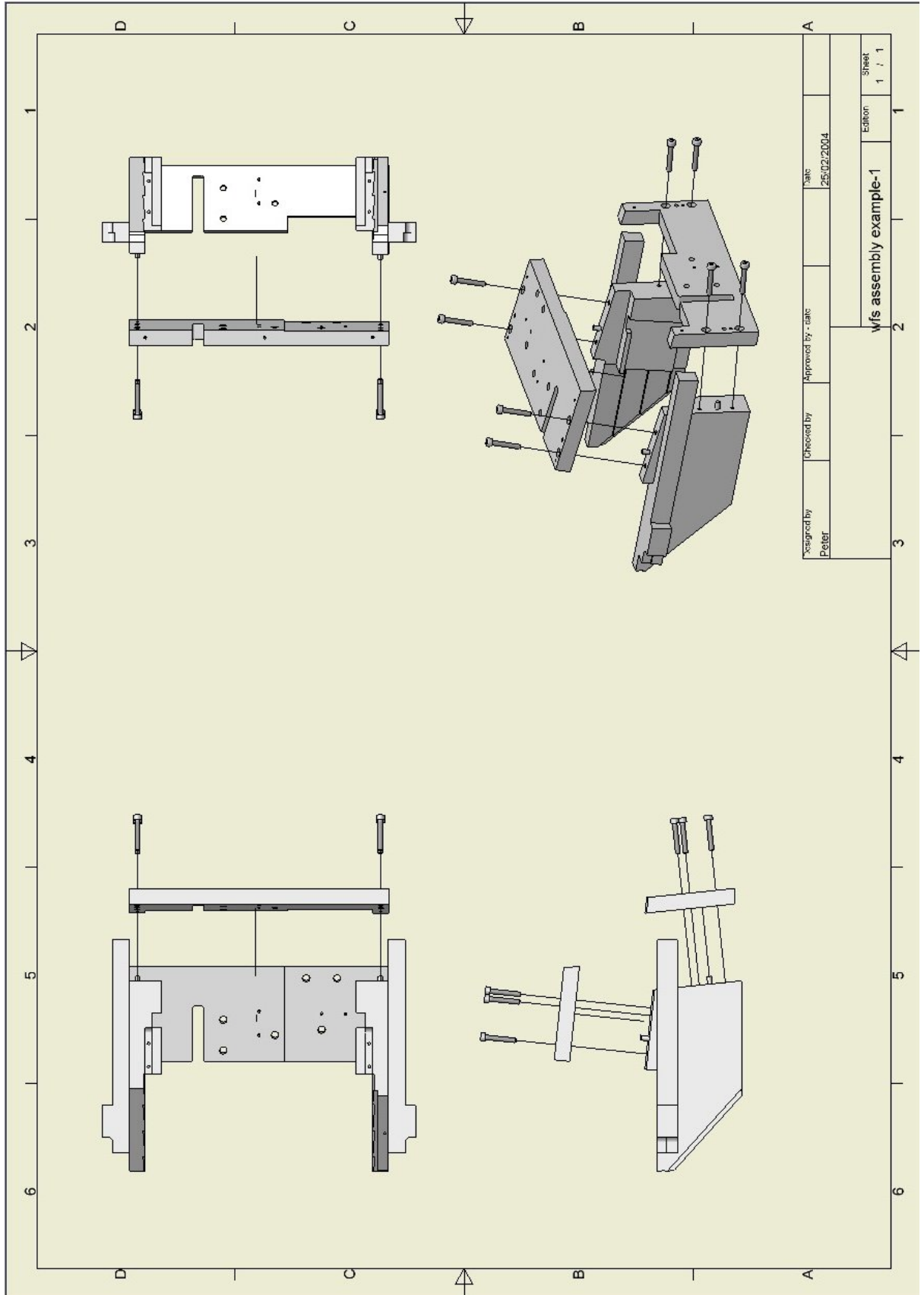
Doc. Number:	VIS-DES-UOD-06042-0001
Date:	8 th March 2004
Issue:	3.0
Page:	Page 58 of 58
Author:	Paul Clark



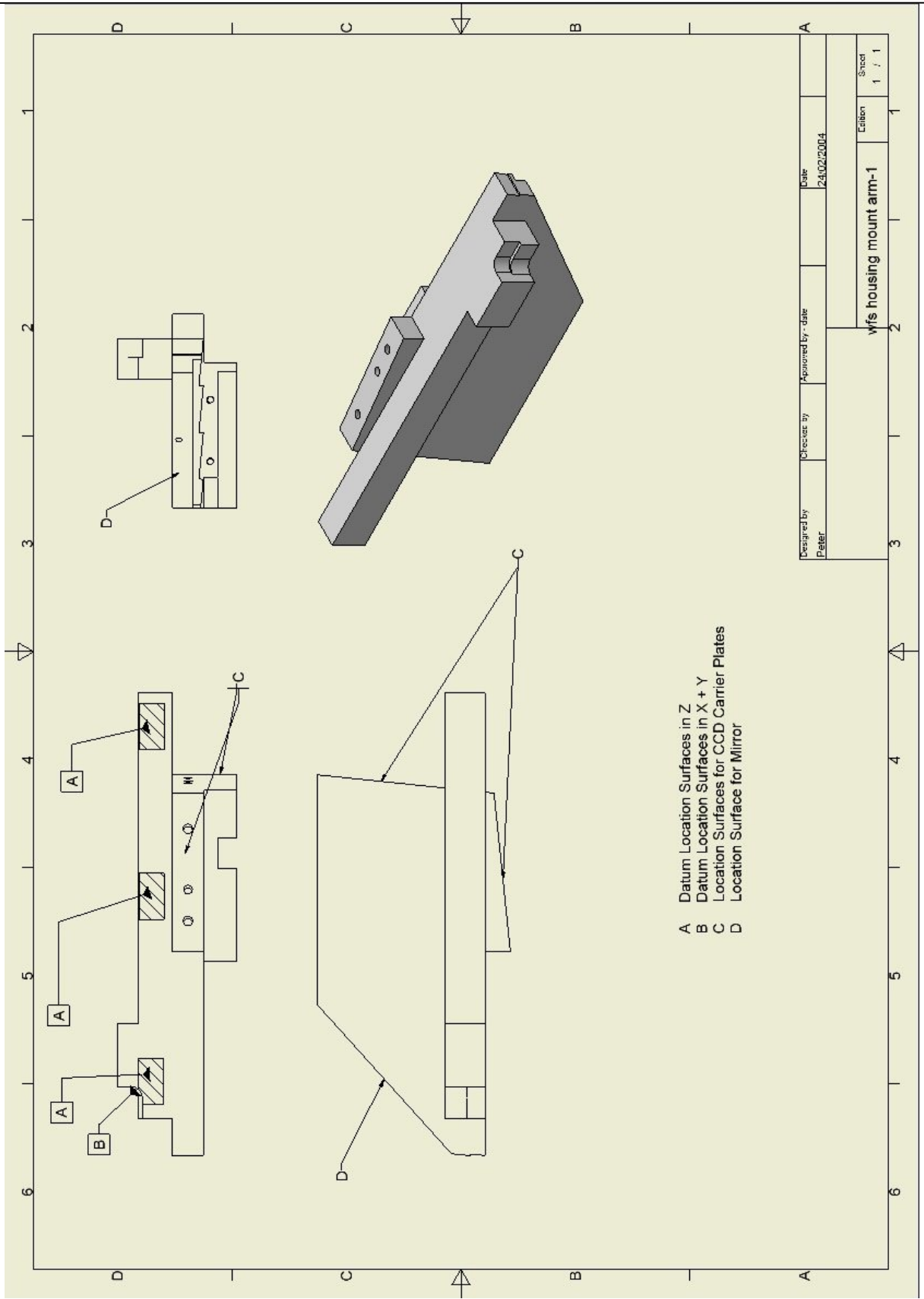
Doc. Number:	VIS-DES-UOD-06042-0001
Date:	8 th March 2004
Issue:	3.0
Page:	Page 59 of 59
Author:	Paul Clark



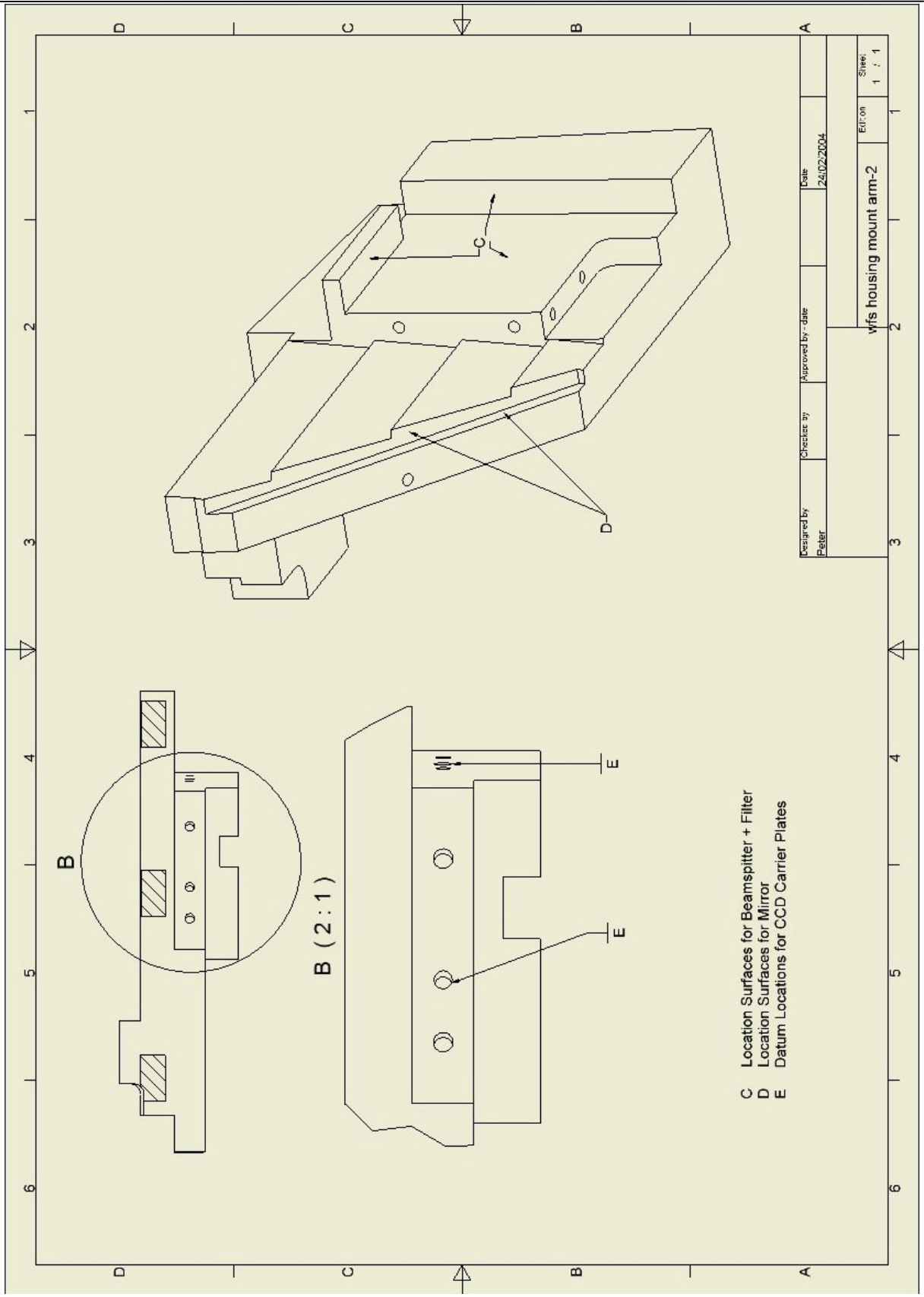
Doc. Number:	VIS-DES-UOD-06042-0001
Date:	8 th March 2004
Issue:	3.0
Page:	Page 60 of 60
Author:	Paul Clark



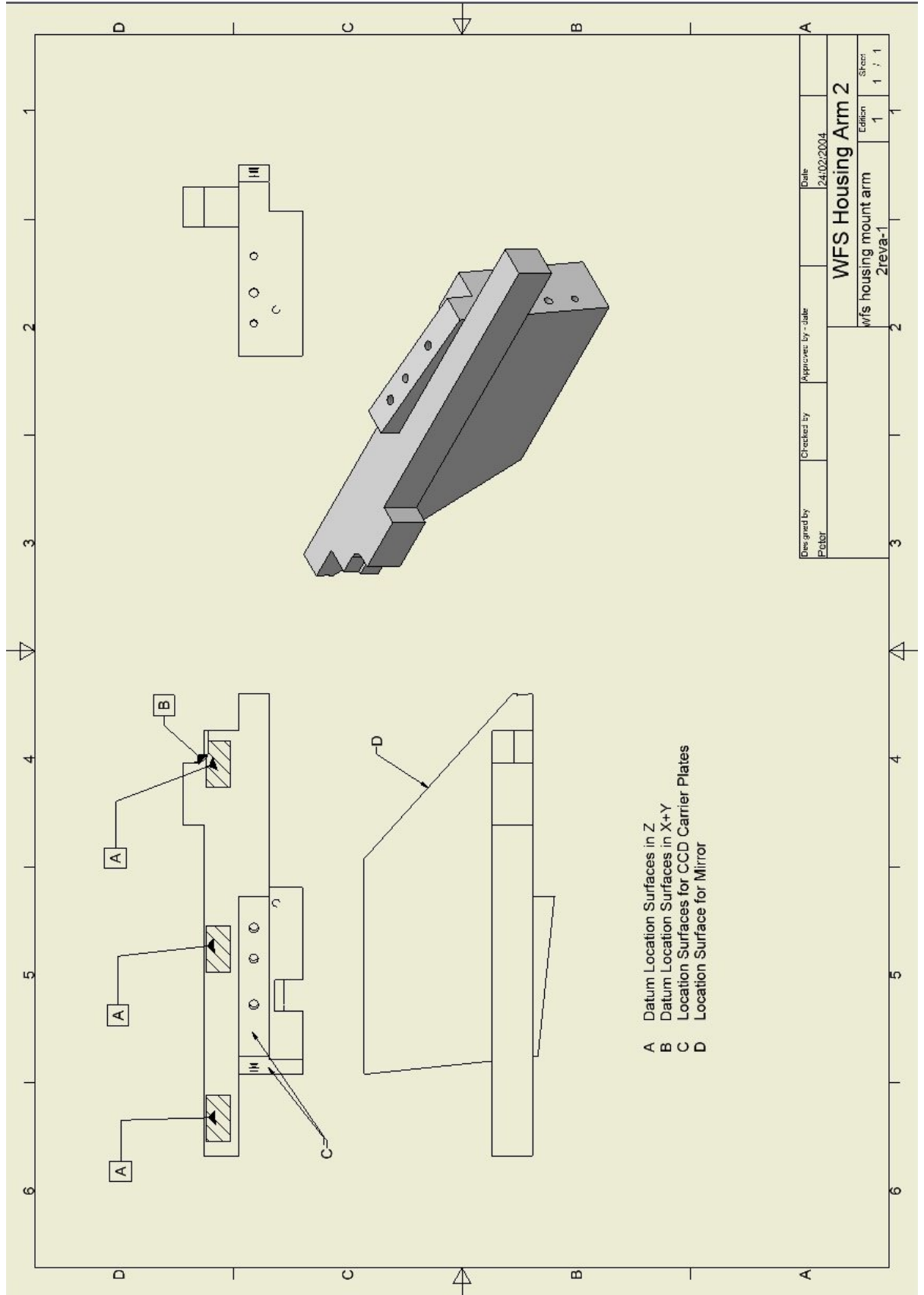
Doc. Number:	VIS-DES-UOD-06042-0001
Date:	8 th March 2004
Issue:	3.0
Page:	Page 61 of 61
Author:	Paul Clark



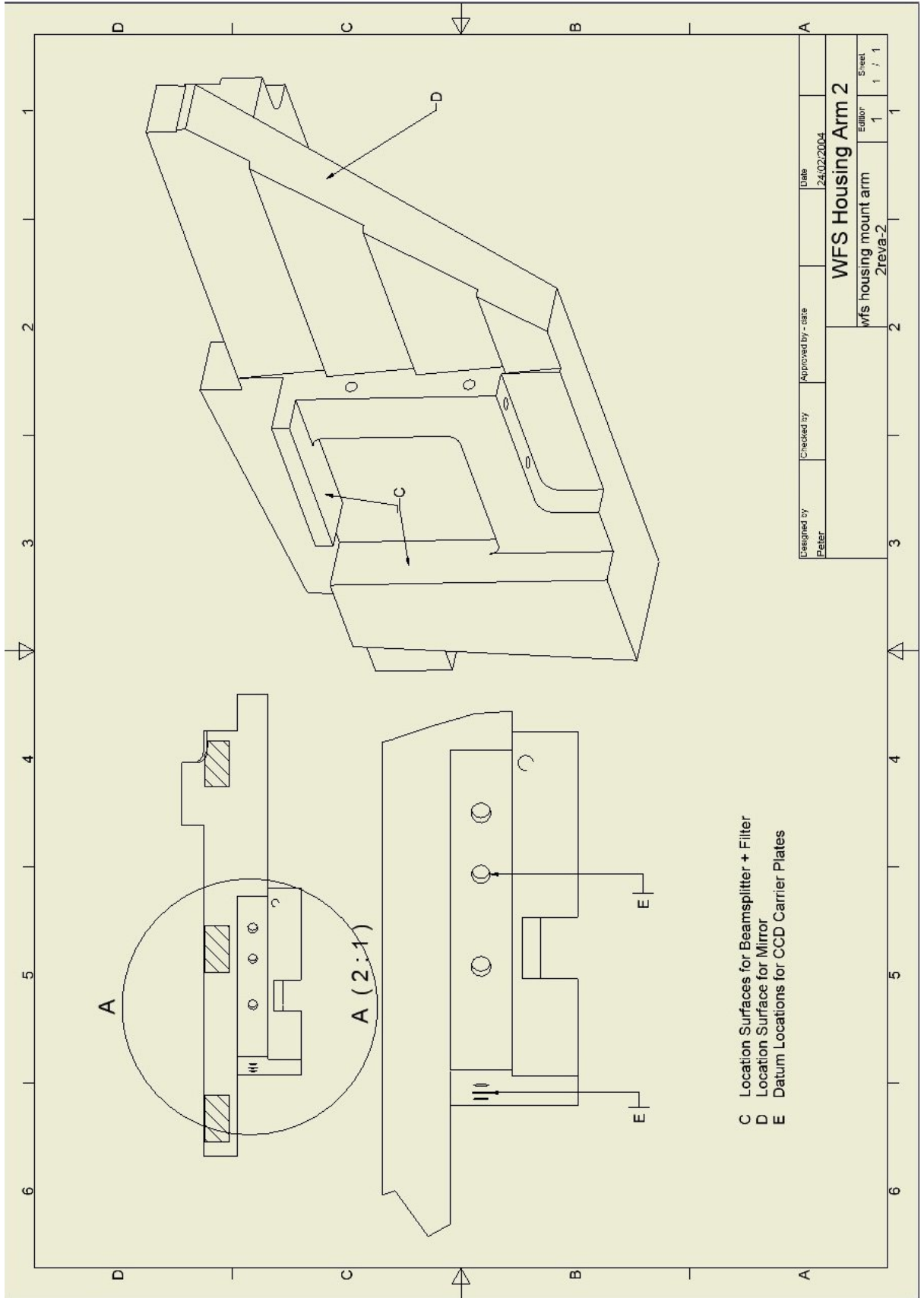
Doc. Number:	VIS-DES-UOD-06042-0001
Date:	8 th March 2004
Issue:	3.0
Page:	Page 62 of 62
Author:	Paul Clark



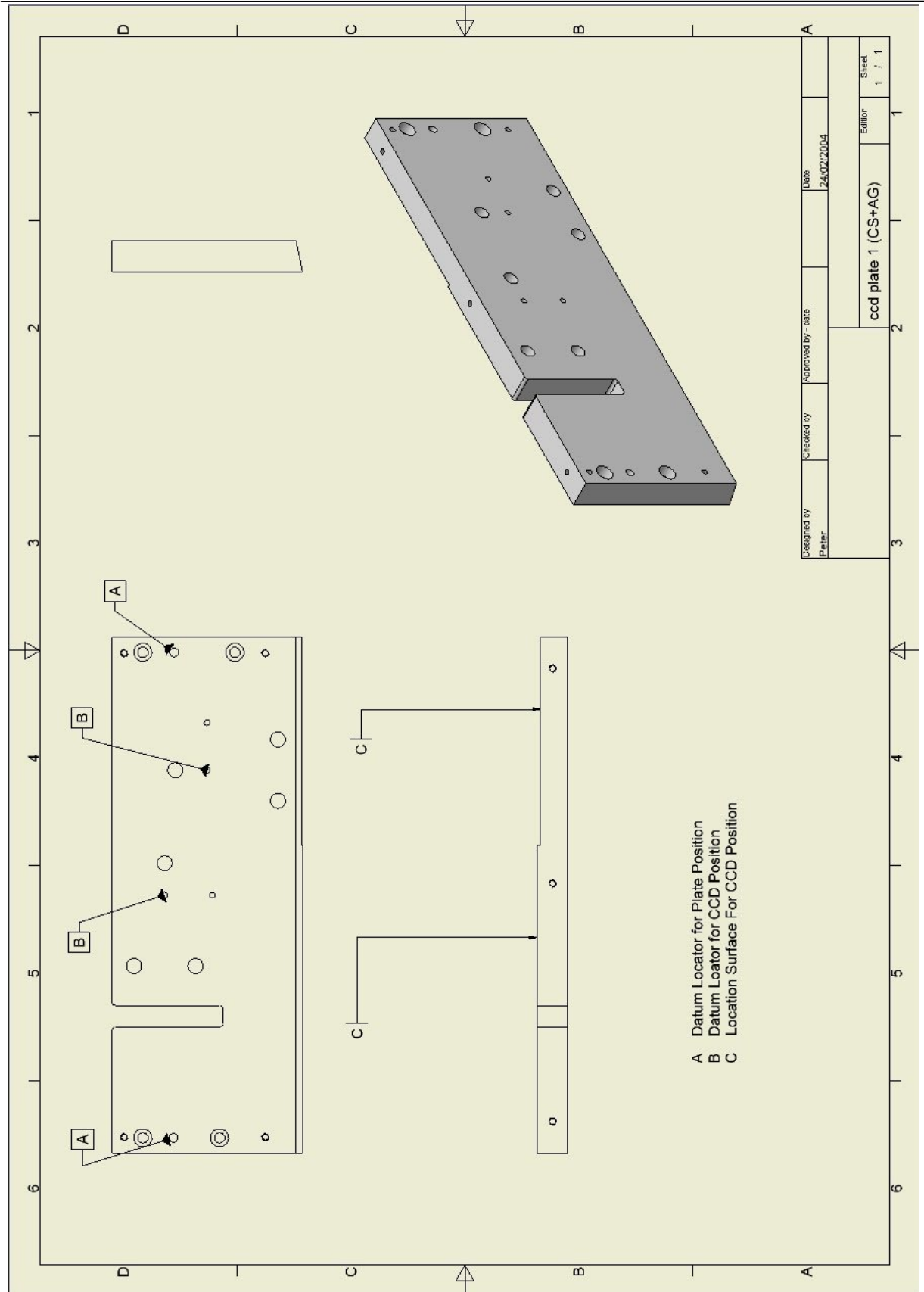
Doc. Number:	VIS-DES-UOD-06042-0001
Date:	8 th March 2004
Issue:	3.0
Page:	Page 63 of 63
Author:	Paul Clark



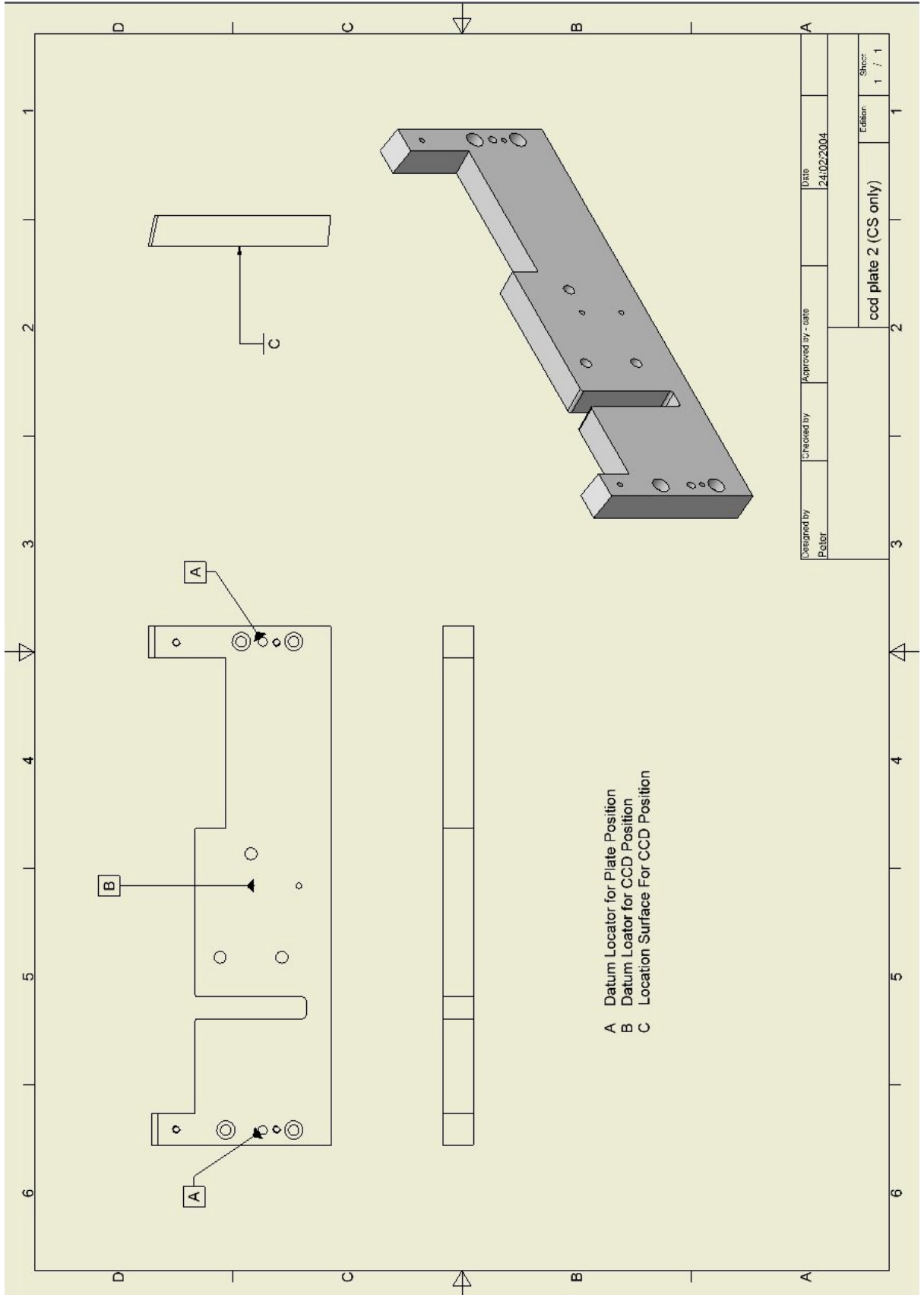
Doc. Number:	VIS-DES-UOD-06042-0001
Date:	8 th March 2004
Issue:	3.0
Page:	Page 64 of 64
Author:	Paul Clark



Doc. Number:	VIS-DES-UOD-06042-0001
Date:	8 th March 2004
Issue:	3.0
Page:	Page 65 of 65
Author:	Paul Clark

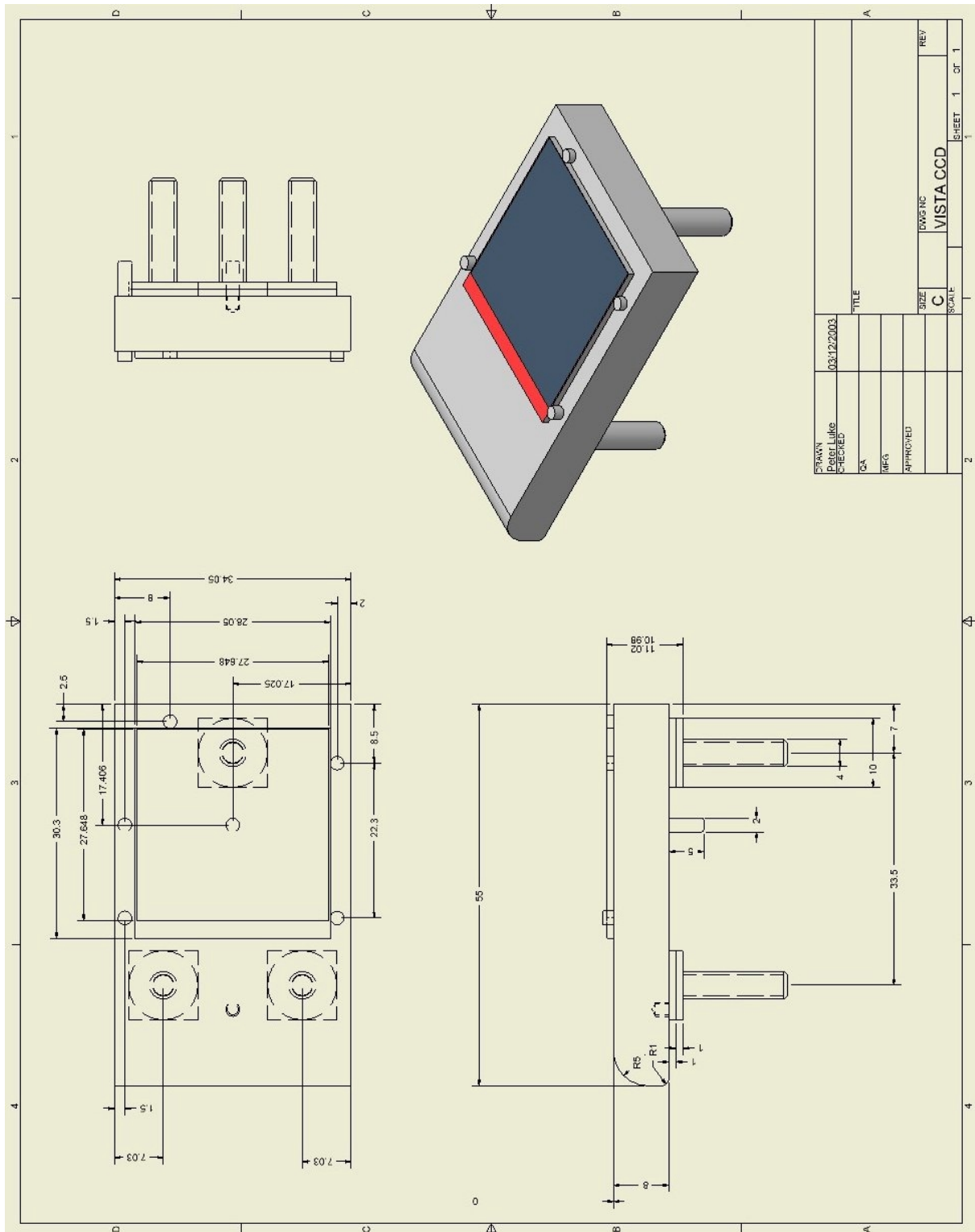


Doc. Number:	VIS-DES-UOD-06042-0001
Date:	8 th March 2004
Issue:	3.0
Page:	Page 66 of 66
Author:	Paul Clark



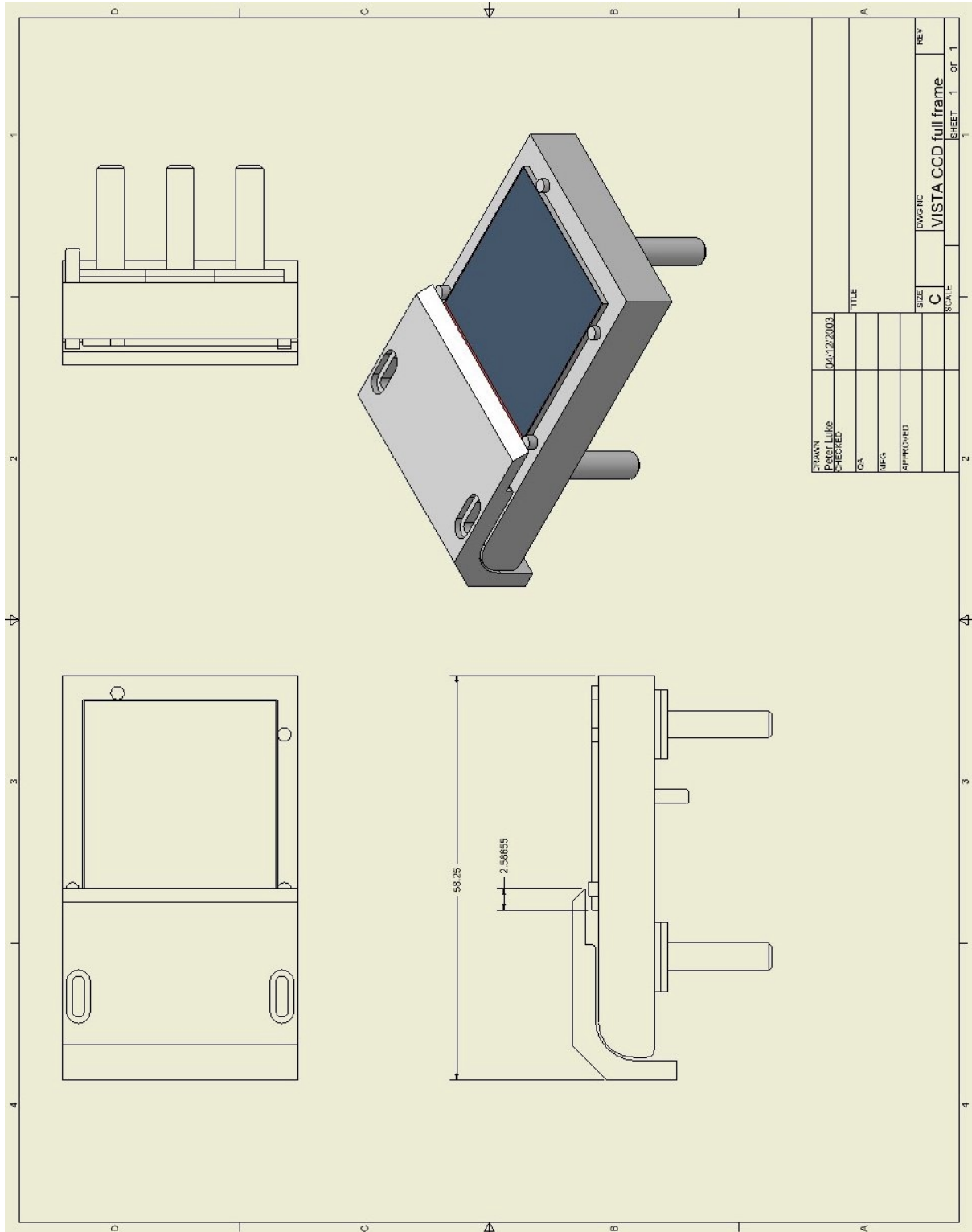
Designed by	Approved by - date	Date	Sheet
Peter		24/02/2004	1 / 1
ccd plate 2 (CS only)			1 / 1

Doc. Number:	VIS-DES-UOD-06042-0001
Date:	8 th March 2004
Issue:	3.0
Page:	Page 67 of 67
Author:	Paul Clark

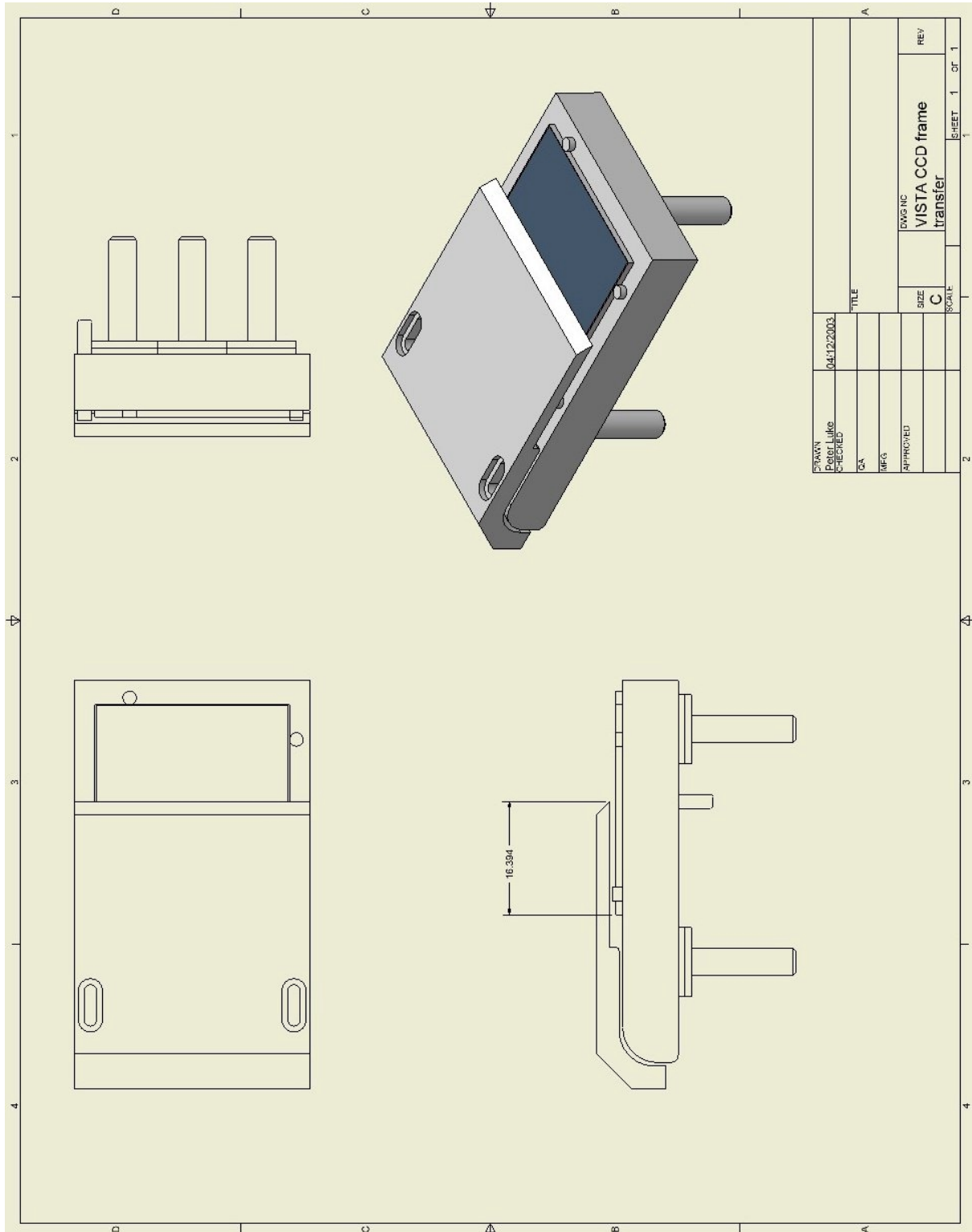


Wavefront Sensors Subsystem Design

Doc. Number:	VIS-DES-UOD-06042-0001
Date:	8 th March 2004
Issue:	3.0
Page:	Page 68 of 68
Author:	Paul Clark



Doc. Number:	VIS-DES-UOD-06042-0001
Date:	8 th March 2004
Issue:	3.0
Page:	Page 69 of 69
Author:	Paul Clark



Doc. Number:	VIS-DES-UOD-06042-0001
Date:	8 th March 2004
Issue:	3.0
Page:	Page 70 of 70
Author:	Paul Clark

17 Appendix 4: Electrical Schematics and Board Layout (Paul Berry)

The following sections contain the: grounding diagram; harness diagram; board schematics; board layout and parts list for the LOCS/AG units.



17.1 Overall EMC Grounding Diagram

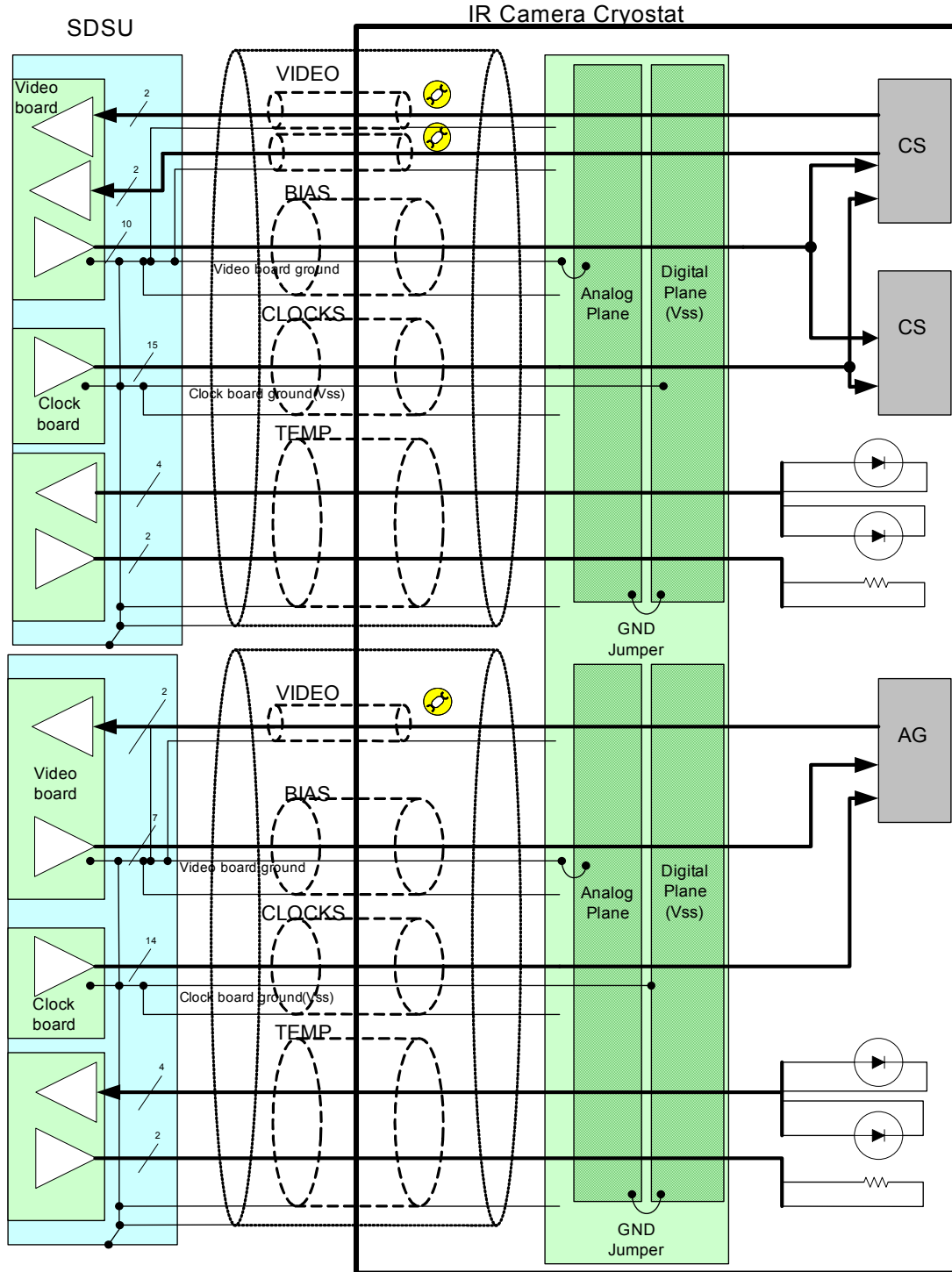


Figure 12.1.1: Overall EMC Grounding Diagram for Wavefront Sensors

Doc. Number:	VIS-DES-UOD-06042-0001
Date:	8 th March 2004
Issue:	3.0
Page:	Page 72 of 72
Author:	Paul Clark

17.2 Cable Harnesses

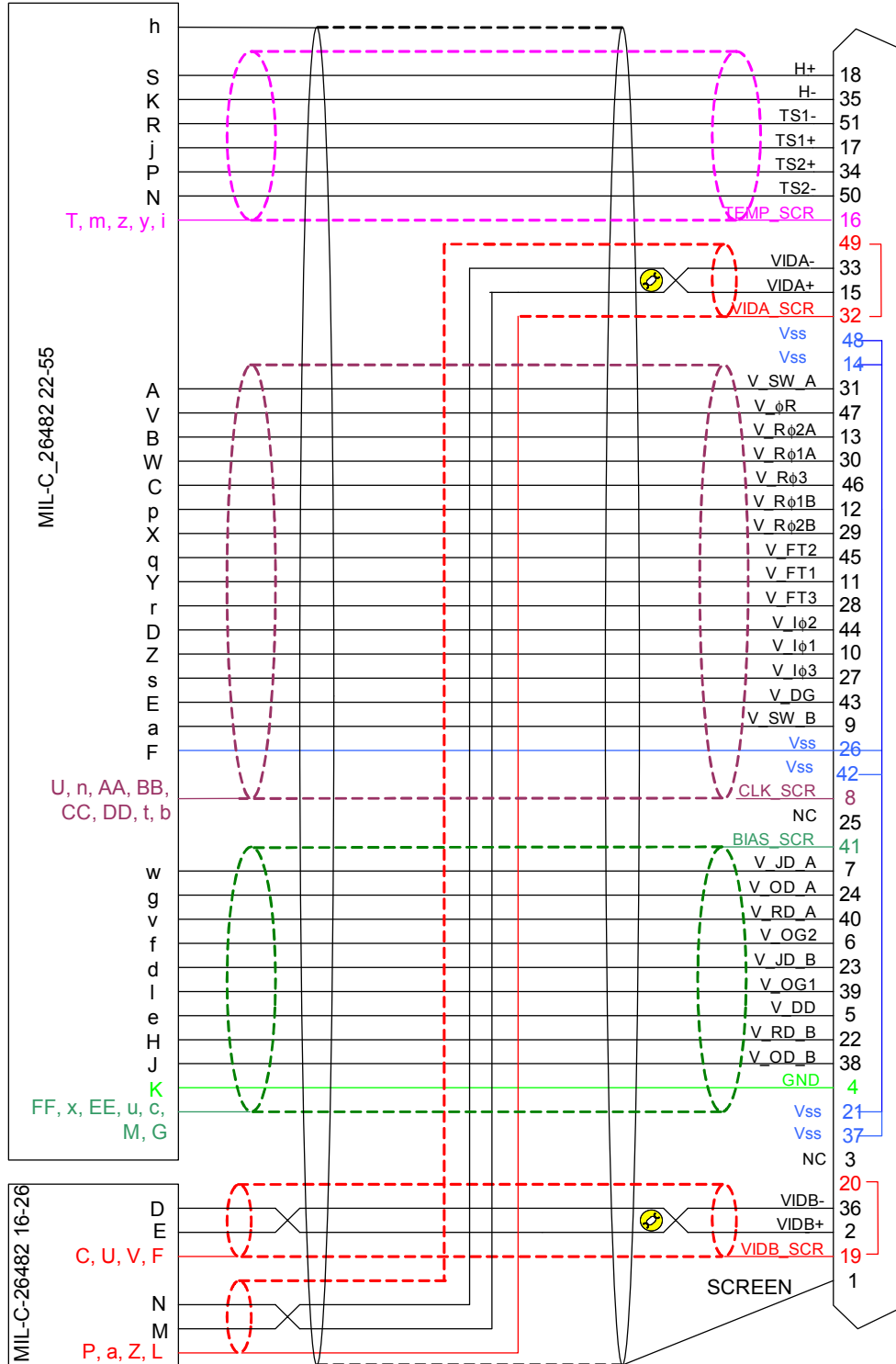


Figure 12.2.1: Cable harness for Curvature Sensors

Doc. Number:	VIS-DES-UOD-06042-0001
Date:	8 th March 2004
Issue:	3.0
Page:	Page 73 of 73
Author:	Paul Clark

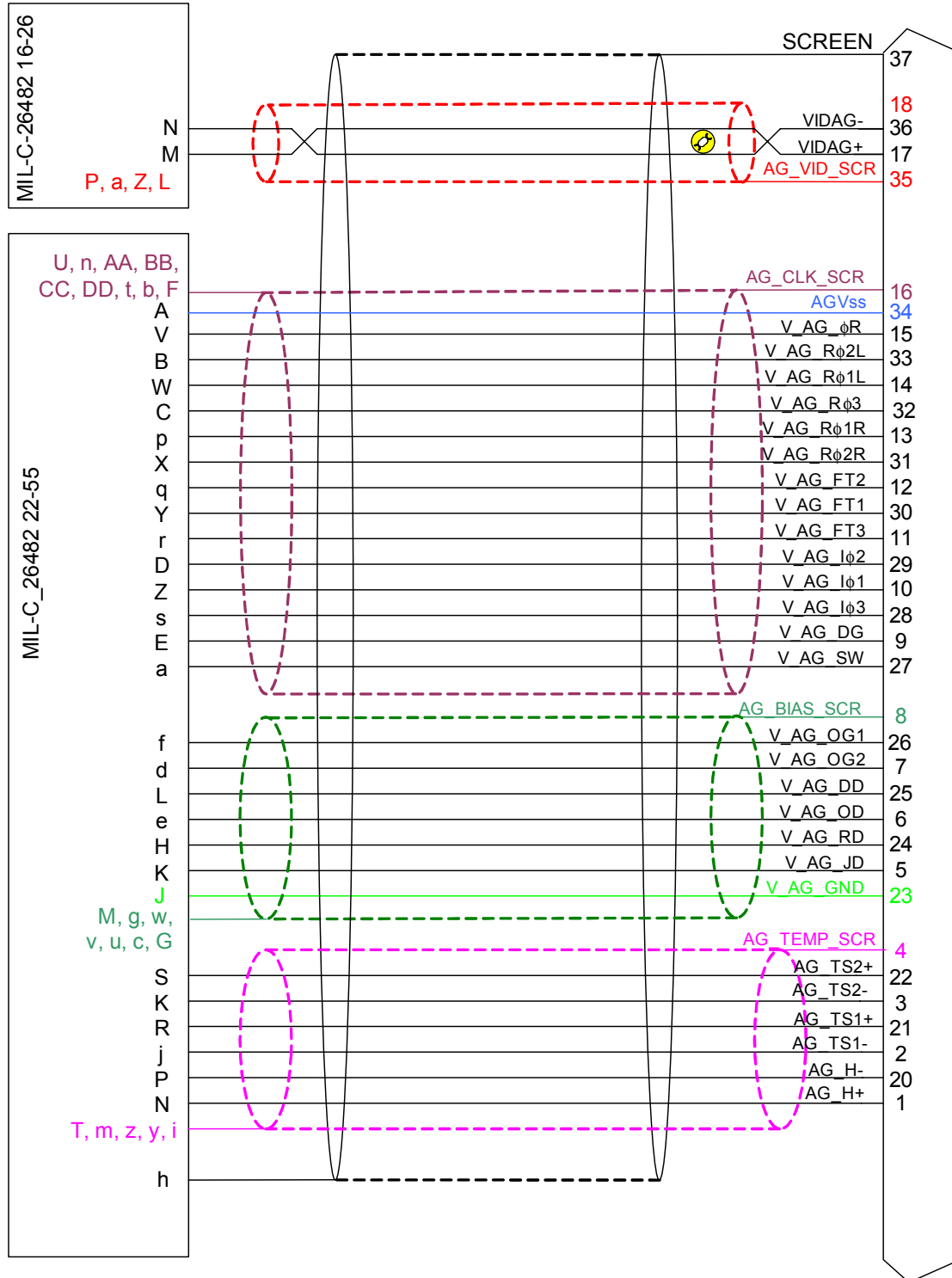
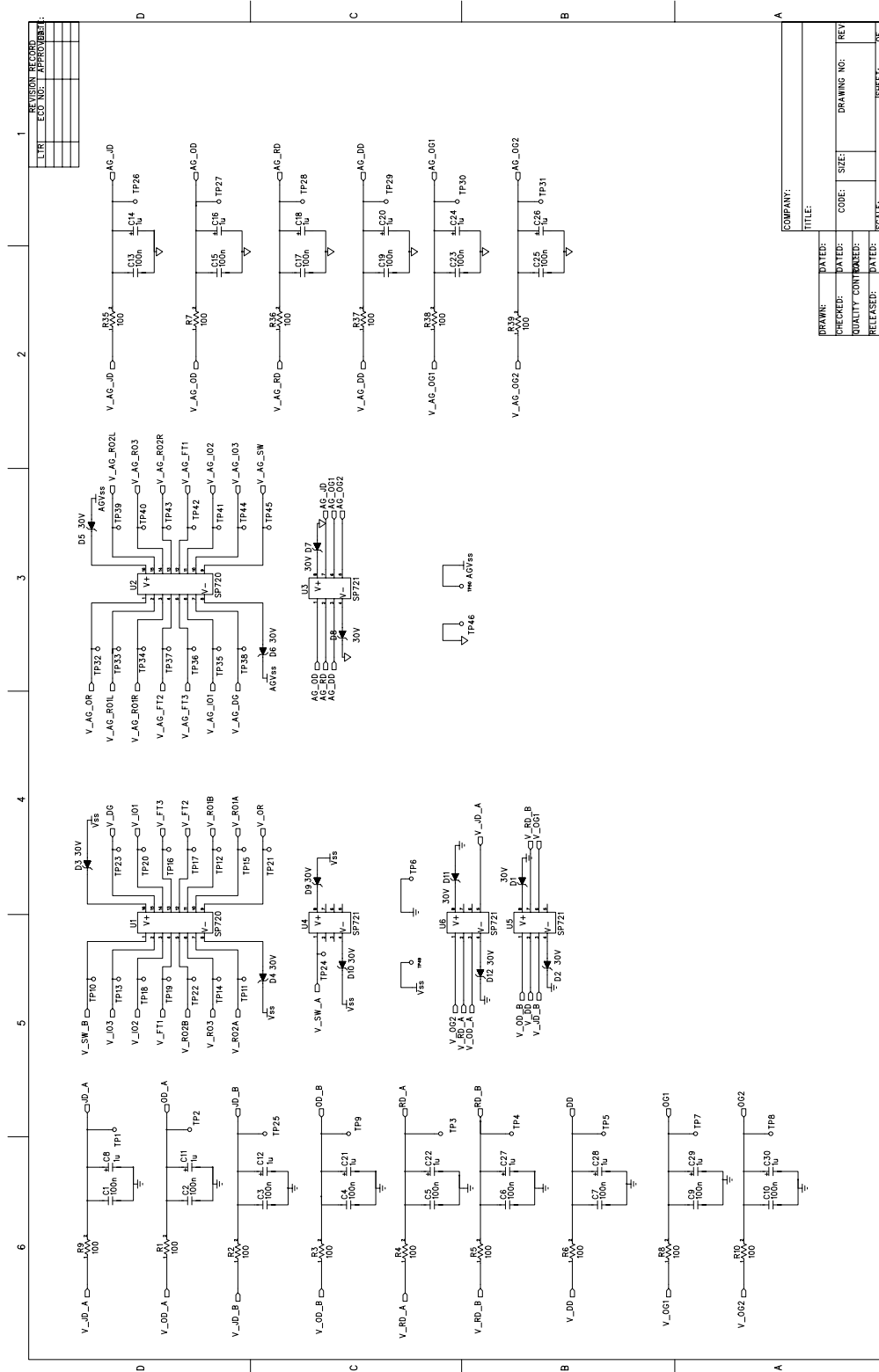


Figure 12.2.2: Cable Harness for Autoguider

Doc. Number:	VIS-DES-UOD-06042-0001
Date:	8 th March 2004
Issue:	3.0
Page:	Page 75 of 75
Author:	Paul Clark

WFS CCD 0.1.sch-2 - Thu Feb 26 14:44:30 2004



COMPANY:	
TITLE:	
DRAWN:	DATE:
CHECKED:	DATE:
QUALITY CONTROLLED:	DATE:
RELEASED:	DATE:
CODE:	SIZE:
DRAWING NO.:	REVISION:
SCALE:	SHEET:

Figure 12.3.2: Schematic showing protection scheme (2 of 3)



Doc. Number:	VIS-DES-UOD-06042-0001
Date:	8 th March 2004
Issue:	3.0
Page:	Page 76 of 76
Author:	Paul Clark

WFS CCD 0.1.sch-3 - Thu Feb 26 14:45:07 2004

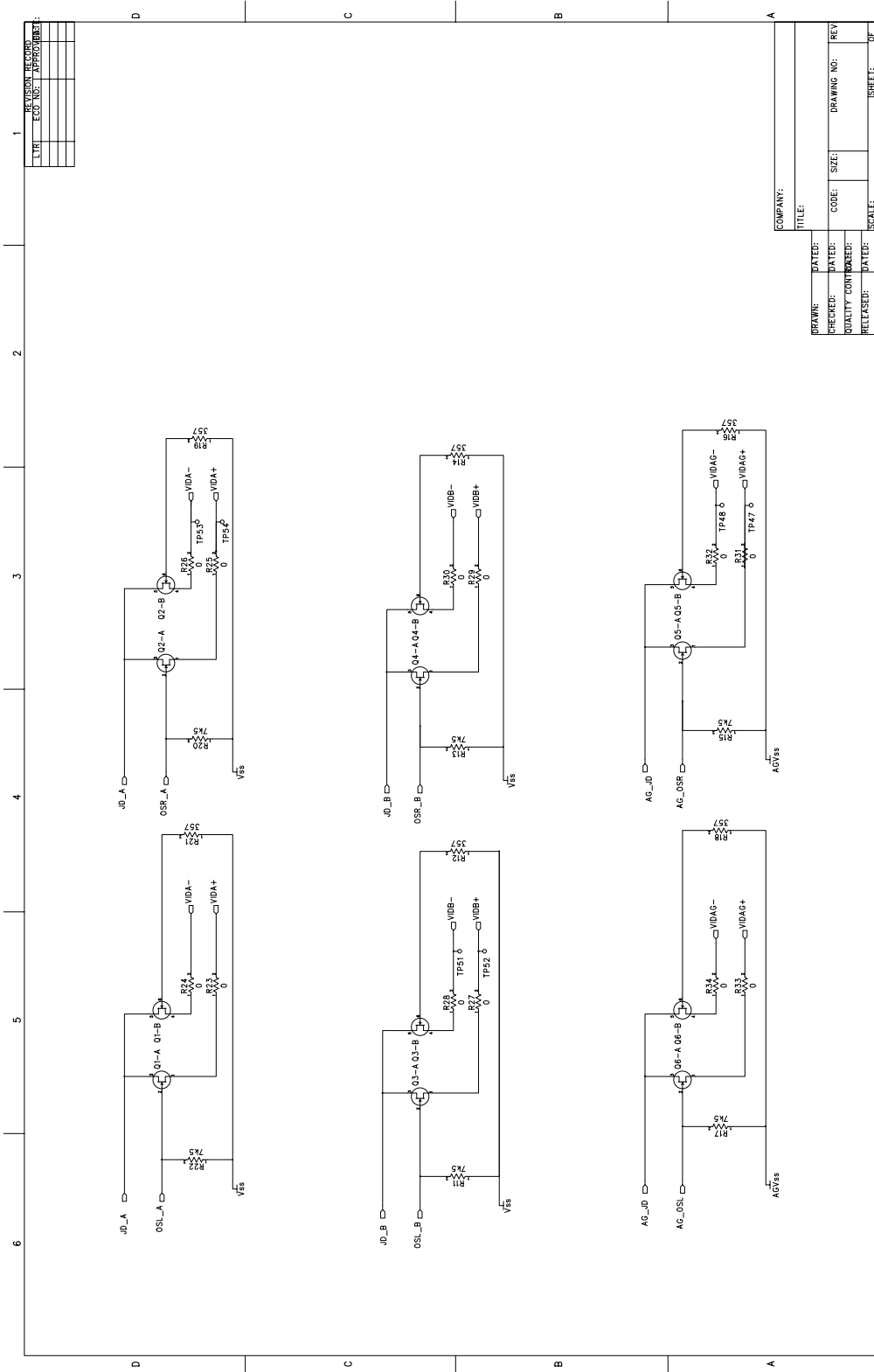


Figure 12.3.3: Schematic showing buffer configuration of CCD outputs (3 of 3)

Doc. Number:	VIS-DES-UOD-06042-0001
Date:	8 th March 2004
Issue:	3.0
Page:	Page 77 of 77
Author:	Paul Clark

17.4 Board Layout

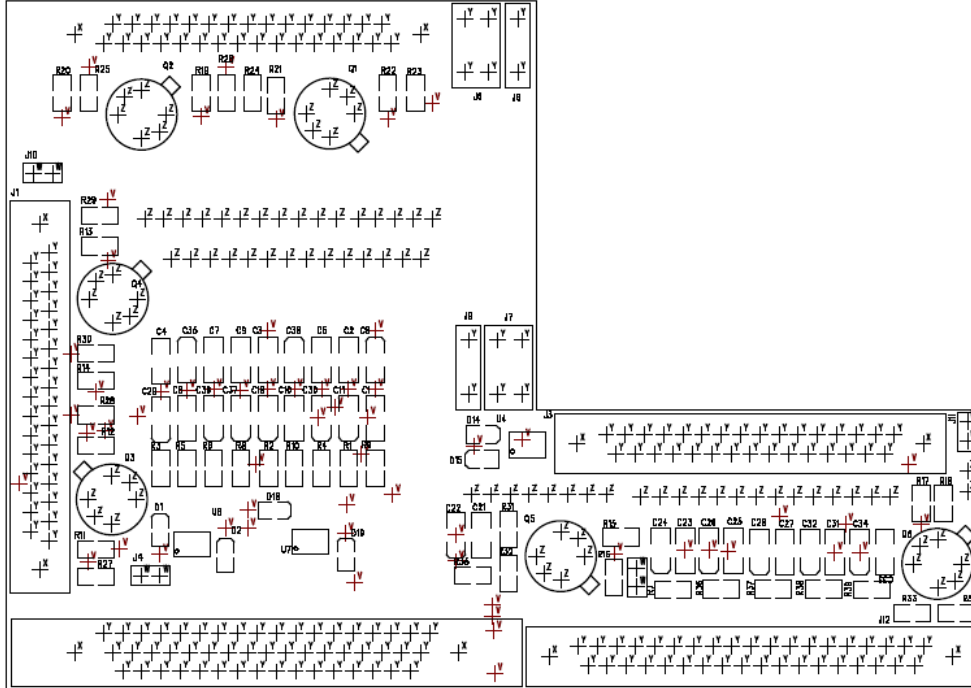


Figure 12.4.1: Board Layout (Component Side)

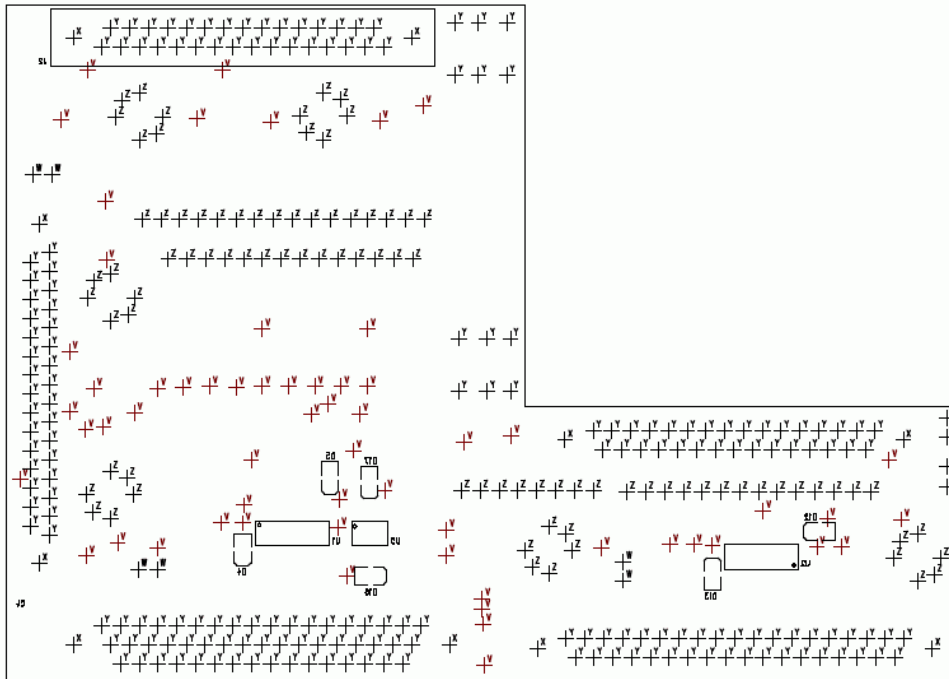


Figure 12.4.2: Board Layout (Reverse Side, Transparent View)

17.5 Parts List

Item	Qty	Reference	Part Name	Part Number	PCB DECAL	Value
1	15	C8 C11 C18 C22 C24 C26 C28-30 C32 C34-38	1206+	RS 367-3415	1206+	1u
2	6	Q1-6	2N5564	2N5555	TO-71	
3	4	J4 J10-11 J13	2PINHEADER		HDR2	
4	15	C1-7 C9-10 C21 C23 C25 C27 C31 C33	CAP1206	RS 264-4179	1206	100n
5	2	J8-9	GFPL2PIN	Positronic GF2M00DS3L	GF2M00DS3LA	
6	2	J6-7	GFPL4PIN	Positronic GF4M00DS3L	GF4M00DS3LA	
7	3	J1-3	MDM31SBS	MDM31SBS	MDM31SBS	
8	1	J12	MDM37PBS	MDM37PBS	MDM37PBS	
9	1	J5	MDM51BSP	MDM51BSP	MDM51BSP	
10	15	R1-10 R35-39	RES0805	RS 215-1532	0805	100
11	6	R16 R18-19 R21 R12 R14	RES0805	RS 215-1942	0805	357
12	6	R22 R11 R20 R13 R17 R15	RES0805	RS 215-3364	0805	7k5
13	12	R28-34 R23-27	RES0805	RS 223-0146	0805	0
14	2	U1-2	SP720	Future Electronics SP720AB	SO16MB	
15	4	U4-7	SP721	Future Electronics SP721AB	SO8M1	
16	54	TP1-50 TP53-56	TESTVIA		TESTVIA	
17	12	D1-2 D4-5 D12-19	ZENER-DIODE	1n6677ur-1	MELF2	30V

18 Appendix 5: Test Plan

The following sections contain the verification matrix and the individual test requirements for the WFS system.

18.1 WFS Verification Matrix

WFS Verification Matrix					
Item	Applicable Document	Section	Description	Who	Warm / Cold
0.1	AD16	7.17	The CCDs will be tested by the supplier to demonstrate compliance with the specification for:		
			Spectral Response	Supplier	Cold
			Full Well Depth	Supplier	Cold
			CTE	Supplier	Cold
			Read Noise	Supplier	Cold
			Surface Flatness	Supplier	Warm
			Surface Positioning	Supplier	Warm
0.2	LOCS/AG Filter Tech Spec		The LOCS/AG filters will be tested by the supplier to demonstrate compliance with the specification for:		
			Surface Flatness	Supplier	Warm
			Spectral Response	Supplier	Warm
			Dimensions	Supplier	Warm
0.3	LOCS/AG Beamsplitter Tech Spec		The LOCS/AG cube beamsplitters will be tested by the supplier to demonstrate compliance with the specification for:		
			Surface Flatness	Supplier	Warm
			Parallelism	Supplier	Warm
			Transmission / Reflectance	Supplier	Warm
			Dimensions	Supplier	Warm
0.4	HOCS Beamsplitter Tech Spec		The HOCS cube beamsplitters will be tested by the supplier to demonstrate compliance with the specification for:		
			Surface Flatness	Supplier	Warm
			Spectral Response	Supplier	Warm
			Parallelism	Supplier	Warm
			Transmission / Reflectance	Supplier	Warm
			Dimensions	Supplier	Warm
1	AD06	9.1.1	LOCS/AG Alignment setting (best focus position)	Durham	Warm & Cold
2	AD06	9.1.2	LOCS/AG Internal stability: thermal & flexure	Durham	Warm & Cold
3	AD06	9.2.1	LOCS/AG Autoguider centroid accuracy	Durham	Warm & Cold
4	AD06	9.2.2	LOCS Zernike coefficients determination accuracy	Durham	Warm
5	AD06	9.2.3	HOCS Zernike accuracy	Durham	Model

Table 18.1.1: WFS Verification Matrix

Doc. Number:	VIS-DES-UOD-06042-0001
Date:	8 th March 2004
Issue:	3.0
Page:	Page 80 of 80
Author:	Paul Clark

18.2 Summary and Description of Test Procedures

The following sub-sections summarise the aims of the individual verification and test procedures.

18.2.1 Verification Procedure 0.1: LOCS/AG CCD Properties

This procedure aims to ensure that the delivered CCDs meet the requirements documented in the technical specification AD16. AD16 section 7.17 specifies the tests that the supplier must perform on each device and document in a test report. The procedure is simply a crosscheck of the test report for each device against the relevant requirement.

18.2.2 Verification Procedure 0.2: LOCS/AG Filter Properties

This procedure aims to ensure that the delivered LOCS/AG filters (Schott RG9) meet the requirements that will be documented in the technical specification. The specification will contain requirements for surface flatness, parallelism, short-pass filter coating spectral response and overall (warm) dimensions. The supplier will be required to provide documented test data showing compliance with each requirement. The procedure is simply a crosscheck of the test report for each filter against the relevant requirement. Since surface flatness and dimension tests are easy to replicate, these will be repeated on delivery.

18.2.3 Verification Procedure 0.3: LOCS/AG Beamsplitter Properties

This procedure aims to ensure that the delivered LOCS/AG cube beamsplitters (fused silica) meet the requirements that will be documented in the technical specification. The specification will contain requirements for surface flatness, parallelism, transmission / reflectance properties and overall (warm) dimensions. The supplier will be required to provide documented test data showing compliance with each requirement. The procedure is simply a crosscheck of the test report for each beamsplitter against the relevant requirement. Since surface flatness and dimension tests are easy to replicate, these will be repeated on delivery.

18.2.4 Verification Procedure 0.4: HOCS Beamsplitter Properties

This procedure aims to ensure that the delivered HOCS cube beamsplitters (fused silica) meet the requirements that will be documented in the technical specification. The specification will contain requirements for surface flatness, spectral response, parallelism, transmission / reflectance properties and overall (warm) dimensions. Requirements will also be specified for the three individual elements of the beamsplitter, each of which will need to be tested prior to cementing. The supplier will be required to provide documented test data showing compliance with each requirement. The procedure is simply a crosscheck of the test report for each beamsplitter against the relevant requirement. Since surface flatness and dimension tests are easy to replicate, these will be repeated on delivery.

Doc. Number:	VIS-DES-UOD-06042-0001
Date:	8 th March 2004
Issue:	3.0
Page:	Page 81 of 81
Author:	Paul Clark

18.2.5 Test Procedure 1: LOCS/AG Alignment Setting (Best Focus Position)

Precision-machining techniques (akin to those used in diamond turning) will be utilised in the manufacture of the LOCS/AG unit aluminium alloy components to ensure positional accuracy of the detectors and optical components relative to the mounting reference surfaces. It is hoped to avoid the need for shimming between components but this remains an option if required.

The warm dimensions of the individual and assembled manufactured parts will be confirmed by precision metrology providing confidence that the detectors, when fitted, will be placed in the correct position. The detectors will be procured with a 20 μ m surface position tolerance relative to the rear mounting pads but the manufacturer will also be requested to provide measurement data of this same distance to a resolution of 5 μ m. If the manufacturer is unable to comply with this request then the detectors will be measured to this accuracy after delivery with a non-contact surface profileometer. In this way a one-time shimming of the CCDs, if required, on installation will achieve the required (focus) positional accuracy of $\pm 25\mu$ m. The detector decentre requirement of $\pm 200\mu$ m is not considered arduous.

The LOCS/AG optical components (pick-off mirror, filter and beamsplitter) will be positioned against reference surfaces machined into the aluminium alloy mount arms and held in place by beryllium copper springs. Precision metrology will be sufficient to establish if the reference surfaces are in the correct warm position. The surfaces will be machined in two iterations if required to deliver the required positional accuracy.

Once constructed, three alignment mirrors will be adhered to the LOCS/AG unit in positions where they can be seen from outside the camera cryostat (see figure 6.7.6). These mirrors are required for subsystem and Camera AIT. The absolute position of these mirrors is not critical. Their position relative to the mounting reference surfaces will be measured by either precision metrology or the use of an alignment telescope. These measurements will then be delivered as a calibration table with each individual LOCS/AG unit.

A warm-to-cold-to-warm alignment test will be conducted with the LOCS/AG unit installed in a test cryostat and cooled by cold heads. A fast reference beam with precision focus adjustment will be directed at the LOCS detectors allowing the required change in focus to be observed as the unit housing contracts with temperature. An alignment scope will be used to monitor the motion of the unit alignment mirrors relative to the test cryostat allowing any such motion to be subtracted from the reference beam results. Expected translation of the reference beam across the detector surface will be measured by CCD readout centroiding.

18.2.6 Test Procedure 2: LOCS/AG Internal Stability (Thermal & Flexure)

As outlined above, the thermal stability of the LOCS/AG units will be confirmed during a warm-to-cold-to-warm alignment test.

Doc. Number:	VIS-DES-UOD-06042-0001
Date:	8 th March 2004
Issue:	3.0
Page:	Page 82 of 82
Author:	Paul Clark

Flexure of the LOCS/AG units is not considered to be a significant issue given their low mass (2.25kg, see section 6.10). Flexure will be tested in the warm state. An individual unit will be mounted in a clean enclosure on a flexure rig and fed by a fast reference beam source, also mounted on the flexure rig. Displacement of the detectors or the optic components will be verified by CCD readout centroiding and FWHM measurement.

18.2.7 Test Procedure 3: AG Centroid Accuracy

Autoguider centroid accuracy will be tested by translating a fast precision test beam across the AG entry aperture. The displacement of the test beam source will be compared to CCD readout centroiding and the accuracy confirmed. This test will be conducted in the warm and cold state.

18.2.8 Test Procedure 4: LOWFS Zernike Coefficient Determination Accuracy

This test will be conducted in the warm state since the non-common-path aberrations introduced by a cryostat window would not be measurable during the course of such a cold test.

A calibrated aberration test source, based on a 97-actuator continuous phase sheet deformable mirror, will be used to inject known aberrations into the LOCS unit. The test source will be independently calibrated and monitored by a phase-shifting interferometer, viewing the surface of the deformable mirror. Non-common path aberrations detected by the LOCS will be subtracted as the measurement tests progress. It may be possible to provide additional verification of the injected aberrations through the use of a separate Shack-Hartmann wavefront sensor but this strategy will only be adopted if the additional aberrations caused by the introduction of the additional optics are not detrimental to the accuracy of the test. A simplified overview of the test set-up is shown in the following figure.

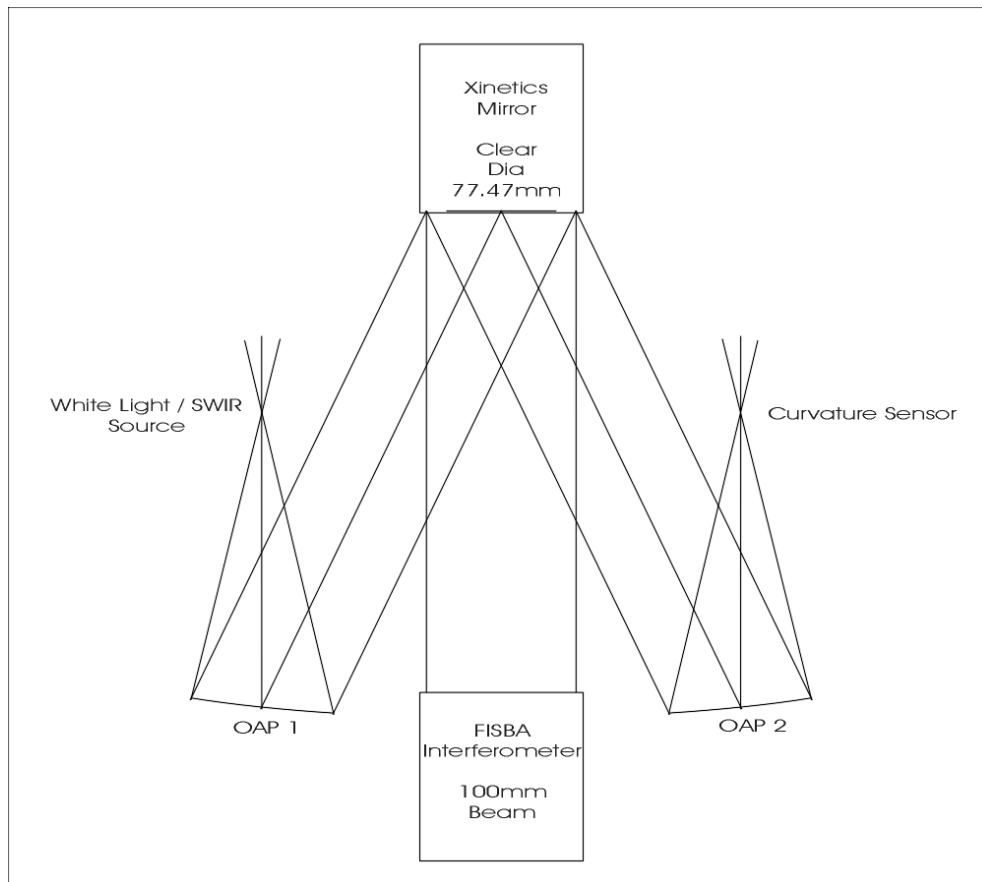


Figure 1: Simplified Aberration Test Source

18.2.9 Test Procedure 5: HOWFS Zernike Coefficient Determination Accuracy

It will not be possible to conduct a test of the HOCS system, using the same test source as the LOCS, due to the need to provide a source operating at science wavelengths (J-band) and a detector system capable of viewing the same. It may be possible to conduct a non-calibrated test during Camera AIT using the test source already specified for that phase. The determination accuracy of the HOWFS system therefore needs to rely upon the modelling work already undertaken and confirmation from the LOCS tests that all is well.

18.3 Verification and Test Procedures

The following sub-sections list the individual verification and test procedures. These procedure tables will be developed and detailed further in planning the test activities.

Doc. Number:	VIS-DES-UOD-06042-0001
Date:	8 th March 2004
Issue:	3.0
Page:	Page 84 of 84
Author:	Paul Clark

18.3.1 Verification Test 0.1

Applicable Specification:	
IR Camera system :	IR Camera
IR Camera sub-system:	WFS: LOCS & AG
Brief title of test	Confirmation of CCD properties
Type of verification	Data check
Location of test	Durham
Applicable documents	VIS-SPE-UOD-06042-0006

Documentation/Test equipment required.		
<ul style="list-style-type: none"> • Manufacturer's test report 		
External specialist required.		
None		
Test procedure or procedure reference		
1. Crosscheck manufacturer's test report against technical specification		
Test performed by		
Tester	Organisation	Date of test
Location	Applicable test report	

Doc. Number:	VIS-DES-UOD-06042-0001
Date:	8 th March 2004
Issue:	3.0
Page:	Page 85 of 85
Author:	Paul Clark

18.3.2 Verification Test 0.2

Applicable Specification:	
IR Camera system :	IR Camera
IR Camera sub-system:	WFS: LOCS & AG
Brief title of test	Confirmation of filter properties
Type of verification	Data check & Measurement
Location of test	Durham
Applicable documents	VIS-SPE-UOD-06042-00??

Documentation/Test equipment required.		
<ul style="list-style-type: none"> • Manufacturer's test report • Phase-shifting interferometer • Metrology equipment 		
External specialist required.		
None		
Test procedure or procedure reference		
<ol style="list-style-type: none"> 1. Crosscheck manufacturer's test report against technical specification 2. Confirm surface flatness measurement using phase-shifting interferometer 3. Confirm dimensions via precision metrology 		
Test performed by		
Tester	Organisation	Date of test
Location	Applicable test report	

Doc. Number:	VIS-DES-UOD-06042-0001
Date:	8 th March 2004
Issue:	3.0
Page:	Page 86 of 86
Author:	Paul Clark

18.3.3 Verification Test 0.3

Applicable Specification:	
IR Camera system :	IR Camera
IR Camera sub-system:	WFS: LOCS & AG
Brief title of test	Confirmation of beamsplitter properties
Type of verification	Data check & Measurement
Location of test	Durham
Applicable documents	VIS-SPE-UOD-06042-00??

Documentation/Test equipment required.		
<ul style="list-style-type: none"> • Manufacturer's test report • Phase-shifting interferometer • Metrology equipment 		
External specialist required.		
None		
Test procedure or procedure reference		
<ol style="list-style-type: none"> 1. Crosscheck manufacturer's test report against technical specification 2. Confirm surface flatness measurement using phase-shifting interferometer 3. Confirm dimensions via precision metrology 		
Test performed by		
Tester	Organisation	Date of test
Location	Applicable test report	

Doc. Number:	VIS-DES-UOD-06042-0001
Date:	8 th March 2004
Issue:	3.0
Page:	Page 87 of 87
Author:	Paul Clark

18.3.4 Verification Test 0.4

Applicable Specification:	
IR Camera system :	IR Camera
IR Camera sub-system:	WFS: HOCS
Brief title of test	Confirmation of beamsplitter properties
Type of verification	Data check & Measurement
Location of test	Durham
Applicable documents	VIS-SPE-UOD-06042-00??

Documentation/Test equipment required.		
<ul style="list-style-type: none"> • Manufacturer's test report • Phase-shifting interferometer • Metrology equipment 		
External specialist required.		
None		
Test procedure or procedure reference		
<ol style="list-style-type: none"> 1. Crosscheck manufacturer's test report against technical specification 2. Confirm surface flatness measurement using phase-shifting interferometer 3. Confirm dimensions via precision metrology 		
Test performed by		
Tester	Organisation	Date of test
Location	Applicable test report	

Doc. Number:	VIS-DES-UOD-06042-0001
Date:	8 th March 2004
Issue:	3.0
Page:	Page 88 of 88
Author:	Paul Clark

18.3.5 Test Procedure 1

Applicable Specification:	
IR Camera system :	IR Camera
IR Camera sub-system:	WFS: LOCS/AG
Brief title of test	Alignment setting
Type of verification	Measurement
Location of test	Durham
Applicable documents	VIS-SPE-RAL-06040-0001

Documentation/Test equipment required.		
<ul style="list-style-type: none"> • Metrology equipment • Test cryostat • Reference beam source • Alignment telescope 		
External specialist required.		
None		
Test procedure or procedure reference		
<ol style="list-style-type: none"> 1. Measure LOCS/AG aluminium components 2. Re-machine optics reference surfaces if required 3. Manufacture CCD shims if required 4. Adhere alignment mirrors to unit housing 5. Measure mirror position relative to mounting reference surfaces. Document. 6. Conduct warm-cold-warm alignment test using reference beam and alignment telescope outside cryostat. Document. 		
Test performed by		
Tester	Organisation	Date of test
Location	Applicable test report	

Doc. Number:	VIS-DES-UOD-06042-0001
Date:	8 th March 2004
Issue:	3.0
Page:	Page 89 of 89
Author:	Paul Clark

18.3.6 Test Procedure 2

Applicable Specification:	
IR Camera system :	IR Camera
IR Camera sub-system:	WFS: LOCS/AG
Brief title of test	Internal stability
Type of verification	Measurement
Location of test	Durham
Applicable documents	VIS-SPE-RAL-06040-0001

Documentation/Test equipment required.		
<ul style="list-style-type: none"> • Flexure rig • Reference beam source • Clean enclosure for LOCS/AG unit 		
External specialist required.		
None		
Test procedure or procedure reference		
1. Test flexure by reading out CCD centroid position at various attitudes. Document.		
Test performed by		
Tester	Organisation	Date of test
Location	Applicable test report	

Doc. Number:	VIS-DES-UOD-06042-0001
Date:	8 th March 2004
Issue:	3.0
Page:	Page 90 of 90
Author:	Paul Clark

18.3.7 Test Procedure 3

Applicable Specification:	
IR Camera system :	IR Camera
IR Camera sub-system:	WFS: LOCS/AG
Brief title of test	AG Centroid accuracy
Type of verification	Measurement
Location of test	Durham
Applicable documents	VIS-SPE-RAL-06040-0001

Documentation/Test equipment required.		
<ul style="list-style-type: none"> Precision fast reference beam source Test cryostat 		
External specialist required.		
None		
Test procedure or procedure reference		
<ol style="list-style-type: none"> Confirm centroid accuracy by translating reference beam across sensor. Observe CCD centroid position. Document. Repeat in test cryostat. Document. 		
Test performed by		
Tester	Organisation	Date of test
Location	Applicable test report	

18.3.8 Test Procedure 4

Applicable Specification:	
IR Camera system :	IR Camera
IR Camera sub-system:	WFS: LOCS/AG
Brief title of test	LOCS Aberration measurement accuracy
Type of verification	Measurement
Location of test	Durham
Applicable documents	VIS-SPE-RAL-06040-0001

Documentation/Test equipment required.		
<ul style="list-style-type: none"> • Calibrated aberration test source • Phase-shifting interferometer 		
External specialist required.		
None		
Test procedure or procedure reference		
1. Confirm aberration measurement accuracy using calibrated test source. Document.		
Test performed by		
Tester	Organisation	Date of test
Location	Applicable test report	

18.3.9 Test Procedure 5

Applicable Specification:	
IR Camera system :	IR Camera
IR Camera sub-system:	WFS: HOCS
Brief title of test	HOCS Aberration measurement accuracy
Type of verification	Measurement
Location of test	RAL
Applicable documents	VIS-SPE-RAL-06040-0001

Documentation/Test equipment required.		
<ul style="list-style-type: none"> • AIT test source • IR Camera AIT Procedures 		
External specialist required.		
None		
Test procedure or procedure reference		
1. Perform non-calibrated measurement during Camera AIT campaign to validate model results. Document.		
Test performed by		
Tester	Organisation	Date of test
Location	Applicable test report	

Doc. Number:	VIS-DES-UOD-06042-0001
Date:	8 th March 2004
Issue:	3.0
Page:	Page 93 of 93
Author:	Paul Clark

19 Appendix 6: LOCS/AG Optical Design Report (Richard Bingham)

Note: This report was written prior to the decision to rotate the autoguider CCD through 90°.

Proposed optical design of the Low-Order Curvature Sensor (LOCS) and the Autoguider for VISTA

Version 1

Richard G. Bingham
11 November 2003

This is part of an optical design project related to the VISTA wavefront sensors.

I investigated different layouts for the LOCS. One solution (not that preferred) compensated successfully for the astigmatism and coma induced by a tilted plate beamsplitter by using correctly angled flat surfaces. However, it was clearly more complicated than the preferred solution, with compound angles on the assembly and also having extra optical components, with no apparent advantage. The use of a cube-type beamsplitter is preferred as it gives the best solution in terms of simplicity as well as in terms of performance.

The proposed solution is modelled in the Zemax file *Tel+Cube13b.zmx*. This Zemax file contains the telescope as well as the beamsplitter optics so that the ray-trace precisely models the real system, with the sensor optics in the required position off-axis.

The CCDs are both shown in focus in *Tel+Cube13b.zmx* so that Zemax demonstrates the available performance. In practice, the two CCDs are to be adjusted to +/- 1 mm defocus.

The system is to be duplicated in the telescope. In each of the two sensor assemblies, this proposed design uses a single cube-type beamsplitter covering both the LOCS and Autoguider fields. In the case of the Autoguider, the fact that the relevant rays pass through the prism serves to throw the image about 15 mm further out than it would be in vacuum, which may be convenient, and the LOCS and Autoguider CCDs are coplanar. Thus part of the prism has a beamsplitter coating on the hypotenuse face, serving the two LOCS detectors. The Autoguider part of the prism has two simple options – either leave the prism clear, or apply a mirror coating on the hypotenuse face. This gives rise to alternative positions for the Autoguider detector, the choice to be made by Durham.



Doc. Number:	VIS-DES-UOD-06042-0001
Date:	8 th March 2004
Issue:	3.0
Page:	Page 94 of 94
Author:	Paul Clark

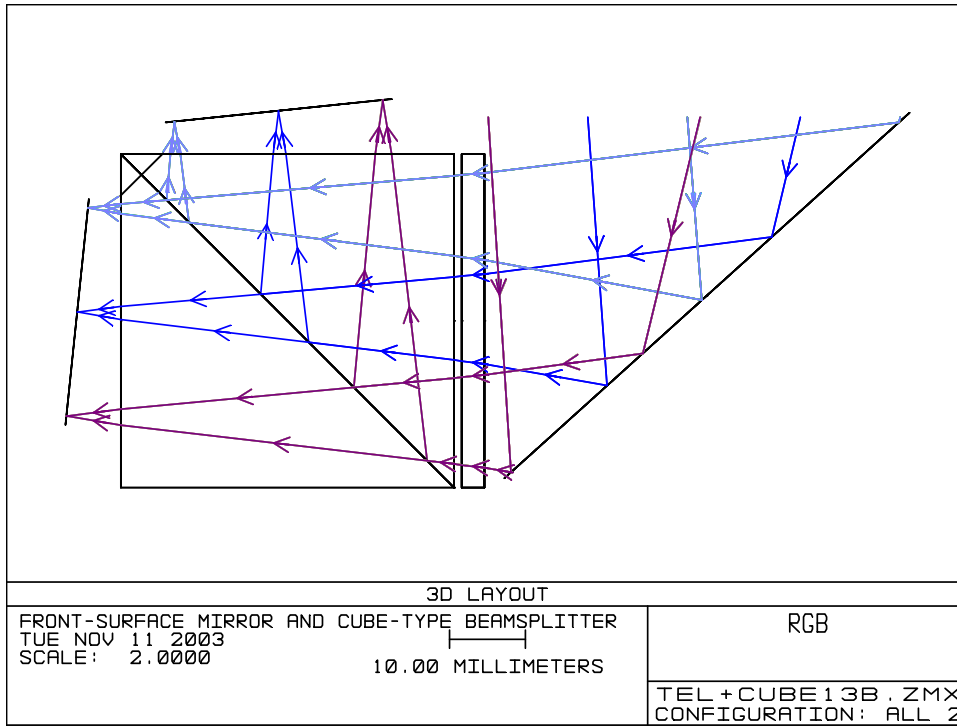


Figure 1

The geometry of the beamsplitter is illustrated above and below (Figures 1 and 2). The two focal planes are shown in the nominally focused position as noted above. The nearest corner of the beamsplitter block can be removed as indicated, if it is necessary to make more space. This prism as shown uses fused silica; if any other material is used as discussed elsewhere, the position of the focal plane needs to be recomputed and is slightly further from the block. (Other dimensions are unchanged.)

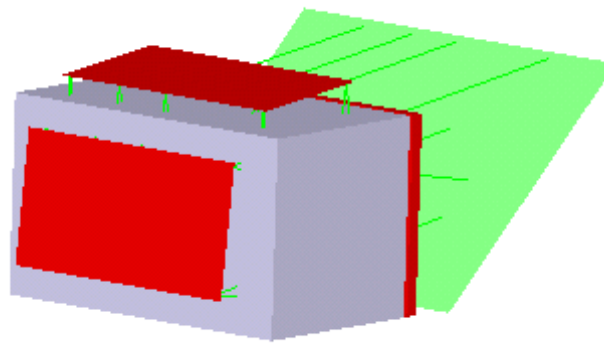


Figure 2

Doc. Number:	VIS-DES-UOD-06042-0001
Date:	8 th March 2004
Issue:	3.0
Page:	Page 95 of 95
Author:	Paul Clark

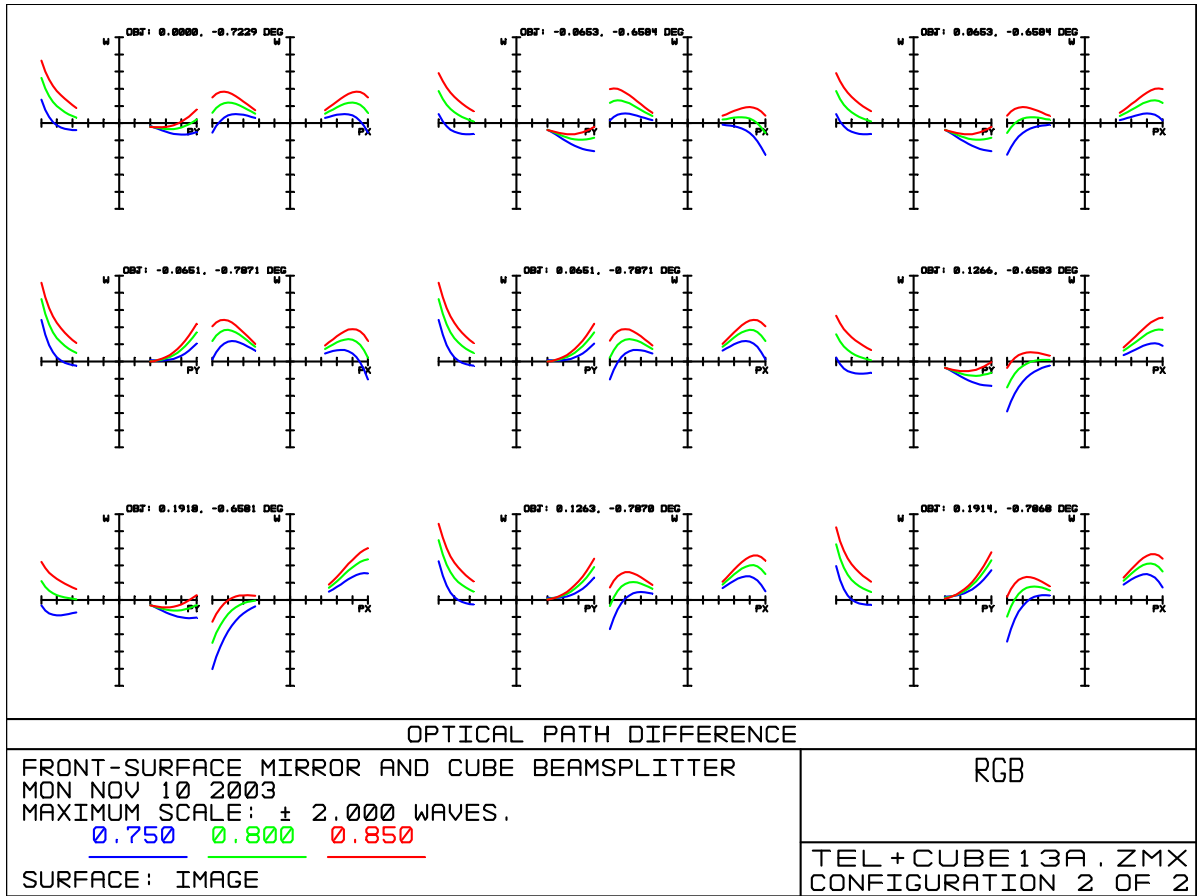


Figure 3

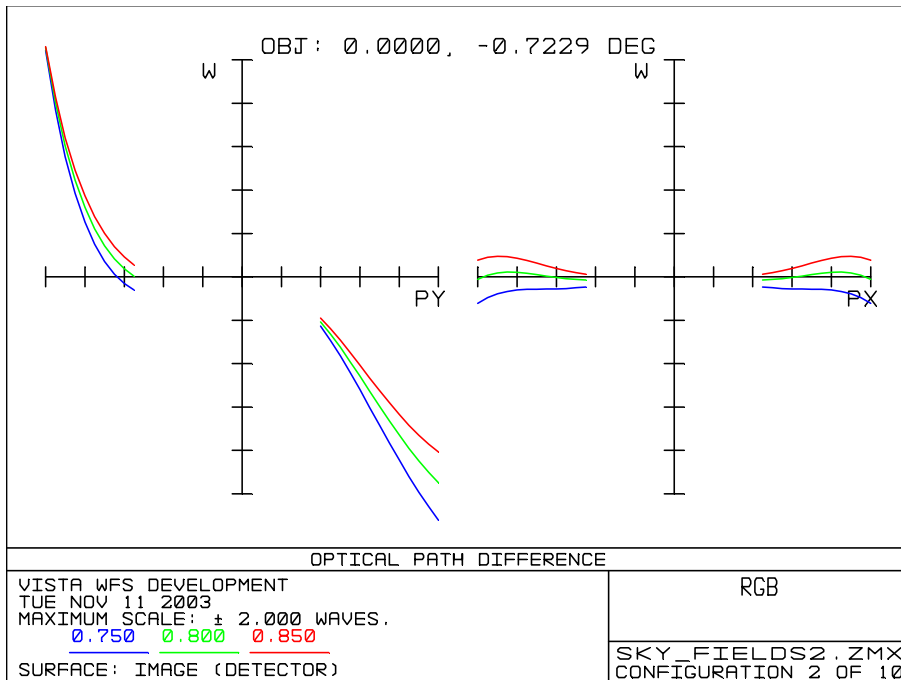


Figure 4

Doc. Number:	VIS-DES-UOD-06042-0001
Date:	8 th March 2004
Issue:	3.0
Page:	Page 96 of 96
Author:	Paul Clark

Figure 3 shows the aberrations (optical path difference) appearing through the silica beamsplitter for nine field positions, being first the centre, then the corners of the LOCS field and then the corners of the Autoguider field. This may also be seen from the Zemax file. The scale is +/- 2 waves. Figure 4 shows aberrations appearing through VISTA without the beamsplitter, at the centre of the LOCS field, on the same scale. {Note: Further detail on the LOCS aberrations is given in Appendix 14.}

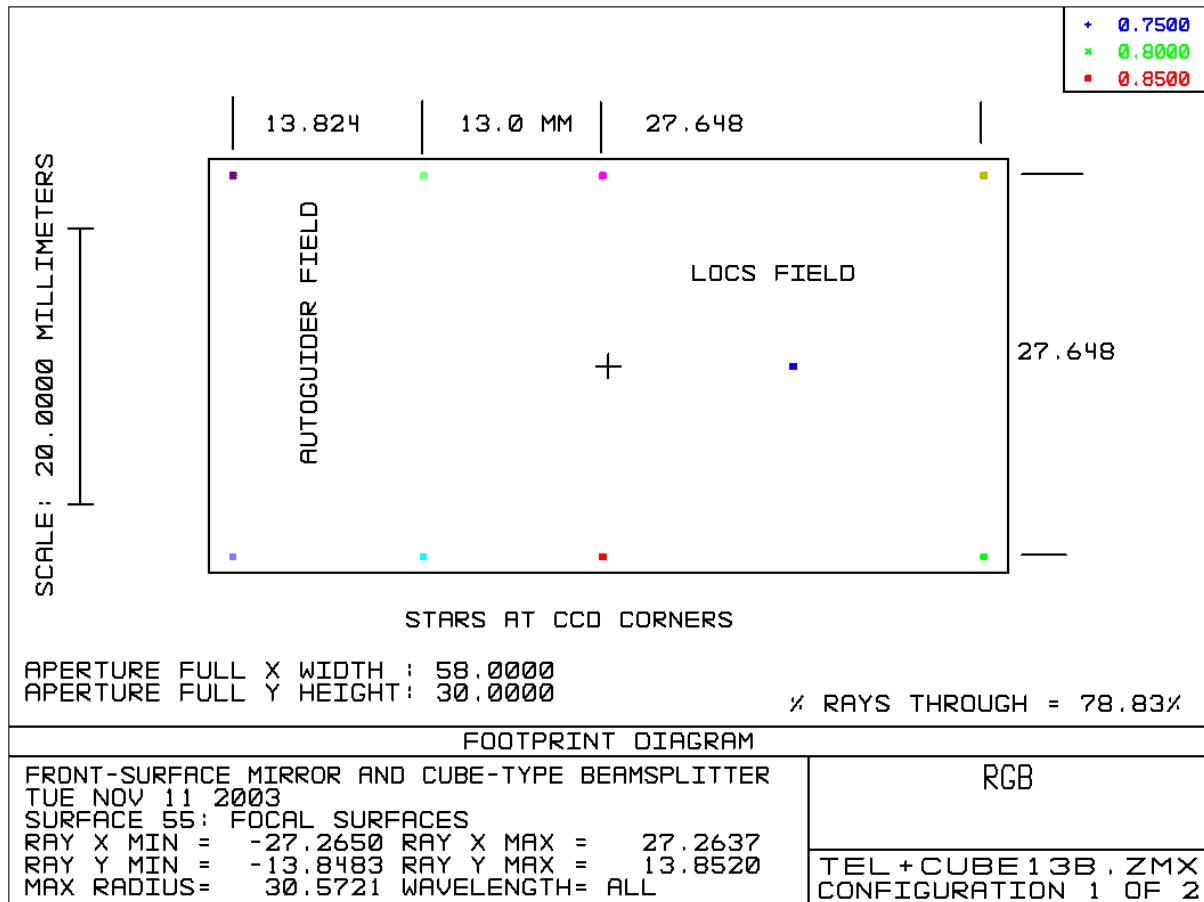


Figure 5

The field of view available at either exit from the beamsplitter is illustrated above in Figure 5. As noted, one exit will be chosen for the Autoguider field. This will be either straight through the prism or in reflection, depending on whether a mirror coating is applied on the relevant part of the beamsplitter hypotenuse face. {Note: the autoguider field has subsequently been rotated through 90°. The CCD is mounted above the cube using the reflected optical path.}

Doc. Number:	VIS-DES-UOD-06042-0001
Date:	8 th March 2004
Issue:	3.0
Page:	Page 97 of 97
Author:	Paul Clark

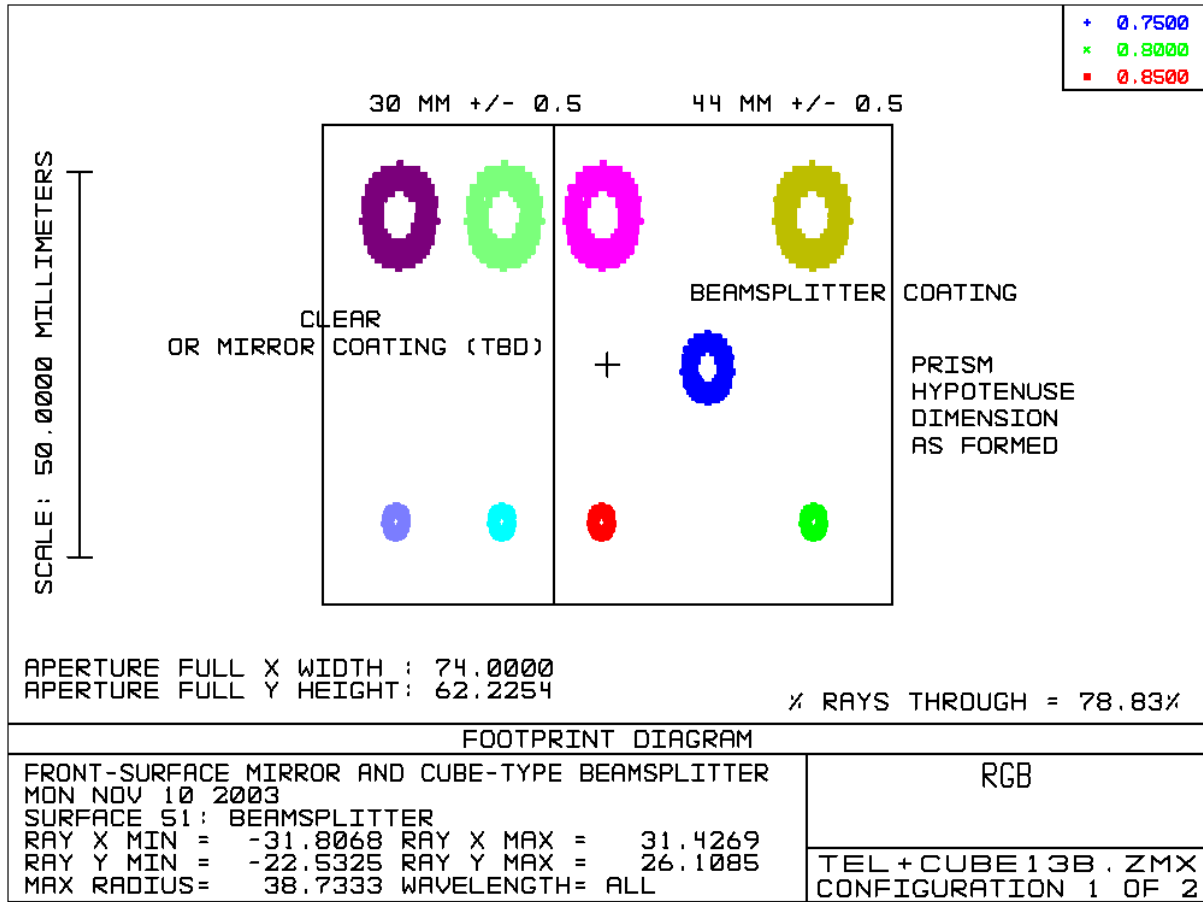


Figure 6

The above Figure 6 and Figures 7 and 8 below indicate details of the beamsplitter block with tolerances.

Doc. Number:	VIS-DES-UOD-06042-0001
Date:	8 th March 2004
Issue:	3.0
Page:	Page 98 of 98
Author:	Paul Clark

Geometry for cutting the beamsplitter prism with tested transmission directions

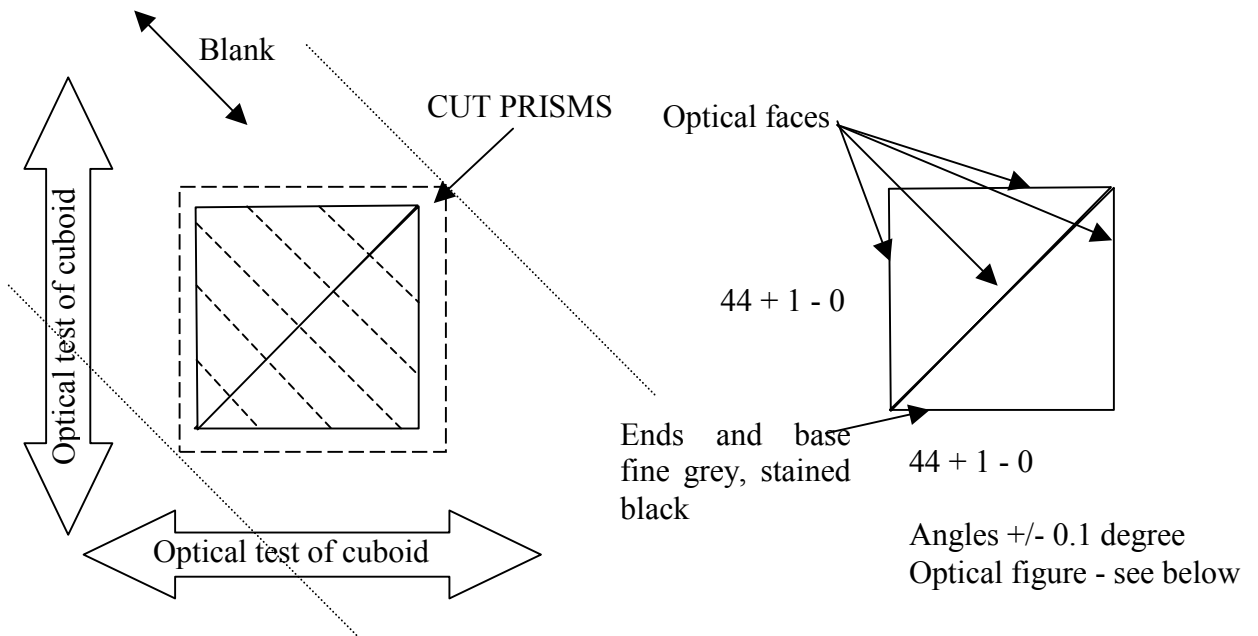


FIGURE 7
Cutting

FIGURE 8
Finished. Sizes in mm

1. Procure or produce a blank giving less than 0.5 wave OPD error in visible light peak to valley in transmission in single pass in ~ 50 mm thickness over ~ 50 mm x 80 mm. Optical tests of the blank need to be performed in two orthogonal directions, as indicated in Figure 7. The dashed lines in Figure 7 show the preferred plane of striations (if any) in the material. (The material supplier will understand this.)
2. Mark out a square prism in relation to the optical test directions, as shown in Figure 7, but allowing for two mm surplus material all over the optical faces, including 2 mm on each mating hypotenuse face.
3. Cut final ends to length.
4. Saw the two 45-degree triangular prisms. Reduce all the optical faces to size by removing approximately 2 mm glass with loose abrasive on each surface. Do not mill.
5. Polish the optical faces.
6. Figure the outer faces flat to 0.5 visible fringe p-v in reflection. Figure the hypotenuse face flat to 0.2 visible fringe p-v in reflection. Flatness tolerances apply to the reflected wavefront (not to the surface height) and are with respect to absolute flatness, the curvature tolerance being zero. All to 2 mm from edges. Generate chamfers approximately 1 mm x 45 degrees.

Doc. Number:	VIS-DES-UOD-06042-0001
Date:	8 th March 2004
Issue:	3.0
Page:	Page 99 of 99
Author:	Paul Clark

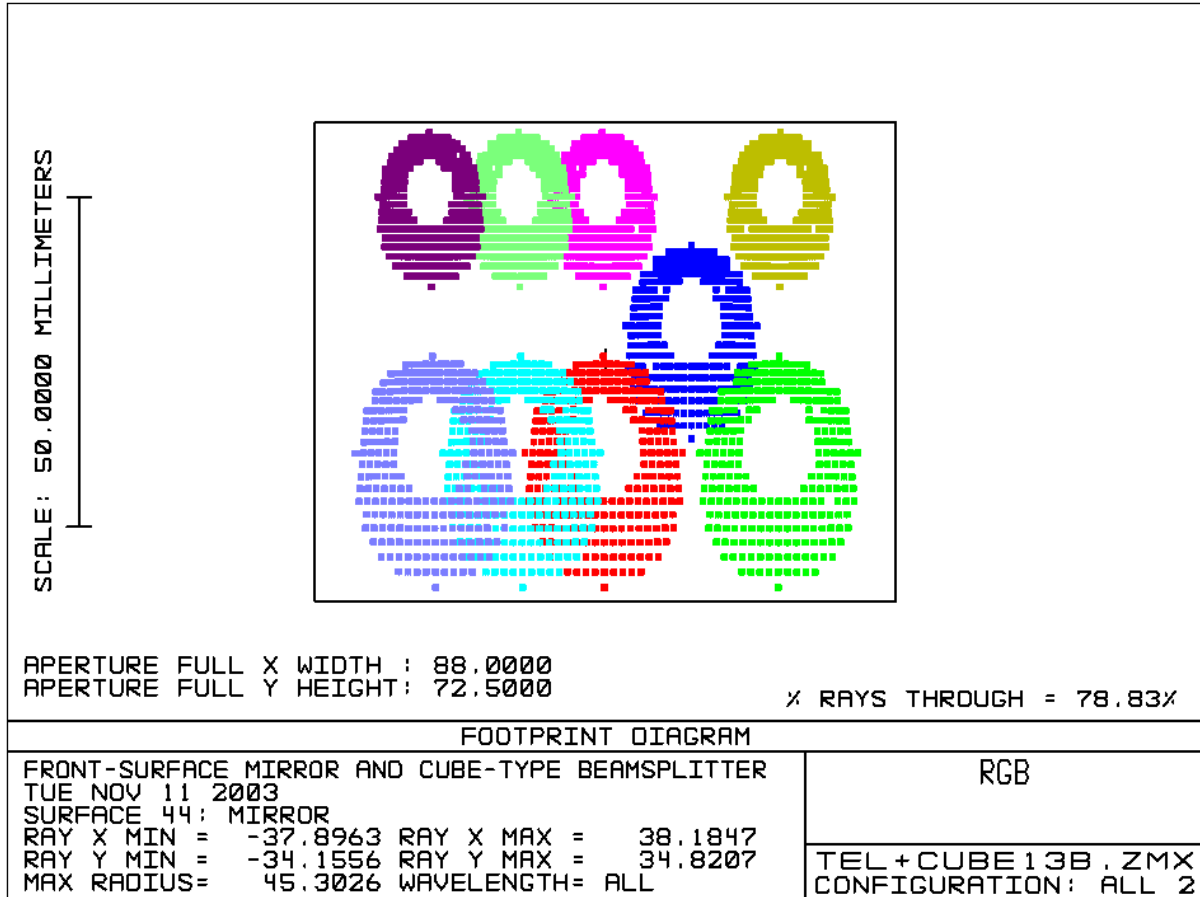


Figure 9

Figure 9 shows the mirror surface 88 x 72.5 mm with illumination patches for the field positions previously discussed. The mirror should be figured to 0.2 visible fringe p-v in the reflected wavefront overall with respect to absolute flatness, and if possible this quality should be maintained to 1.5 mm from the long edges, including any chamfer up to 0.5 mm. To achieve this on a stiff component, the mirror should be produced as the hypotenuse face of a triangular block.

Doc. Number:	VIS-DES-UOD-06042-0001
Date:	8 th March 2004
Issue:	3.0
Page:	Page 100 of 100
Author:	Paul Clark

The filter (Figure 10) is modelled as 74 x 44 x 3 mm. Figure each side flat to 0.5 visible fringes p-v in the reflected wavefront. Filter type to be specified by Durham. The LOCS and Autoguider areas are just separated (by 0.25 mm) at this point.

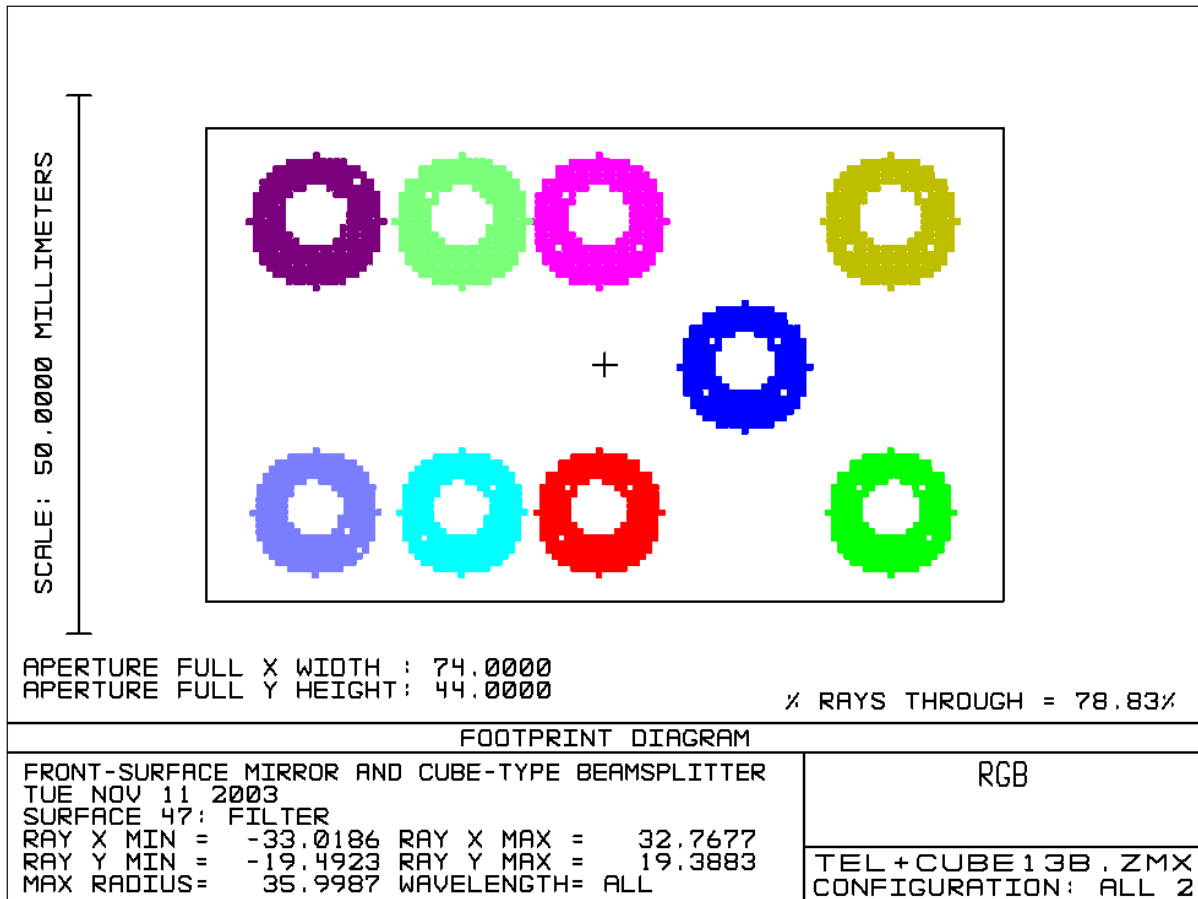
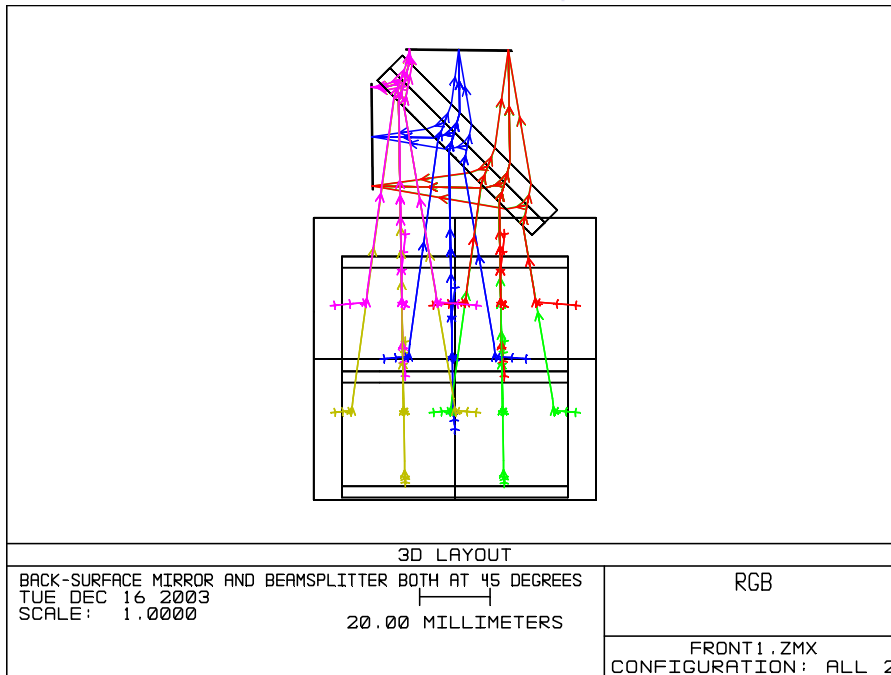
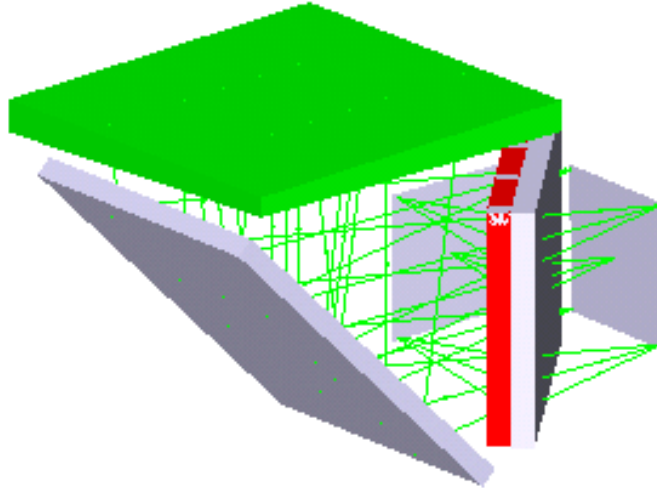


Figure 10

20 Appendix 7: Alternative Non-Cemented LOCS Design (R Bingham)



This solution aims to correct the astigmatism and coma in a beamsplitter of significant thickness. To do this it uses a back-surface mirror and a front corrector (shown green) that is wedged at a compound angle. This solution works in aberration terms but was not recommended, owing to the existence of the cube-beamsplitter solution; the cube solution avoids stray reflections from the close parallel surfaces of the mirror and beamsplitter and appears easier to produce.

Note. The plates of the beamsplitter shown above need not be cemented. The alternative is to use AR and beamsplitter coatings designed for 45 degrees incidence in vacuum, with thin shims (say 10 μm) providing a gap. Assemble in the optics factory.

21 Appendix 8: HOCS Optical Design Report (Richard Bingham)

Proposed optical designs for the High-Order Curvature Sensor (HOCS) for VISTA Optical Design and Analysis - Report

Richard G. Bingham
28 January 2004

21.1 Introduction and Summary

This is part of an optical design project for the VISTA wavefront sensors. The High Order Curvature Sensor is a passive optical device feeding one of the VISTA science detectors. It uses beamsplitters providing a pair of stellar images on the same detector surface at different positions of focus. Alternative layouts are based on:

Type A: A suggestion by Martin Caldwell, document VIS-TRE-UOD-06042-0004, page 13, 22 May 2003.

Types B and C: A suggestion by Richard Bingham dated 11 November 2003 (email to Paul Clark).

The sensor is required to operate at J and K_s wavebands. The following wavelengths are used here.

Band	Wavelength (microns)		
	50 % point	Centre	50 % point
J	1.16	1.25	1.34
K _s	1.99	2.15	2.31

The designed defocus distances are: 1.0, 1.5 and 2.1 mm. Type A provides images at these distances as + or -, one lying each side of focus. Types B and C provide one image at the stated defocus and one image in-focus. These designed defocus distances are changed by altering the thicknesses of the optical components. Type A will be seen to provide the best function. Type B is a lower-cost option as regards optical manufacturing. Type C is a similar low-cost option that is included for completeness, but it requires a wide dynamic range of measured intensity and would need further study.

{Note: Types B & C would potentially allow the HOWFS to be implemented as a Phase Diversity sensor, rather than a Curvature Sensor. They are included here for completeness but only Type A is currently being considered for inclusion within the IR Camera. Phase

Doc. Number:	VIS-DES-UOD-06042-0001
Date:	8 th March 2004
Issue:	3.0
Page:	Page 103 of 103
Author:	Paul Clark

diversity has previously been used by the NAOS-CONICA development team to analyse aberrations within the instrument.}

It may be noted that in any of these arrangements, with an even number of reflections in both the light paths, each out-of-focus image will have the same parity as the other in relation to the main optics. Where an image passes through the focus, it is effectively rotated 180 degrees without reversal of parity.

All optical studies included the complete optical system of the telescope, but not seeing. This report also includes reasonably comprehensive consideration of stray and scattered light. Geometrical ray tracing is used in the main, but a trial with coherent imaging is also shown. The two operating wavebands, two layout options and three defocus distances give rise to twelve possible designs. There are also options for the beamsplitter's splitting fractions.

In principle, any of these devices may be moved either laterally or in the focus (axial) direction.

21.2 Materials

In common with the LOCS, these devices are formed with cemented prism elements that must resist cooling. This technology is possibly subject to further discussion and experiment, but the most likely material to be selected is Heraeus Infrasil and that is adopted here. A change of material would not be excessively complicated to introduce in this design phase, but there would be small changes to the thicknesses of the optical elements.

21.3 Beamsplitter coatings

Transmission, reflection and absorption coefficients are stated for various coatings used in this design exercise, and it is indicated how the choice of these coefficients affects the results. For procurement, the beamsplitter coatings should be specified in terms of desired coefficients.

21.4 Optical Diagrams for Type A, on axis

The six Figures 1a to 1f show Type A devices for the two wavebands and three defocus distances. Actual dimensions are tabulated later. The beamsplitter blocks are cuboids with square end faces. Ray tracing and diagrams relate to the whole optical system including the lenses of the infrared camera, but for clarity, only the beamsplitter section is reproduced. It may be seen that the model includes multiple reflections. Figures 1a to 1f do *not* show that some rays correspond to greatly reduced intensities (this is quantified later).

To model both the required rays and the stray light, the end surfaces of the prism block are assigned nominal $\lambda/4$ anti-reflection coatings. The side faces are modelled with a purely

Doc. Number:	VIS-DES-UOD-06042-0001
Date:	8 th March 2004
Issue:	3.0
Page:	Page 104 of 104
Author:	Paul Clark

nominal black surface, absorbing 95 per cent. Of the five per cent reflected light from these side faces, 30 per cent is specular and 70 per cent is scattered according to the Lambertian rule. The whole VISTA optical system is included here (although out of the diagram) and again the lens faces of the IR camera are assigned nominal $\lambda/4$ anti-reflection coatings. In practice, stray reflections from the lens faces, and scattered light, contribute negligible brightness in Types A and B.

A single angle, 25 degrees, is used for the tilted slab in all these cases. Other angles were investigated, but no advantage was found. In any case, using a variety of angles within the range of devices would complicate production. The chosen value is not critical but there are general considerations. Angles much less than 25 degrees give less satisfactory clearance between the images and the unwanted, subsidiary reflections that ray tracing discloses. Angles much larger than 25 degrees give a rather thin edge on the outer elements (as the length of the cuboid is fixed for a given defocus), making manufacturing unnecessarily critical. 25 degrees is also, incidentally, about the largest angle that can be used on some beamsplitters without introducing significant polarisation, although low polarisation was not specified in this project.

The devices are inserted in substitution for the colour filters, and provide the calculated defocus on the standard science focal plane array, having removed the known filter thicknesses. The devices themselves require the application of colour filters on the entrance face.

Doc. Number:	VIS-DES-UOD-06042-0001
Date:	8 th March 2004
Issue:	3.0
Page:	Page 105 of 105
Author:	Paul Clark

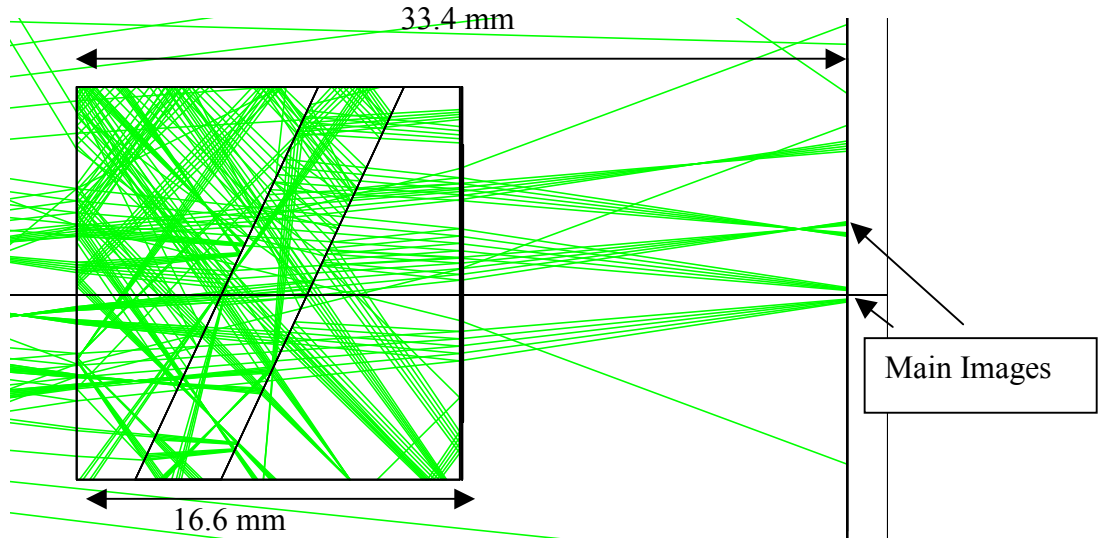


Figure 1a. HOCS type A, J band, with +/- 2.1 mm defocus. For other dimensions, see table. The front surface of each HOCS device shown in this paper is 33.4 mm ahead of focus.

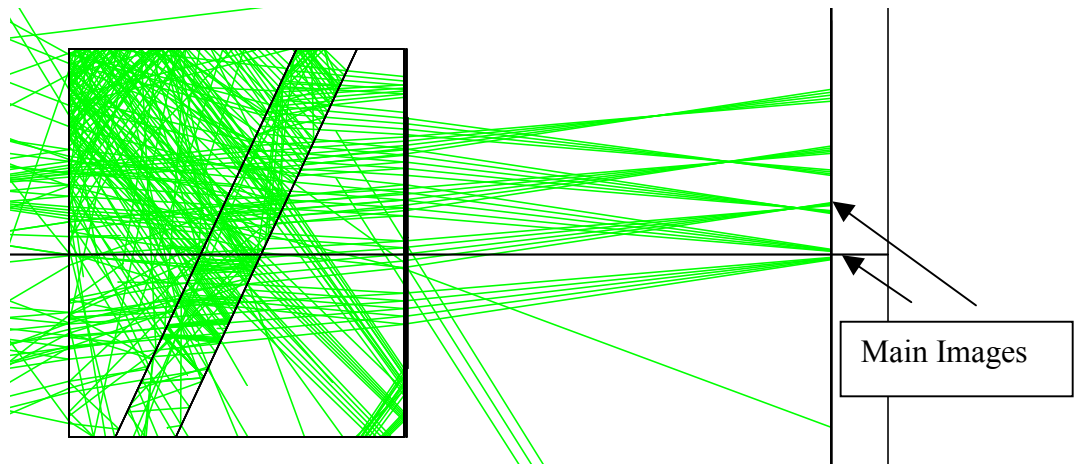


Figure 1b. HOCS type A, J band, with +/- 1.5 mm defocus

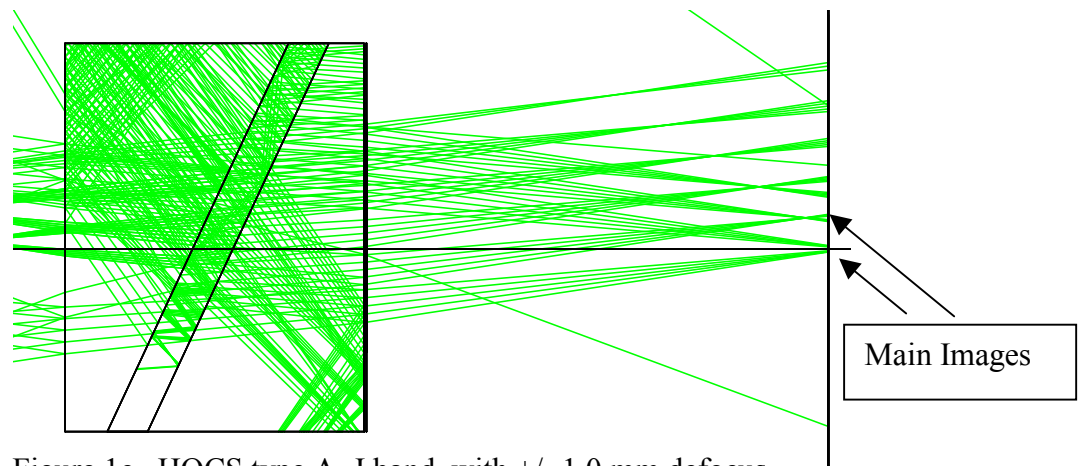


Figure 1c. HOCS type A, J band, with +/- 1.0 mm defocus

Doc. Number:	VIS-DES-UOD-06042-0001
Date:	8 th March 2004
Issue:	3.0
Page:	Page 106 of 106
Author:	Paul Clark

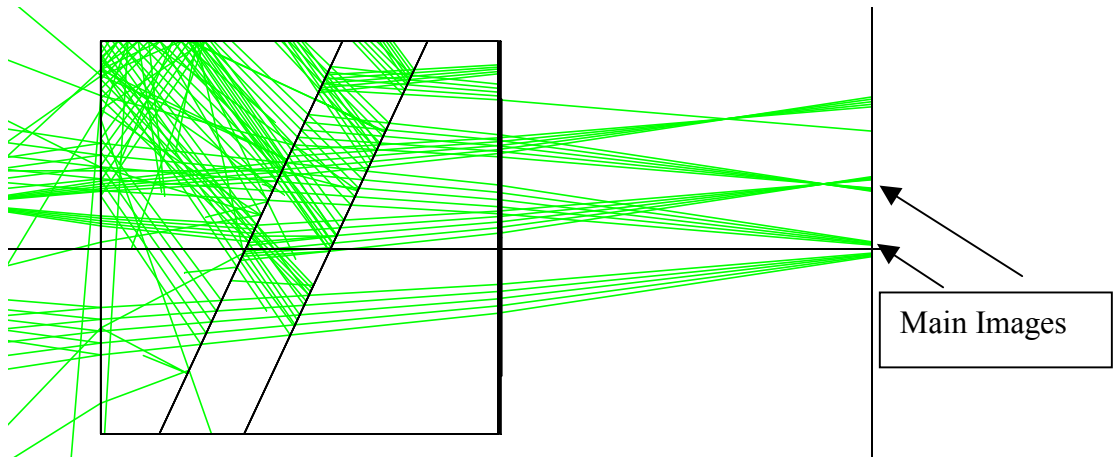


Figure 1d. HOCS type A, Ks band, with +/- 2.1 mm defocus. For other dimensions, see table.

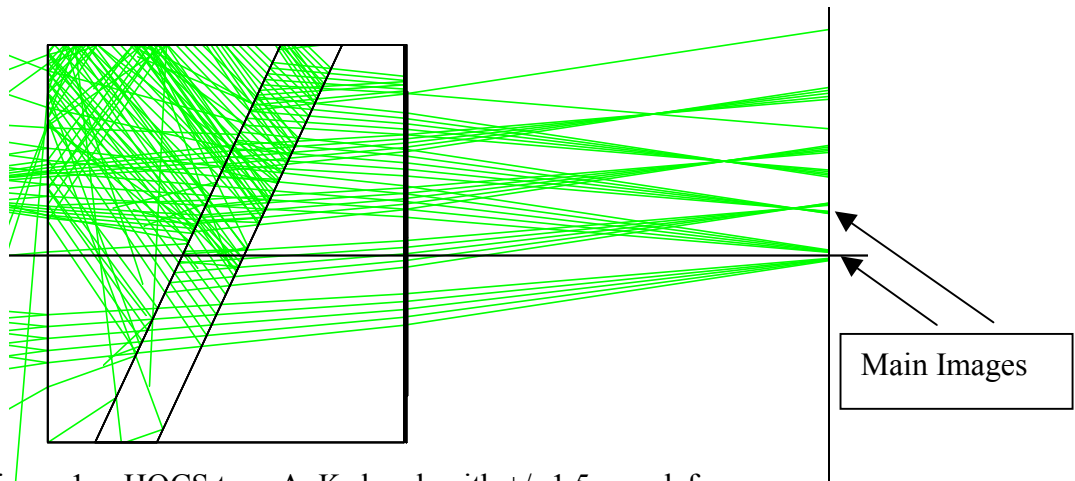


Figure 1e. HOCS type A, Ks band, with +/- 1.5 mm defocus

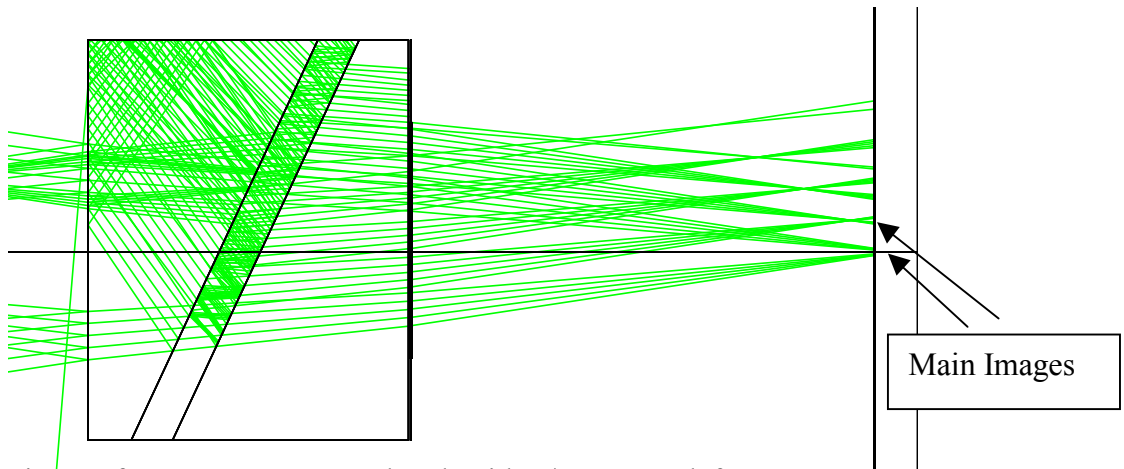


Figure 1f. HOCS type A, Ks band, with +/- 1.0 mm defocus

Doc. Number:	VIS-DES-UOD-06042-0001
Date:	8 th March 2004
Issue:	3.0
Page:	Page 107 of 107
Author:	Paul Clark

21.4.1 Dimensions and tolerances for Type A

The fabricated cuboid blocks for the six sub-type devices of Type A have the same sized entrance and exit faces (17 mm square) and the same angles for the immersed beamsplitter slab. However, the six devices have significantly different overall lengths. The immersed beamsplitters require only slightly differing thicknesses for J and Ks, so that an average can be used and only three different thicknesses are required in that case.

Figure 2 shows the construction of a device and the symbols used in Table I for the dimensions.

Dimension D is that used for ray tracing, whereas dimension C is required for production.

$C = D \times \cosine (25 \text{ degrees})$.

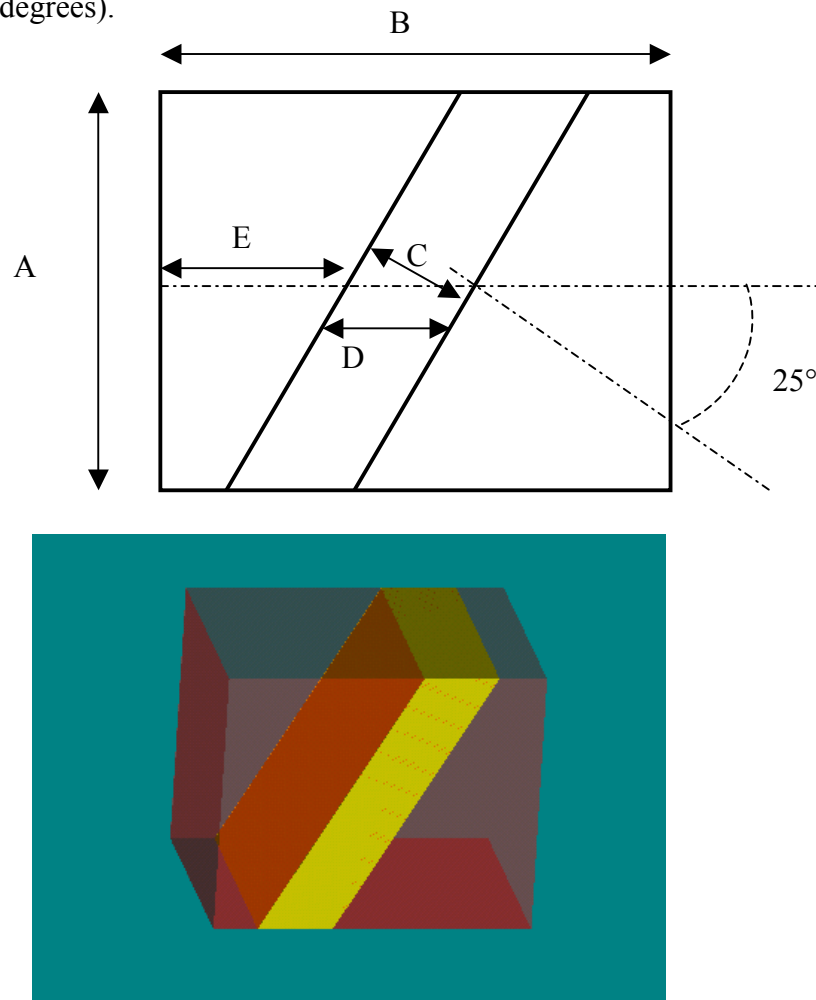


Figure 2. Diagram and illustration showing the construction of the device and the symbols used here for its dimensions.

Table 1

	HOCS beamsplitter Type A Dimensions in mm			
		J	Ks	Mean J & Ks
+/- 2.1 mm defocus	Overall cube length B	16.60	17.20	
	Tilted splitter, axial D	3.72	3.68	3.70
	Normal to splitter C			3.35
	Immersion depth E	6.50	6.50	
	Min. exit aperture diameter	12	12	
+/- 1.5 mm defocus	Overall cube	14.68	15.23	
	Tilted splitter, axial D	2.65	2.63	2.64
	Normal to splitter C			2.39
	Immersion depth E	6.00	6.00	
	Min. exit aperture diameter	11	11	
+/- 1.0 mm defocus	Overall cube	13.07	13.60	
	Tilted splitter, axial D	1.77	1.75	1.76
	Normal to splitter C			1.60
	Immersion depth E	5.80	5.80	
	Min. exit aperture diameter	10	10	

Material – Heraeus Infrasil

Entrance and exit faces are 17.0 mm square (dimension A).

The beam size on the entrance face of the HOCS on-axis is 10.6 mm diameter.

Dimensions D are axial segments as used in ZEMAX. The thickness of the splitter normal C to the beamsplitter surfaces is obtained by multiplying these figures by cosine 25 degrees.

All the HOCS devices in this document are shown with a front surface that is 33.4 mm ahead of the focal plane, but if so required, they can be moved towards the focal plane.

Table 2

Dimensional tolerances	mm
A	+/- 0.1
B	+/- 0.03
C	+/- 0.01
D	Not a specified dimension
E	+/- 0.20
Angles	+/- 1 arc min
Mount square	+/- 0.1 mm across A

Clear apertures of polished faces are up to 2 mm smaller all round than the overall size. Within this, chamfer 0.5 mm x 45 degrees. Thus the polished clear apertures of the entrance and exit faces should be >13 mm square. For an on-axis device, if required, the entrance face

Doc. Number:	VIS-DES-UOD-06042-0001
Date:	8 th March 2004
Issue:	3.0
Page:	Page 109 of 109
Author:	Paul Clark

can be limited to 12 mm diameter and the exit face to the diameters shown in Table I. However, limiting these apertures to circles may slightly reduce the ability to find stars subject to small pointing errors and is not recommended for devices used off-axis, as a special study might be required for placing the device accurately.

Polish the square ends to ± 0.3 visible fringe p-v. Apply colour filter coatings and anti-reflection coatings for relevant wavelength ranges.

Polish the diagonal faces on all three parts to 0.1 visible fringe p-v. Beamsplitter coatings on front face of immersed part and front face of following part.

Side faces to be fine grey, true to shape to ± 0.1 mm. Finish sides black.

21.4.2 Sample Images

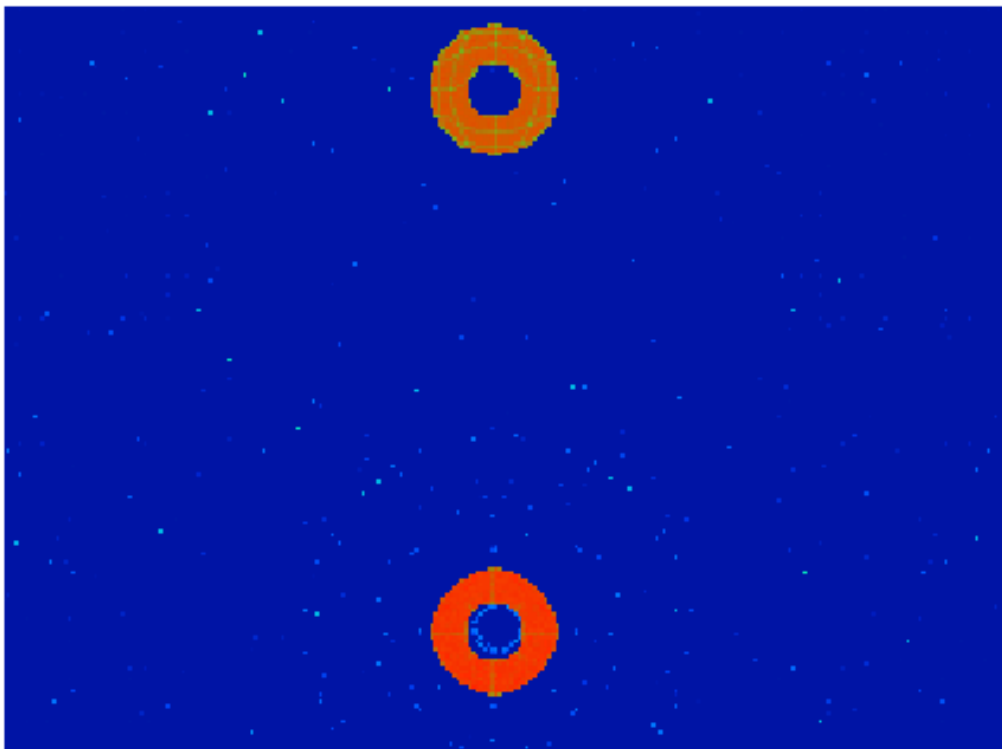


Figure 3. The image yielded by this system with a 14:70:16 beamsplitter (see text). See Figure 4 for the colour scale.

Figure 3 shows a typical intensity distribution on the focal surface, including some scattered light and multiple reflections, which fortunately, are low in brightness. Figure 4 is the same

Doc. Number:	VIS-DES-UOD-06042-0001
Date:	8 th March 2004
Issue:	3.0
Page:	Page 110 of 110
Author:	Paul Clark

plot on a small scale, showing subsidiary reflections and including the logarithmic scale of relative intensities.

The two major images have comparable relative intensities due to assumptions adopted for the beamsplitter, defining the reflection and transmission coefficients. In this case, transmission is 14%, reflection 70%, and absorption 16% (14:70:16).

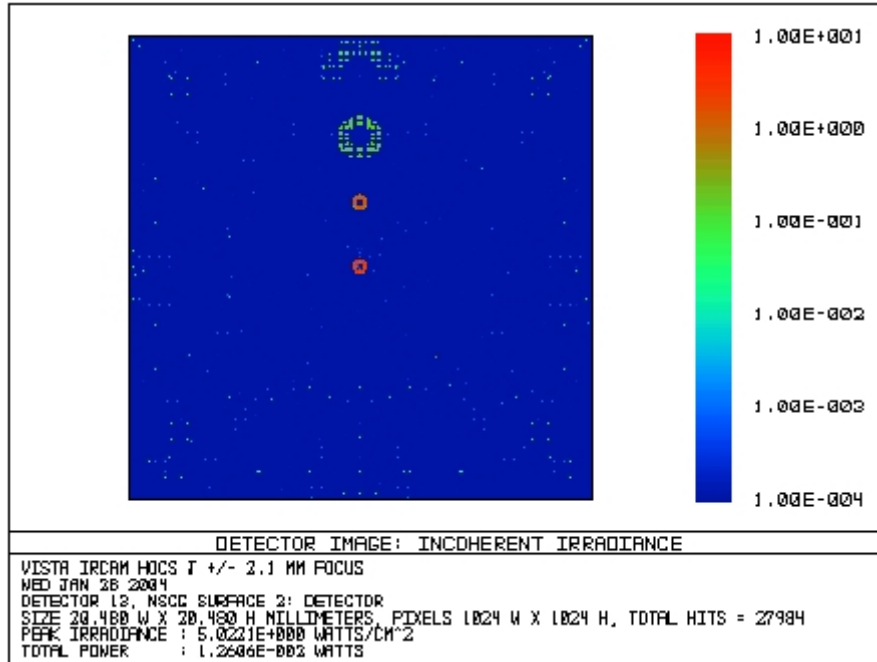


Figure 4. As Figure 3, with intensity scale. The image is obtained with a 14:70:16 beamsplitter.

Figure 5 shows the illumination provided by a “50-50” beamsplitter (see caption). The colour key is the same as in Figure 4. The image sampling is illustrated in more detail in Figure 6, where the illustration resolves the 20-micron pixels.

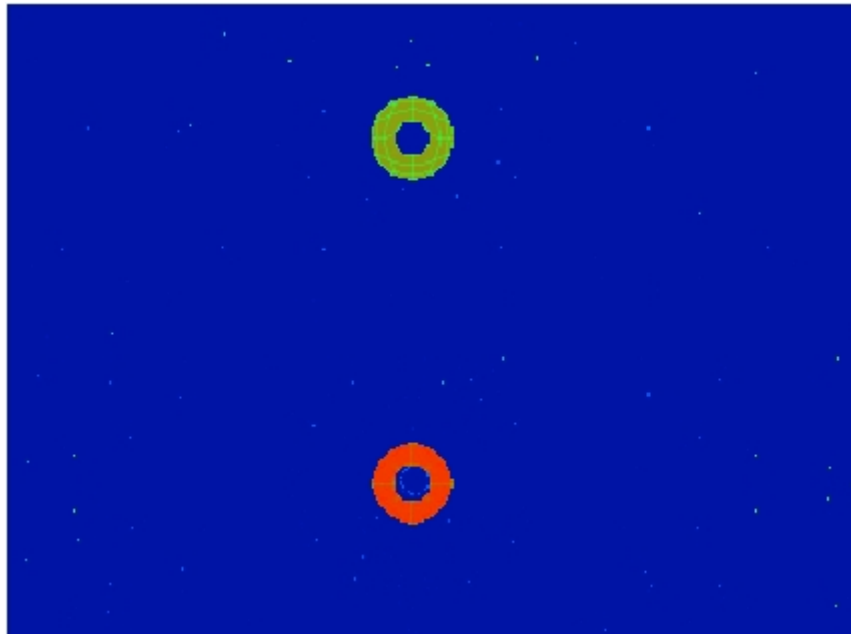


Figure 5. This image is obtained with ± 2.1 mm defocus in J and a 41:39:20 beamsplitter. The colour key for $\log(\text{relative irradiance})$ is the same as in Figure 4. (A larger number of rays is used for these images, giving a more realistic appearance to the size of the central shadows than appears in the ray diagrams.)

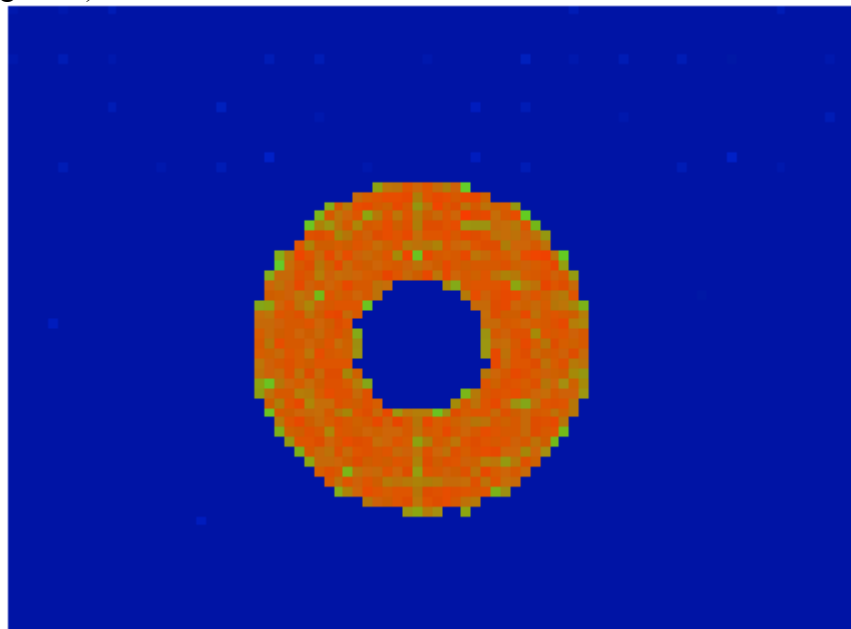


Figure 6. A typical polychromatic image 2.1 mm past focus in J (incoherent summation in this case). This illustrates the sampling with 20-micron pixels. The optics of the telescope are fully modelled, without the atmosphere.

21.4.3 A Trial Aberration in the Telescope

In Figures 7 to 9, a possible application of the sensor has been tested by means of setting up a trial aberration in the telescope, such as might occur in practice. For this exercise, the conic constant of the primary mirror has been changed by +0.0003, giving an increment of about 1.6 microns of spherical aberration in reflection. Figure 7 first shows images obtained from the nominal, unmodified telescope at ± 1.0 mm focus shift. Figures 8 and 9 show how the sensor responds to the trial aberration, which may also be seen as a plot of the wavefront profile by comparing Figures 10 and 11. The images have not been re-analysed but appear satisfactory.

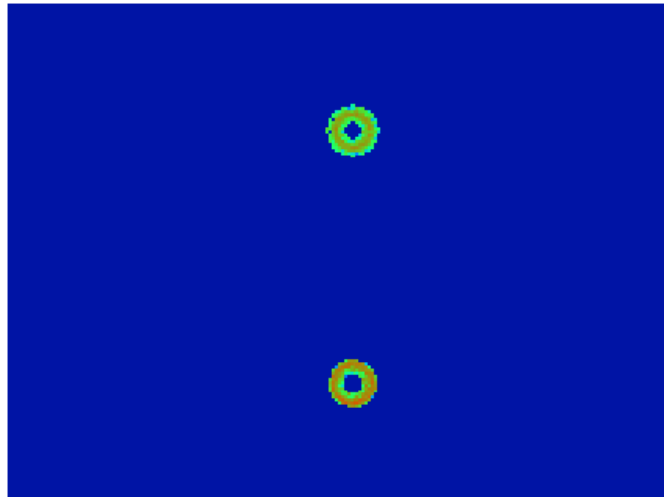


Figure 7. Monochromatic 1.25 nm, coherent (9 microns coherence length), nominal telescope, ± 1 mm defocus (no seeing)

Figure 8 shows the effect obtained when the aberration is present.

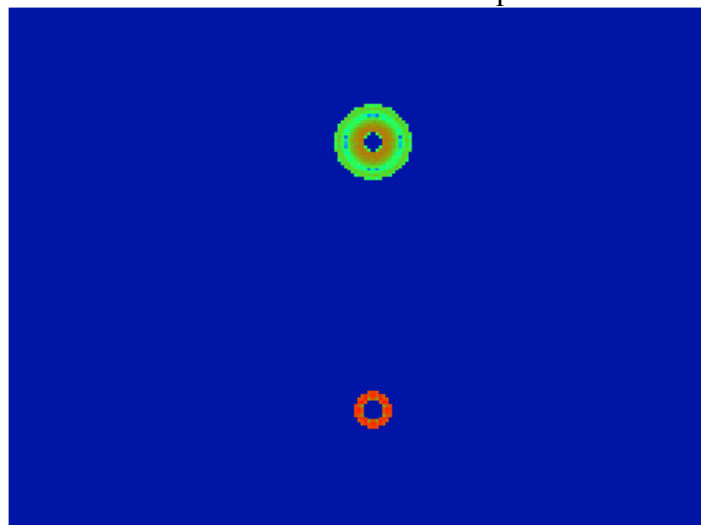


Figure 8. Monochromatic 1.25 nm, coherent, aberrated primary mirror

Doc. Number:	VIS-DES-UOD-06042-0001
Date:	8 th March 2004
Issue:	3.0
Page:	Page 113 of 113
Author:	Paul Clark

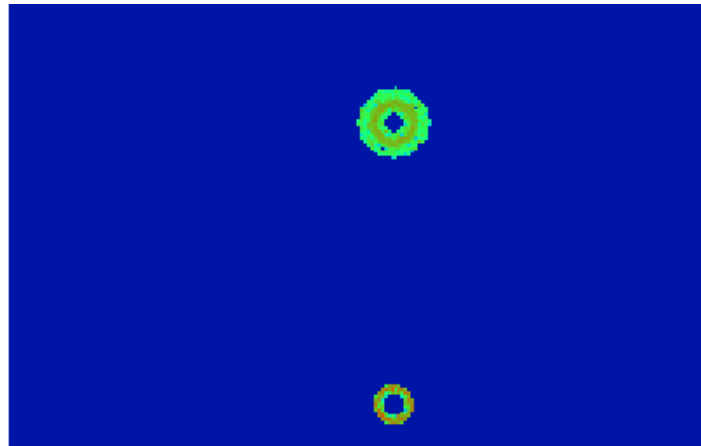


Figure 9 With the three J wavelengths, separately coherent, aberrated primary mirror (In this exercise, the separation of the two images on the detector is slightly larger than in the final design of the sensor.)

Doc. Number:	VIS-DES-UOD-06042-0001
Date:	8 th March 2004
Issue:	3.0
Page:	Page 114 of 114
Author:	Paul Clark

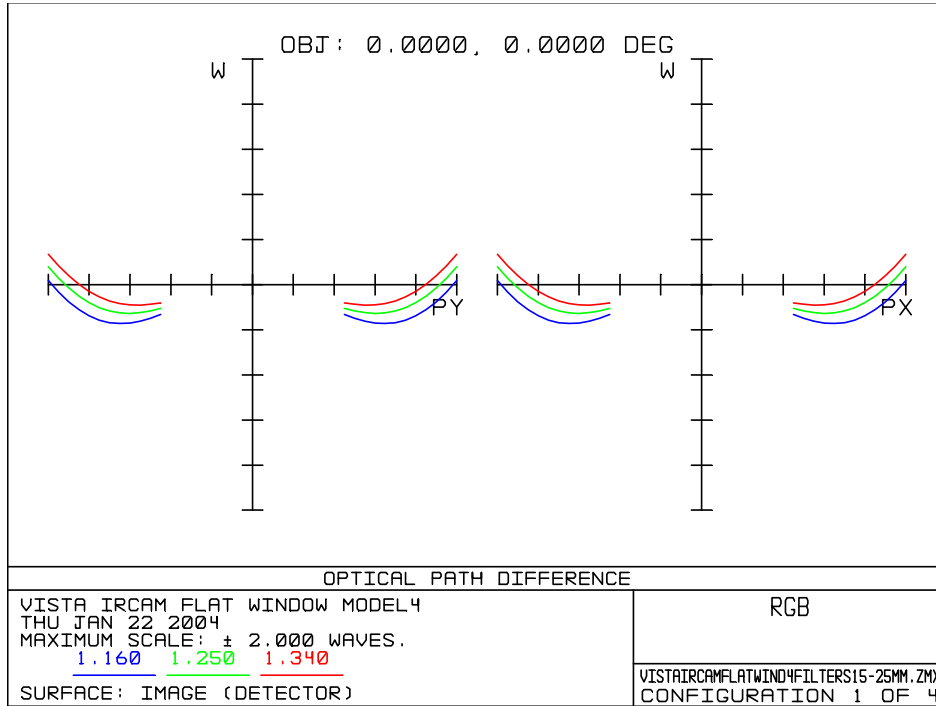


Figure 10. A diagram of wavefront aberration in the nominal telescope. Scale +/- 2 waves

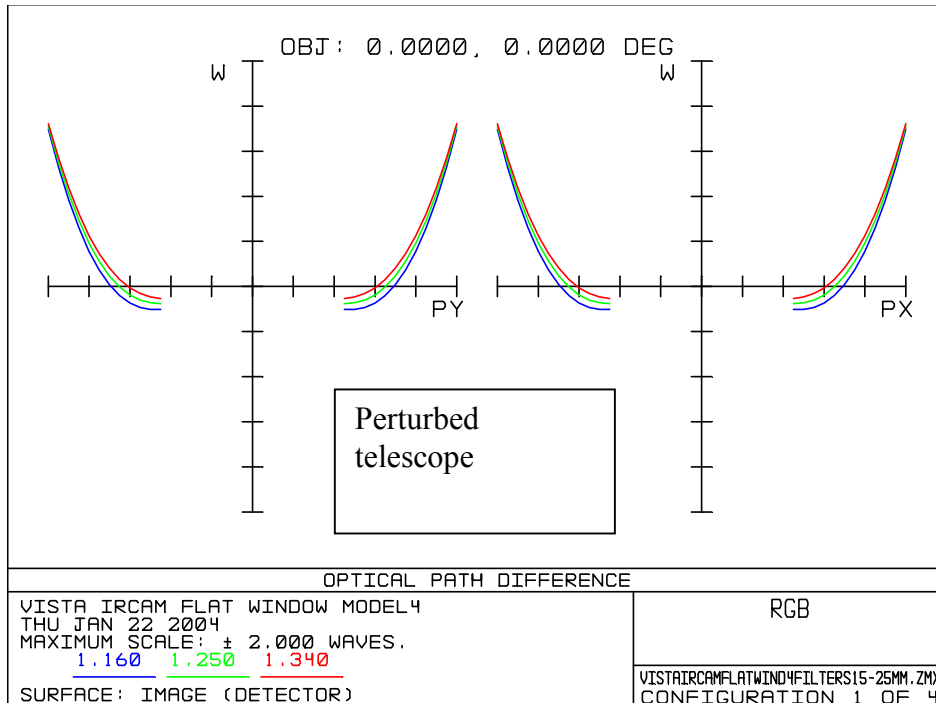


Figure 11. A diagram of wavefront aberration in the notionally perturbed telescope on the same scale.

Doc. Number:	VIS-DES-UOD-06042-0001
Date:	8 th March 2004
Issue:	3.0
Page:	Page 115 of 115
Author:	Paul Clark

21.4.4 Aberrations in the beamsplitters

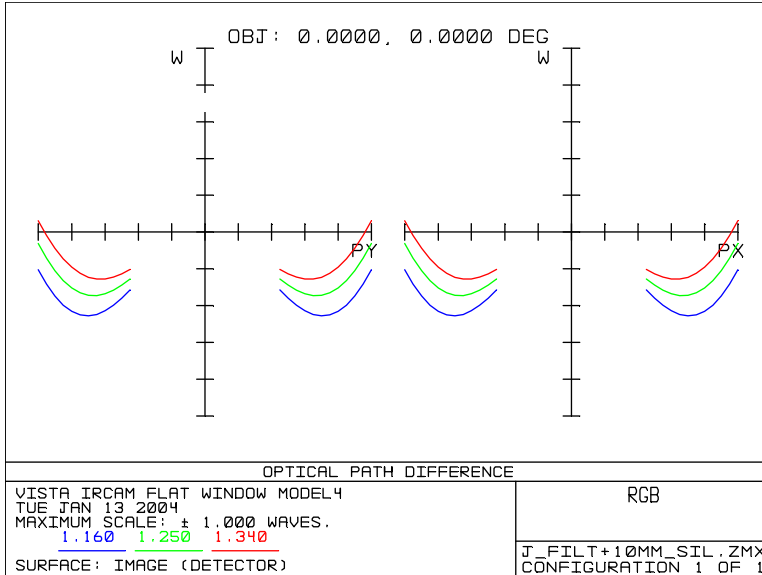
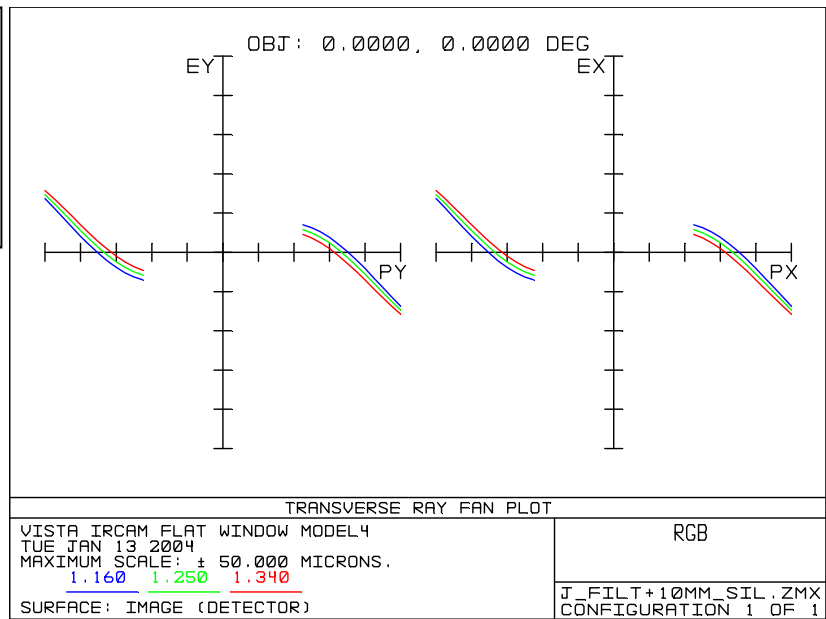


Figure 12. OPD aberrations with the standard 10 mm filter and no HOCS. Scale +/- one wavelength.

Figure 13. Transverse ray aberrations with the standard 10 mm filter and no HOCS. Scale +/- 50 microns.



Figures 12 and 13 above show the aberrations of VISTA re-focused for the best image on-axis in the J band with the standard 10 mm filter thickness, scale +/- 1 wave.

Figures 14 and 15 below show the aberrations of VISTA refocused again on-axis in the J band with 25 mm additional optical path in the prism block. The additional aberration is proportional to this thickness, the value of 25 mm being used here as a reference. It may be seen that aberrations are not much affected by the insertion of the HOCS elements, which have up to only 16.6 mm thickness.

Doc. Number:	VIS-DES-UOD-06042-0001
Date:	8 th March 2004
Issue:	3.0
Page:	Page 116 of 116
Author:	Paul Clark

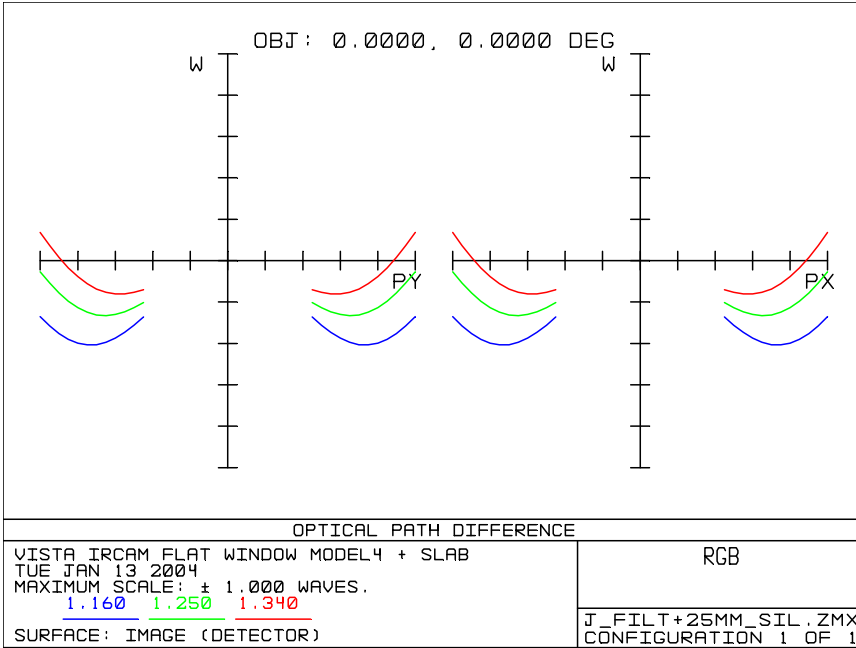


Figure 14. OPD aberrations with 25 mm silica. Scale +/- one wavelength.

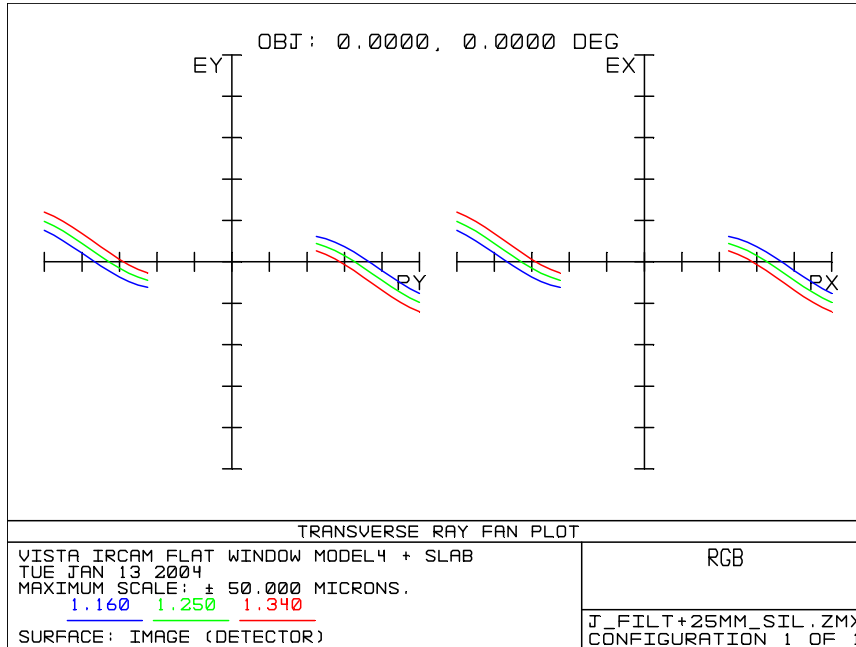


Figure 15. Transverse ray aberrations with 25 mm silica. Scale +/- 50 microns

Doc. Number:	VIS-DES-UOD-06042-0001
Date:	8 th March 2004
Issue:	3.0
Page:	Page 117 of 117
Author:	Paul Clark

21.4.5 The Curvature Sensor placed Off-Axis

There is a requirement to use the High Order Curvature Sensor up to 137.2 mm off-axis. This requirement has been investigated by moving a device and a star image off-axis in the ray trace. Figure 16 shows the ray diagram. It may be seen that the off-axis effect is quite large. With a fairly fast optical system such as this, pupil aberrations are present and may be more apparent off-axis. The effect is that rays having passed through the lens system no longer appear to originate from a uniform circular aperture on-axis with a symmetrical central obscuration. Whilst the effect can be analysed, it may raise a degree of complexity for the curvature sensor.

In Figure 17, the corresponding image intensity is analysed for this off-axis position. Large distortions of the apparent pupil may be seen. These out-of-focus images are not in planes where the pupil is imaged, but they are nevertheless affected by pupil aberrations. This effect will require special consideration in the reduction algorithms.

{Note: The Simplex-based curvature sensing aberration measurement algorithm includes a model of the telescope and camera. The extra focal images are produced by ray tracing and take into consideration the off-axis position of the central obscuration. As described in AD02 section 4, the accuracy of the technique has been validated by comparing the ray-traced extra-focal images against those produced by Fresnel-propagation image generation.}

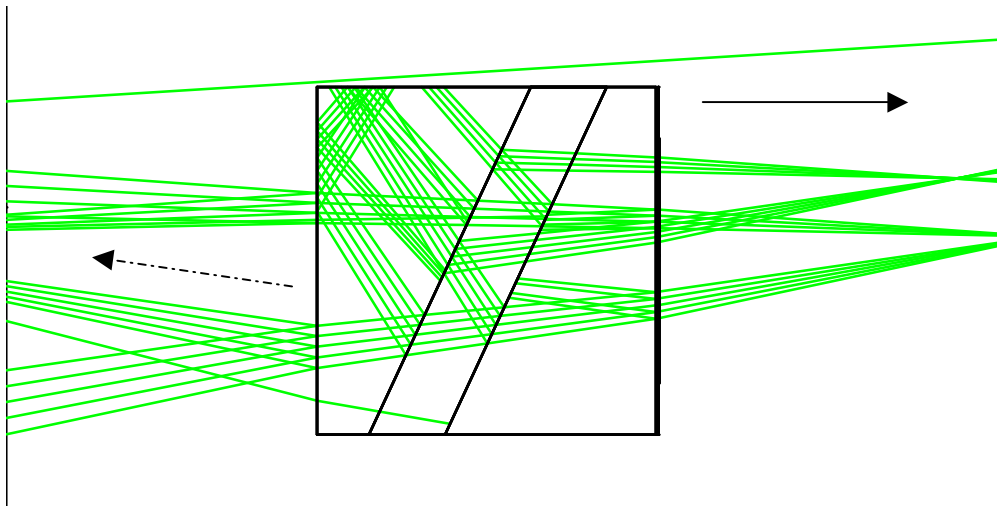


Figure 16. The diagram shows the HOCS type A with ± 2.1 mm defocus in the J waveband. This ray diagram is obtained with the device placed 136 mm off-axis for a field point at 137.2 mm.

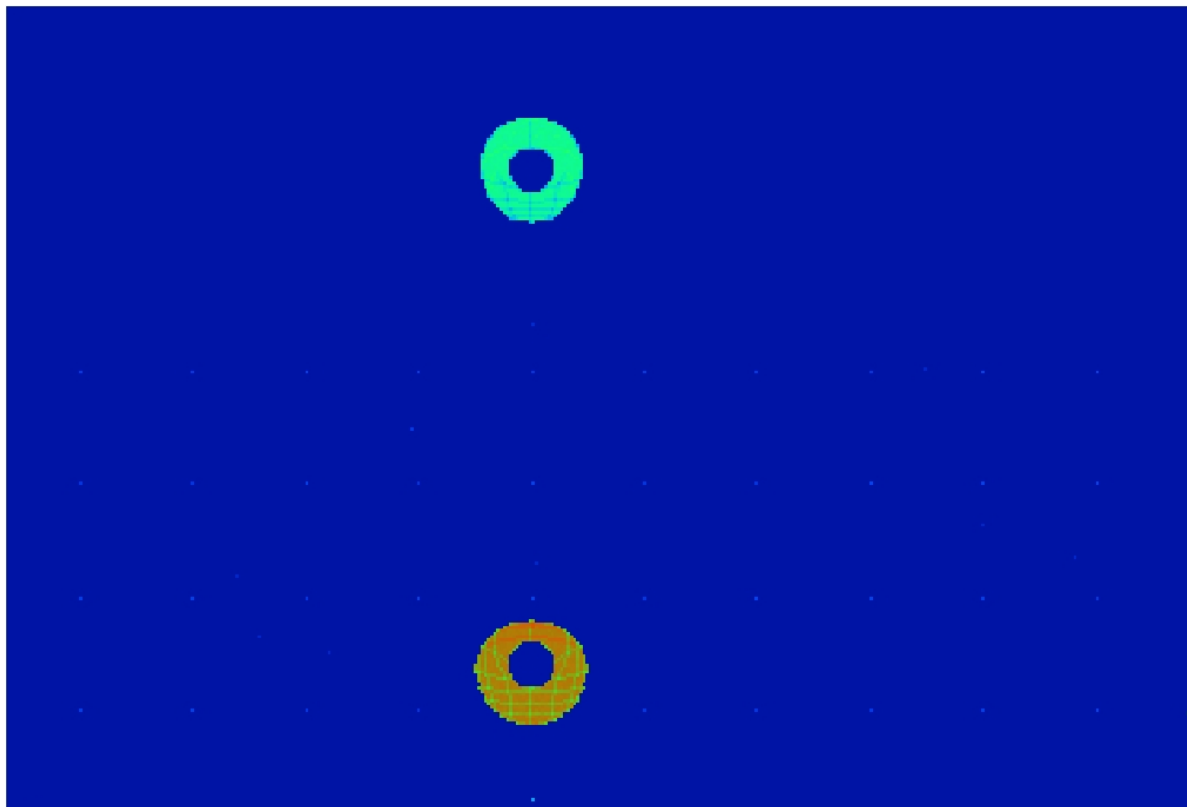


Figure 17. The intensity plot for an off-axis star as in Figure 16

21.5 Curvature Sensor Type B

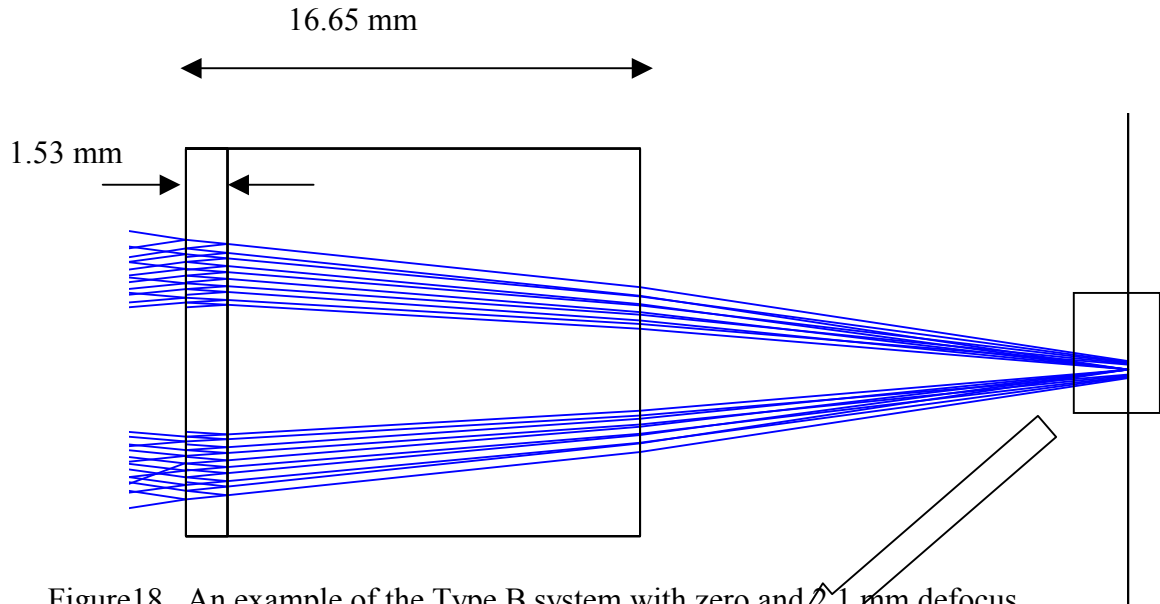


Figure18. An example of the Type B system with zero and 2.1 mm defocus

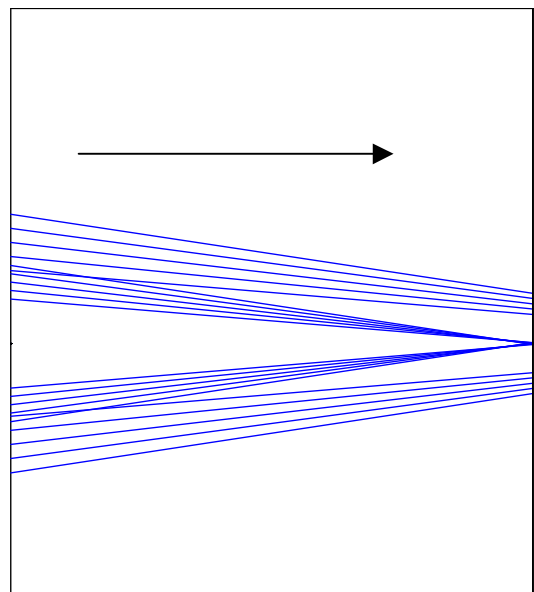


Figure19. Formation of inner and outer images in Layout 2

Figures 18 and 19 show devices of type B. An outer image is defocused to the right, beyond the detector. The defocus distance (2.1 mm in this case) is provided by the total thickness of glass, and an inner image is brought back into focus by the two reflections at the beamsplitter part. The inner image appears in the central shadow in the main image, as shown in the enlarged diagram in Figure 19. In this case, the beamsplitter is not tilted to obtain a separate

image and also, need not be immersed. If it is satisfactory as a curvature sensor, this arrangement may have a considerably lower cost. A decision on this choice will involve the algorithm for using this type of sensor (with one image in focus), and will involve the effect of seeing.

In Type B, it is possible to reduce the relative brightness of the in-focus image by giving the beamsplitter surfaces high transmission and low reflectivity. Clearly, the in-focus image should not be *fainter* than the diffuse image. Figure 20 shows images computed through the whole VISTA system for beamsplitter surfaces of 4:1 transmission to reflection ratio and a defocus of 2.1 mm for the outer image. The relatively low reflectivity has also served to suppress multiple reflections within the beamsplitter section.

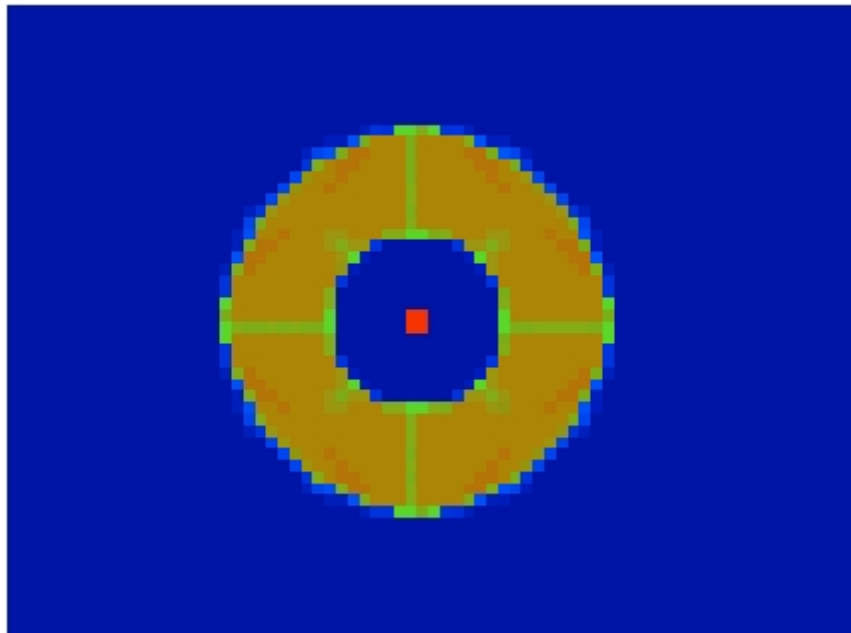


Figure 20. Concentric images in Type B. The colour scale is the same as before. No seeing. This analysis includes the use of 20 micron pixels that are resolved in the figure.

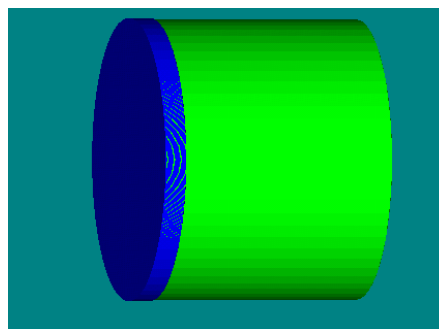


Figure 21. Further illustration of the device type B.

21.6 Curvature Sensor Type C

There exists an alternative arrangement to type B in which the direct image is in focus and the defocused image is pulled forward by the beamsplitter. The defocused image in that case is beyond focus rather than short of focus. This is shown in Figure 22.

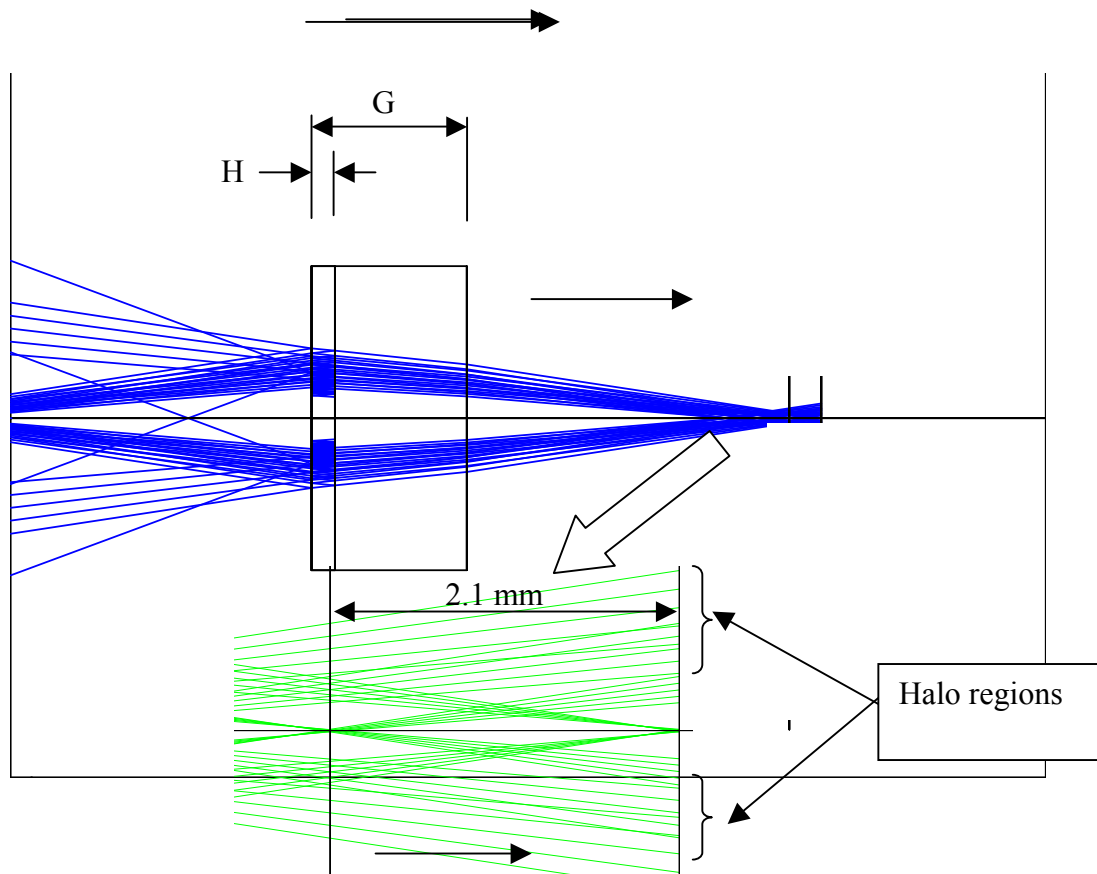


Figure 22. Type C. A normal image in focus, plus an image pulled back 2.1 mm by double reflection on the immersed beamsplitter layers. Diameter 20 mm, clear aperture 16 mm. The outer rays illustrate an additional double reflection (see text).

Type C is problematical owing to the dynamic range of intensity. In this Type C, the focused image cannot be kept down in surface brightness, owing to the two fewer reflections that it sees. High reflectivities may help (albeit with a loss of transmission), but cannot brighten the diffuse image to balance the smaller size of the focused image. Also, multiple reflections within the beamsplitter layer would be enhanced by high reflectivity and give rise to an outer halo as shown in Figure 22. It is possible that such halo regions can be kept outside the main image, but for these reasons, further investigation would be needed before Type C could be implemented.

21.7 Dimensions of devices types B and C

HOCS beamsplitter Type B Dimensions in mm			
		J	Ks
+2.1 & 0 mm defocus	Overall thickness G	16.60	17.21
	Splitter part, axial H	1.53	1.51
+1.5 & 0 mm defocus	Overall thickness G	14.67	15.24
	Splitter part, axial H	1.09	1.08
+1.0 & 0 mm defocus	Overall thickness G	13.07	13.60
	Splitter part, axial H	0.73	0.72

HOCS beamsplitter Type C Dimensions in mm			
		J	Ks
-2.1 & 0 mm defocus	Overall thickness G	9.87	10.32
	Splitter part, axial H	1.53	1.51
-1.5 & 0 mm defocus	Overall thickness G	9.87	10.32
	Splitter part, axial H	1.09	1.08
- 1.0 & 0 mm defocus	Overall thickness G	9.87	10.32
	Splitter part, axial H	0.73	0.72

G is the *total* thickness and is toleranced.

Tolerances are the same as for Type B.

Average thicknesses for the splitter part can be used (for J and Ks).

22 Appendix 9: Stray Light Analysis (Marc Ferlet)

Ghost analysis IRCAM / WFS

Marc Ferlet, RAL/SSTD-OSG (20/02/2004)

22.1 Introduction

This note summarises the evaluation of the ghost images formed on the IRCAM FPA from bright objects in the WFS FoV. These are expected to arise from non-absorbed multiple reflections within the refractive filtering element of the WFS system located just after the pick-off mirror (POM). Section 2 below attempts to quantify the equivalent brightness of possible ghosts from the knowledge of the WFS component characteristics while the optical model runs are described in section 3. Conclusions are drawn in section 4.

22.2 Model for ghost equivalent brightness

Following the same approach as in RD1, the approximate equivalent magnitude of the ghost eventually generated at the IRCAM focal plane can be estimated via:

$$m_{ghost} \approx M_{star} - 2.5 \log\left(\frac{Att_{ghost}}{S_{ghost}}\right)$$

with S_{ghost} being the size of the ghost image extent at

the IRCAM focal plane (converted in arcsec² via the plate scale) and Att_{ghost} being the attenuation of the point source illumination generating the ghost image after interaction. From the properties of the WFS present design (RG9 glass substrate), one can then estimate the relative attenuation for a beam out-of-WFS band but in IRCAM science band, being reflected by the interference filter on the back surface (beamsplitter side). The table below summarises this with the following assumption: attenuation at the POM is based on transmission (~98%) at the front AR coating, double pass after reflection (~98%) on the interference filter coating. Attenuation at FPA is the same with an added 1.5% reflection on any camera lens.

Lambda (nm)	Bulk transmission (for 3mm thick RG9)	Bulk transmission for RG9 (double pass)	Imaginary part of the refractive index	Ghost relative attenuation WFS POM	Ghost relative attenuation at FPA
690	0.00%		2.11E-04		
700	0.30%		1.08E-04		
710	8.00%		4.76E-05		
720	32.00%		2.18E-05		
730	61.00%		9.57E-06		
740	80.00%		4.38E-06		
750	90.00%		2.10E-06		
760	94.00%		1.25E-06		
770	95.00%		1.05E-06		
780	96.00%		8.45E-07		
790	96.00%		8.55E-07		
800	96.00%		8.66E-07		
850	94.00%		1.40E-06		
900	89.00%	79.21%	2.78E-06	1.52%	0.023%
950	80.00%	64.00%	5.62E-06	1.23%	0.018%
1000	65.00%	42.25%	1.14E-05	0.81%	0.012%
1060	36.00%	12.96%	2.87E-05	0.25%	0.004%
1100	17.00%	2.89%	5.17E-05	0.06%	0.001%
1200	0.70%		1.58E-04		
1300	0.60%		1.76E-04		
1400	0.08%		2.65E-04		
1500	0.03%		3.23E-04		
1600	0.09%		2.98E-04		
1700	0.09%		3.16E-04		
1800	0.10%		3.30E-04		
1900	0.90%		2.37E-04		
2000	4.00%		1.71E-04		
2100	8.00%		1.41E-04		
2200	15.00%	2.25%	1.11E-04	0.04%	0.001%
2300	23.00%	5.29%	8.97E-05	0.10%	0.002%
2400	30.00%	9.00%	7.66E-05	0.17%	0.003%
2500	33.00%	10.89%	7.35E-05	0.21%	0.003%
2600	33.00%	10.89%	7.65E-05	0.21%	0.003%
2700	32.00%	10.24%	8.16E-05	0.20%	0.003%
2800	7.00%		1.98E-04		
2900	5.00%		2.30E-04		
3000	4.00%		2.56E-04		

Table 1: RG9 spectral transmission properties. The limit at $\sim 2.5\mu\text{m}$ stands as the approximate science detector cut-off. The spectral regions where the RG9 double pass transmission is $>1\%$ are highlighted.

For a series of star (point source) integrated magnitudes in the worst-case science band ($0.9\mu\text{m}$ - $1.0\mu\text{m}$ i.e. in the Zsloan & Y bands) and for different possible ghost image diameter, one can estimate the ghost image equivalent magnitude (in $\text{mag}/\text{arcsec}^2$) for comparison with the sky background; taking into account the reflected double pass and the front reflection.

M_{star}	Ghost image diameter at FPA		
	50 arcsec	75 arcsec	100 arcsec
4	~ 20.2	~ 21	~ 21.8
5	~ 21.2	~ 22	~ 22.8
6	~ 22.2	~ 23	~ 23.8
7	~ 23.2	~ 24	~ 24.8

Doc. Number:	VIS-DES-UOD-06042-0001
Date:	8 th March 2004
Issue:	3.0
Page:	Page 125 of 125
Author:	Paul Clark

The straylight specifications for the IRCAM ghosting requires diameter $<75\text{arcsec}$ for a magnitude $M=6$ star. Assuming the sky background in the worst-case science band to be $\sim 18.5\text{mag/arcsec}^2$ (TBC), it would be desirable to induce, from the WFS path, an eventual ghost no brighter than $\sim 1\%$ of the sky background i.e. of magnitude $\sim 23.5\text{mag/arcsec}^2$, highlighted in the table above. The consequence is that the larger the induced ghost image is, the brighter the point source can be allow in the WFS FoV, with the typical example values given above.

Table 1 shows that at the long wavelength edge of the Ks band there would be also some fraction of WFS in-field light reflected back through the filter but with a factor 10 in attenuation compared to the Y-Zsloan worst-case band. The sky background being also higher ($\sim 13\text{mag/arcsec}^2$) in Ks band, no extra constraint would be derived from the Ks band edge case.

22.3 Optical model description and results

22.3.1 Model assumptions

The same ASAP optical model as developed and used for previous ghost analysis (see RD1) was updated here with the geometry of the WFS elements as per the original Zemax model **Tel+Cube16v.ZMX**. The Zemax model was initially translated into ASAP for comparison of the overall design post-translation with previously validated ASAP model; then, the WFS components were extracted and implemented in the previous ASAP model (after applying matrix transformations in order to recover the orientation in the reference frame). Model geometry is displayed in Figure 1 below.

The following science band reflectivity values were implemented:

- L1, L2, L3 , window: $R=1.5\%$ per interface
- Science filter: front $\rightarrow R=5\%$, back $\rightarrow R=0.5\%$ (geometry of filter holder plate in not implemented)
- WFS filter: front (POM side) $\rightarrow R=2\%$, back (beamsplitter side) $\rightarrow R=98\%$
- FPA coating: $R=20\%$ assumed worst case at short science wavelengths and a 0.85mm thick detector substrate in highly refractive material (index taken as 3.7 to simulate HgCdTe or CdZnTe type of substrate) is implemented between the image plane (detector active layer) and AR coating location.

The WFS filter is model as a 3mm thick element with refractive index 1.53 and some simulations (see section 3.4) include the imaginary part of the optical constant as the values in the above spreadsheet (see Table 1).

Doc. Number:	VIS-DES-UOD-06042-0001
Date:	8 th March 2004
Issue:	3.0
Page:	Page 126 of 126
Author:	Paul Clark

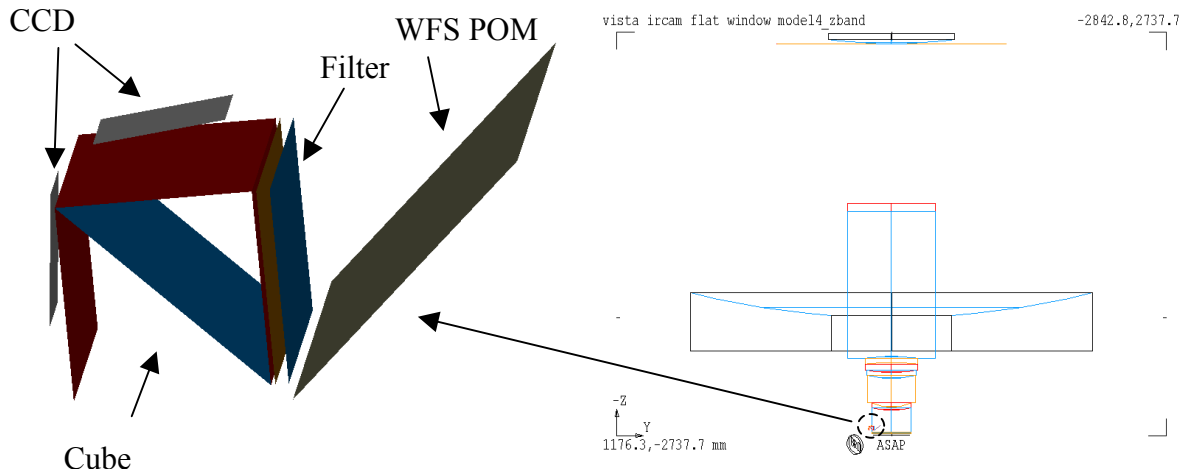


Figure 1: Model geometry used in the optical model

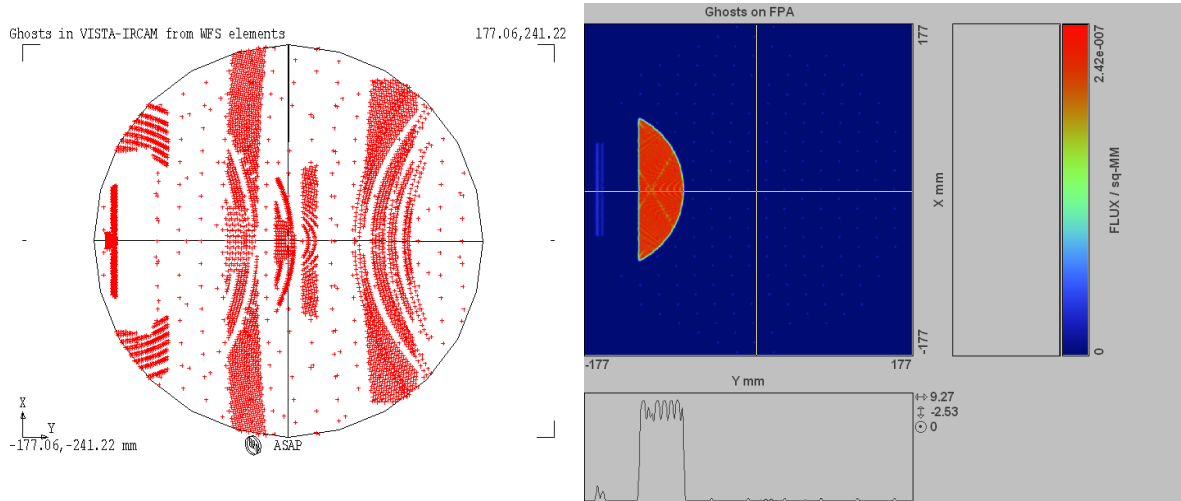
From the above considerations, nominal test wavelengths are $0.9\mu\text{m}$ and $1.0\mu\text{m}$ with unpolarised point source illumination filling the VISTA telescope entrance pupil, tilted to hit the WFS at the centre of its FoV. Angle dependent Fresnel reflection coefficients are used at every interface non-null reflectivity.

22.3.2 Ghost images at IRCAM focal plane

Below are presented a series of results from optical model ray-tracing. Splitting at specific component is performed in order to identify the component responsible of the most critical ghost (usually the smallest) on the FPA, after redirection of the bright source flux back reflected from WFS filter. For each case, a view of the geometric ray-trace impacts on the full FoV FPA and at a linear scale map of the relative irradiance in the full FoV image (sampled on a grid with step size of $500\mu\text{m}$ or 25 FPA pixels, equivalent to $\sim 8.6\text{arcsec}$ on sky).

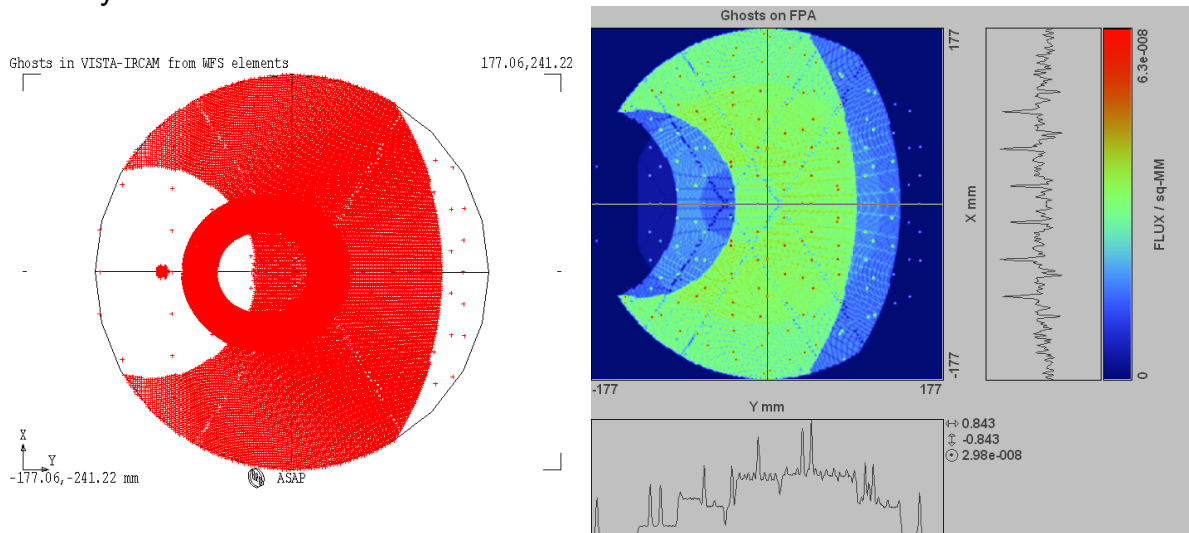
Doc. Number:	VIS-DES-UOD-06042-0001
Date:	8 th March 2004
Issue:	3.0
Page:	Page 127 of 127
Author:	Paul Clark

- L3 only (i.e. all other IRCAM components assumed perfectly transmissive; both L3 surfaces set to $R=1.5\%$):



Multiple features are present on the geometric map but are actually too faint to be seen on linear irradiance. A log scale plot would prove that they are present but orders of magnitude fainter. The only half of the ghost is seen due to vignetting of this defocused image by the WFS POM.

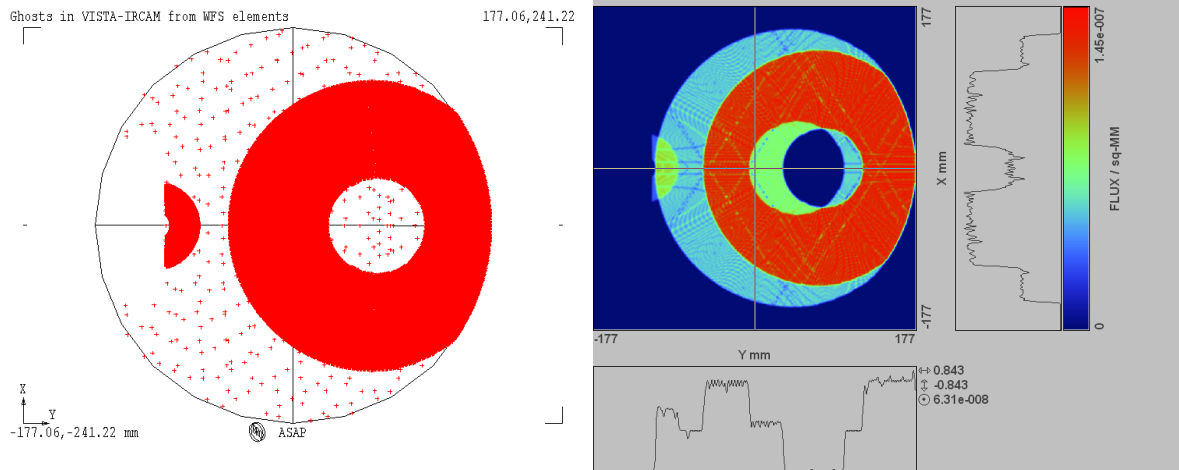
- L2 only:



Most of the ghost images are large scale and/or of low irradiance level even if they add as they are superimposed on each other. The random red spots on the irradiance map are artefacts of the illumination source grid sampling.

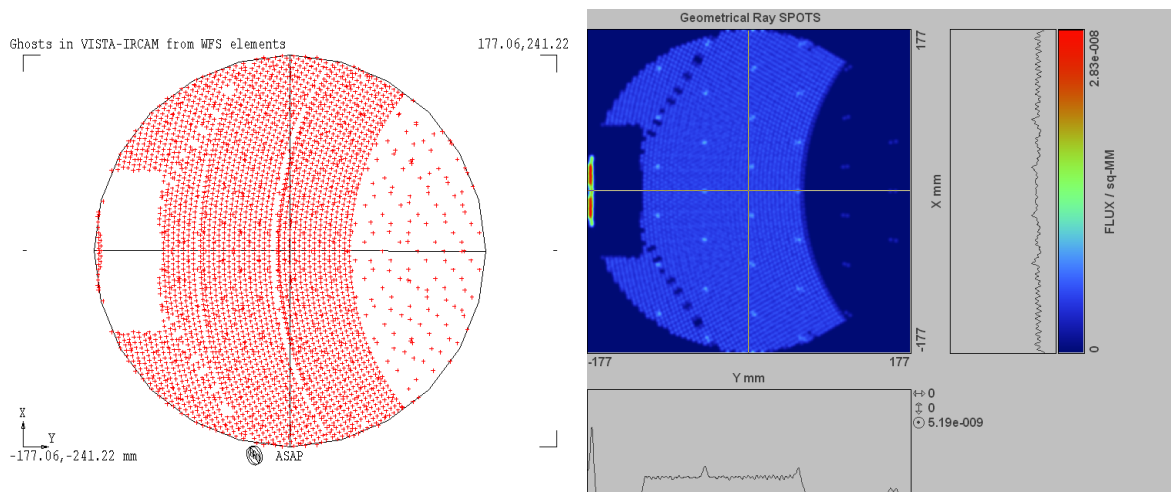
Doc. Number:	VIS-DES-UOD-06042-0001
Date:	8 th March 2004
Issue:	3.0
Page:	Page 128 of 128
Author:	Paul Clark

-L1 only:



The irradiance map reveals more ghost images than the geometric raytrace but the largest one is a diffuse large scale one. Again the smallest (incomplete shape due to the shadow of the WFS POM) ghost on the left side is incomplete due to vignetting by the WFS POM.

-Window only:



The illumination is relatively uniform and spread over a large fraction of the entire FPA. Shadow of the WFS POM is clearly visible in the ghost image. Strong localised illumination is found at the extreme edge of the full FoV circular FoV due to reflection back from the window into the cavity formed by WFS POM and the WFS filter. It is assumed that this particular path is in reality blocked by the mounting structure of the POM, the filter holder and/or the support structure surrounding the detector arrays at the FPA.

Doc. Number:	VIS-DES-UOD-06042-0001
Date:	8 th March 2004
Issue:	3.0
Page:	Page 129 of 129
Author:	Paul Clark

- All non-perfectly transmitting interfaces (including FPA coating and science filter interfaces) taken into account:

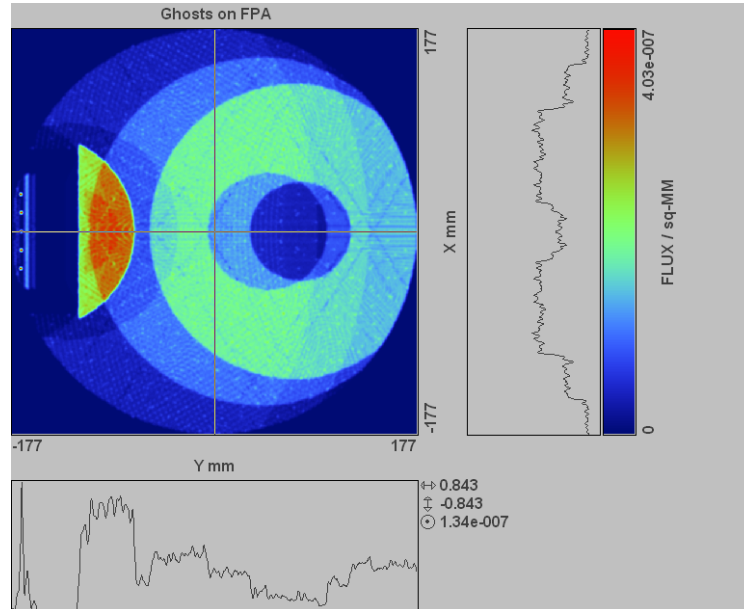


Figure 2: Full FoV image at IRCAM FPA including the effect of imperfect transmission for all camera elements

For comparison, below is shown the results of identical simulation but with the WFS interference filter located in place of the broadband AR coating i.e. on the front surface of the WFS filter. The pattern of defocused images is similar to the one above: their shape and position of ghost images is dominantly determined by the location of the filter device along the optical path in the system, not the level of reflectivity at the filter interfaces.

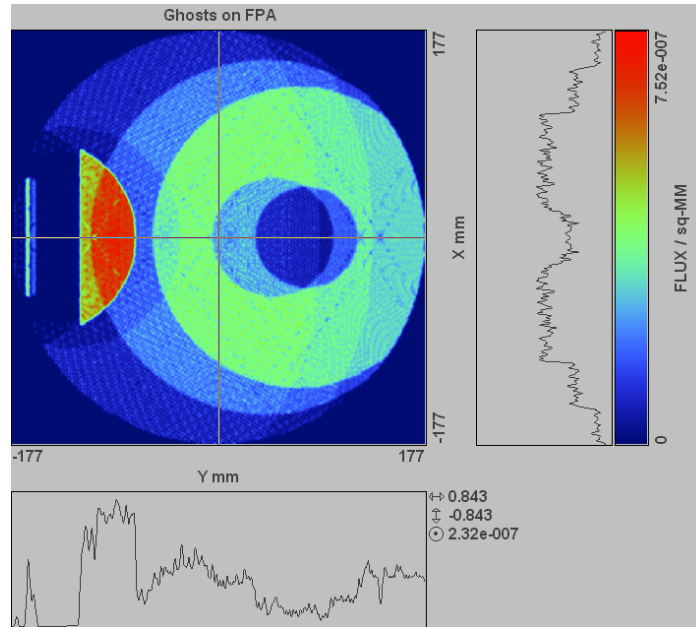


Figure 3: Idem as Figure 2 for the case of interference filter on the front surface of the WFS filter (R~98%)

In both cases, the smallest brightest zone¹ (red zone, local irradiance peaks on the extreme left leaking below the WFS POM and filter are not considered as an issue here) in the above image is covering a surface equivalent to a disk of diameter ~235arcsec. Even the superposition of all brightest ghosts from individual component (here mainly from reflections on L3 and L1) would lead to a ghost equivalent magnitude $m_{ghost} \sim M_{star} + 19.1$. Assuming a sky background in the 0.9-1.0 μ m band of the order of ~18.5mag/arcsec² (TBC), for celestial objects as bright as M=2 in the WFS FoV, the ghost image at IRCAM FPA would still be estimated to be no brighter than ~10% of the sky background.

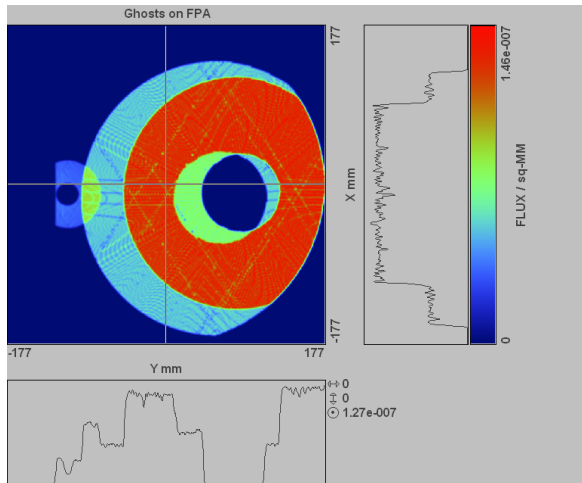
22.3.3 Field positions

The above results were obtained for the central field position (Y=0.72288deg, X=0deg). Point sources at other field positions were implemented to check for an eventual displacement and shape variations of the ghost images. The other field positions are taken as the corner ones defined in the Zemax model **Tel+Cube16v.ZMX** and reproduced below.

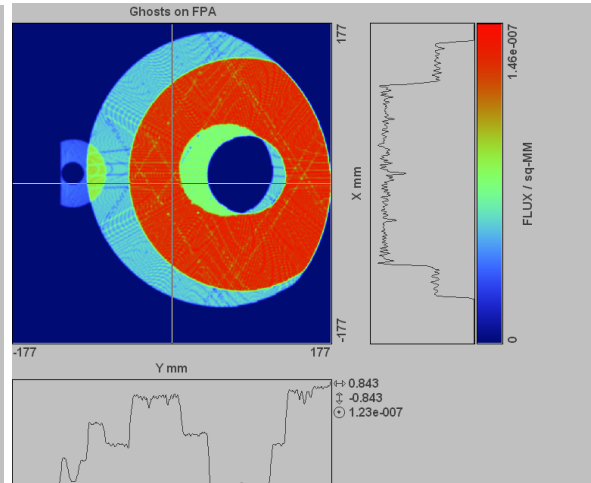
¹ Possibly difficult to isolate anyway from the diffuse background due to the superimposition of a lot of ghost images with close level or irradiance.

WFS edge field pos.	X (deg)	Y (deg)
1	-0.065258	0.6584
2	0.065258	0.6584
3	-0.065107	0.78708
4	0.065107	0.78708

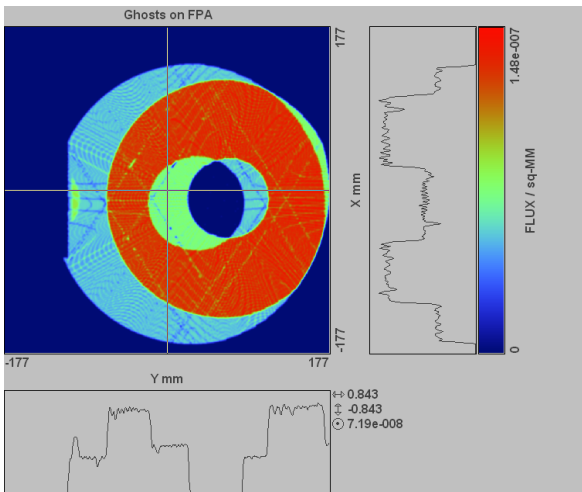
Results in section 3.2 above suggest using the case of “L1 only” as above to assess the impact of different field positions. The 4 pictures below are respectively associated with the above field positions.



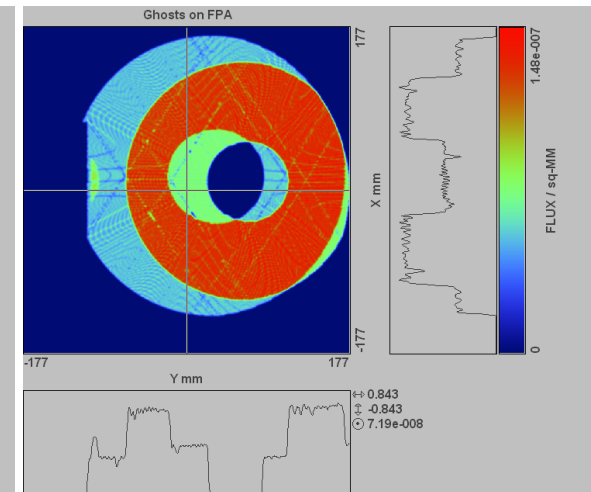
Field pos. 1



Field pos. 2



Field pos. 3



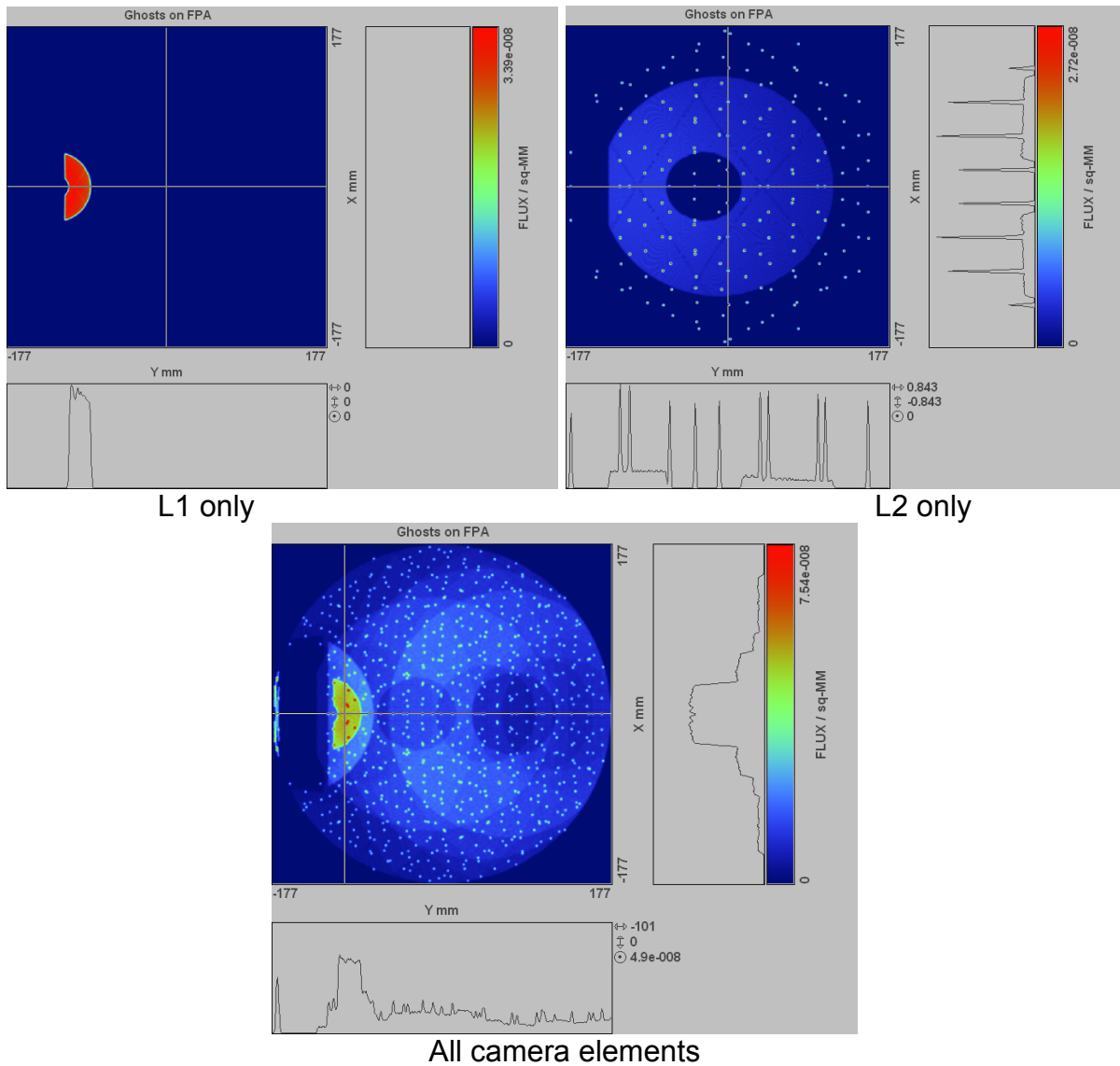
Field pos. 4

Doc. Number:	VIS-DES-UOD-06042-0001
Date:	8 th March 2004
Issue:	3.0
Page:	Page 132 of 132
Author:	Paul Clark

Small displacement of the ghost images is found. The ghost with highest irradiance level is not getting smaller in size. Secondary but smaller ghosts are still present only for field positions 1 and 2. No worst effect is therefore detected for this case.

22.3.4 Case of real (absorbing) WFS filter substrate

The discussion in the above sub-sections deal with ideal filter substrate leading to a worst-case scenario as from Table 1 one can see that at least the double pass propagation in RG9 would be expected to be reduced by 20% minimum (i.e. at 900nm). Implementation of the absorption properties of the filter substrate was made in the optical model and some illustrated results (full FoV irradiance map) are displayed below.



Doc. Number:	VIS-DES-UOD-06042-0001
Date:	8 th March 2004
Issue:	3.0
Page:	Page 133 of 133
Author:	Paul Clark

The attenuation through the WFS filter is reducing the number of ghosts on top of the overall irradiance level attenuation. The smallest (half image due to the WFS POM shadow) ghost is relatively more dominant over the large scale diffuse background of superimposed fainter defocused images. Rapid estimation of the ghost magnitude lead to $m_{ghost} \sim M_{star} + 22.4$, meaning that, for object of magnitude $M=1$ or fainter, the brightest ghost would still be $\sim 1\%$ or less of the sky background in Y-Zsloan bands. If the interference filter coating is located on the front surface of the filter, an increased by factor ~ 30 in illumination at FPA is expected leading to $m_{ghost} \sim M_{star} + 18.7$ for the same main ghost image. In that case, it would be better to avoid point source brighter than magnitude $M=5$ in the WFS FoV in order to maintain a low level of ghost background at the FPA.

22.4 Conclusion

An estimation of the defocused images at IRCAM FPA (not for the WFS detectors) generated by multiple reflections inside WFS filter and IRCAM elements was made, based on an updated optical model. IRCAM focal plane images show the presence of many ghost most of them of very large scale if not full FPA scale. The smaller and brighter ones are found to be located close to the shadow formed by the WFS POM. Their size is large enough so that they are not expected to generate large background signal compared to IRCAM in-field sky background. Quantitative approximate estimations of the equivalent induced ghost brightness were performed in order to give an idea of the magnitude of the brightness object allowed in the WFS FoV without inducing ghost on the IRCAM FPA larger than a small fraction (typically 1%) of the science in-band sky background.

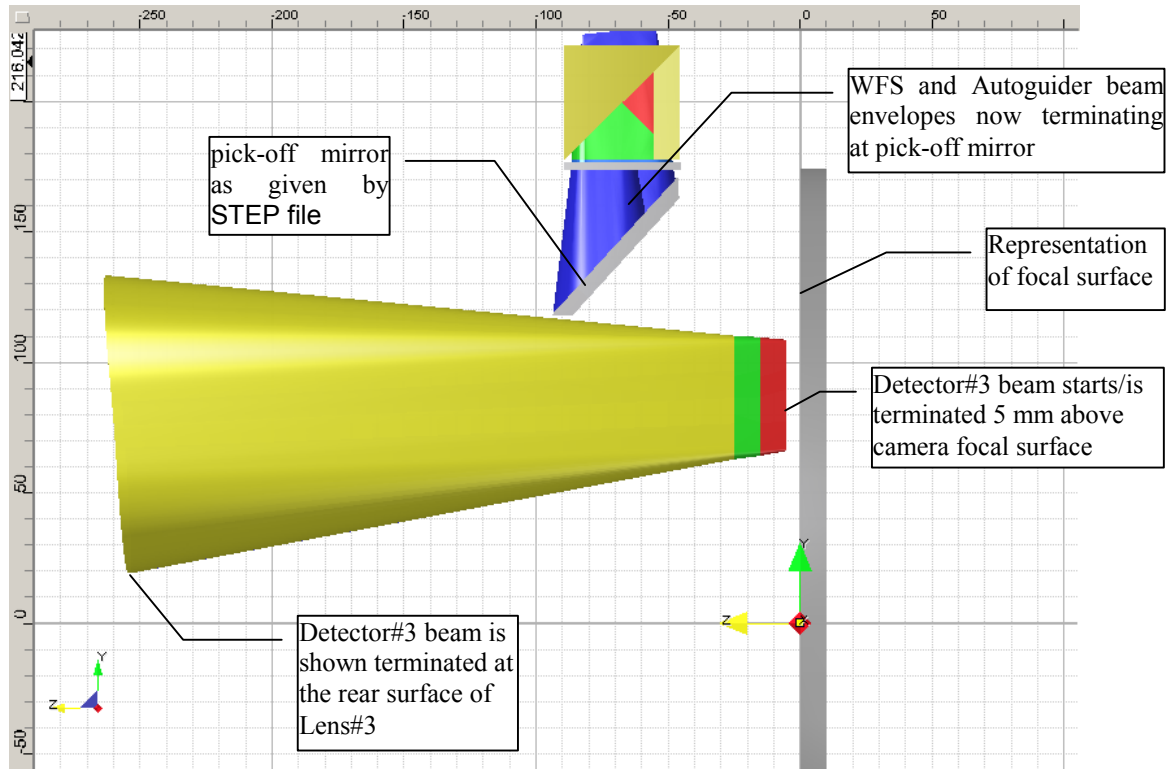
Reference document

RD1 VIS-TRE-RAL-06013-2002 Issue 1.0, *Ghost analysis update for the flat-window design* (13/06/03)

Doc. Number:	VIS-DES-UOD-06042-0001
Date:	8 th March 2004
Issue:	3.0
Page:	Page 134 of 134
Author:	Paul Clark

23 Appendix 10: Science Beam Clearance (Tony Richards)

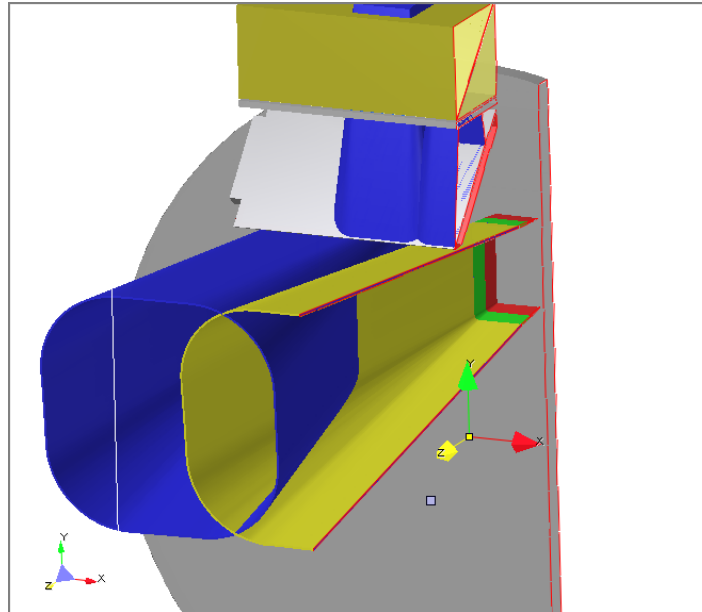
The first picture shows the WFS STEP model imported into the 3-D CAD viewer along with some detector beams.



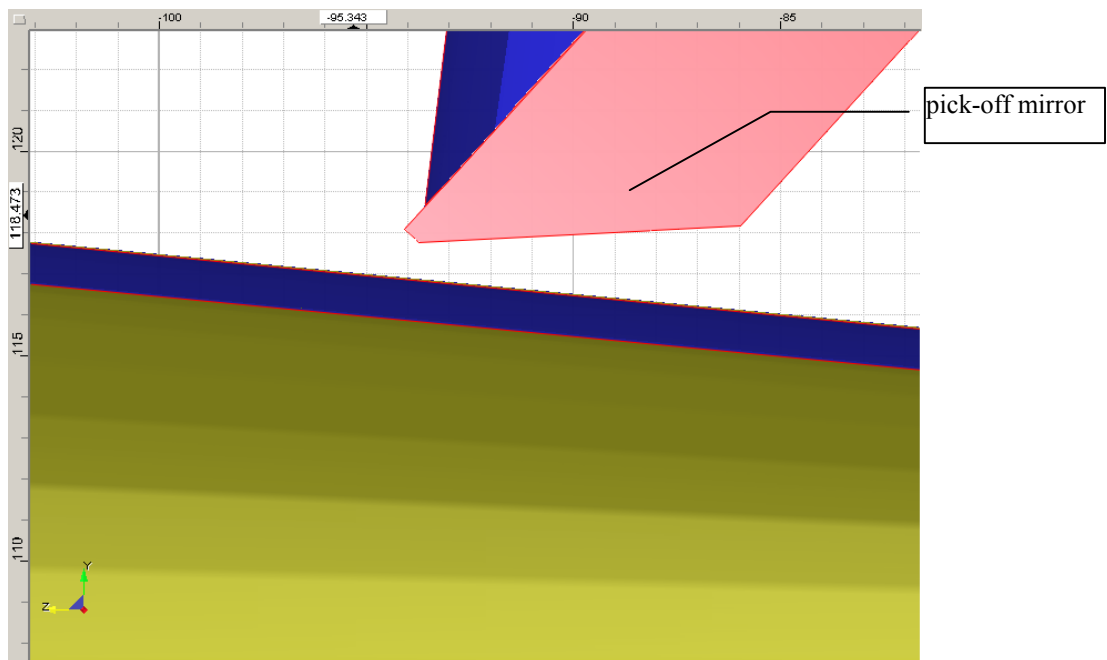
Doc. Number:	VIS-DES-UOD-06042-0001
Date:	8 th March 2004
Issue:	3.0
Page:	Page 135 of 135
Author:	Paul Clark

23.1 Clearance between Pick-off mirror and nearest detector beam

The next two pictures show slices through a detector beam where it passes closest to the edge of the pick-off mirror. The first one shows the sectional plane through the autoguider part of the WFS used beam where it is closest to the nearest detector beams.

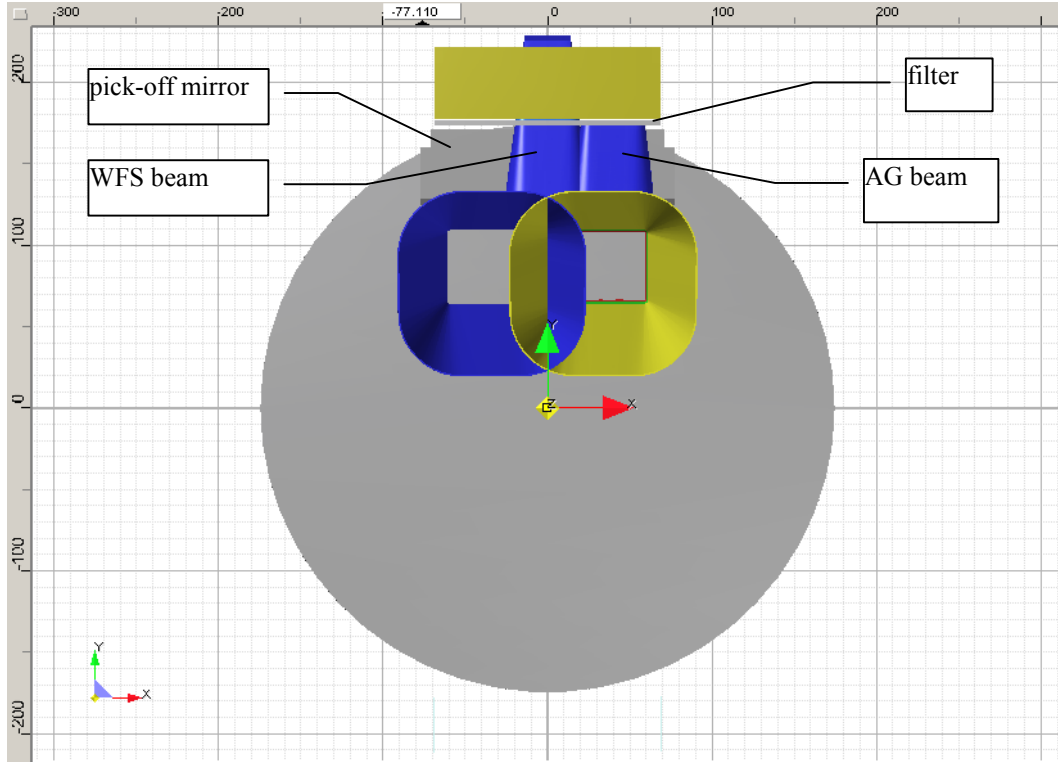


The second picture is of a close-up view in the sectional plane, which shows the minimum clearance between pick-off mirror and detector beam to be about 1 mm.



Doc. Number:	VIS-DES-UOD-06042-0001
Date:	8 th March 2004
Issue:	3.0
Page:	Page 136 of 136
Author:	Paul Clark

The final picture is a plan view from above that shows the WFS beam that passes straight through the beam splitter, terminating just in front of the WFS detector, and an Autoguider beam path alongside.



Doc. Number:	VIS-DES-UOD-06042-0001
Date:	8 th March 2004
Issue:	3.0
Page:	Page 137 of 137
Author:	Paul Clark

24 Appendix 11: Cube Beamsplitter Qualification Test

As described in sections 6.3 and 7.1, cube beamsplitter designs have been adopted for both the low and high order curvature sensors. A qualification test of the beamsplitter has been performed to allay fears of cracking or delaminating on cooling/warming.

A 40mm BK7 cube beamsplitter was subjected to repeated submersion in liquid nitrogen. In each of ten runs, the cube was lowered into a tall dewar with ~1 litre of liquid nitrogen at the bottom, over a period of approximately 10 hours (a descent rate of 1mm/min). The air temperature gradient within the dewar was approximately linear apart from variations near to the opening caused by turbulence. The air temperature gradient across the cube, before submersion, was therefore approximately 13K at all times. After having been submerged in liquid overnight, the cube was raised back up into ambient temperature air over a period of approximately 5 hours.

This was regarded as a severe test for the cube to withstand and at least an order of magnitude more severe than the cooling/warming rate to be incurred within the camera cryostat. The test was performed using a BK7 cube primarily on the grounds of cost and availability but also as BK7 has a CTE eight times higher than the fused silica which will be used in the actual system. A 40mm cube was chosen to ensure the test was representative of the size of beamsplitter in the chosen design.

The cube beamsplitter suffered no damage during the tests other than some very minor chipping of the adhesive layer on the on the bottom surface of the cube which was always lowered into the liquid first. Figure 1 depicts this. The top and corner edges of the adhesive layer were completely undamaged.

The test is regarded as a complete success indicating that the adopted fused silica cube beamsplitter design will function well and will not be damaged by cooling / warming cycles within the camera cryostat.

A separate test is underway to investigate the performance of an identical BK7 cube which is being cooled under vacuum, mounted in a dewar using beryllium retaining springs as per the mechanical design. The results of this test are not available at the time of writing but can be reported at the FDR is required. Both BK7 cubes will be made available for inspection at the FDR.

Doc. Number:	VIS-DES-UOD-06042-0001
Date:	8 th March 2004
Issue:	3.0
Page:	Page 138 of 138
Author:	Paul Clark

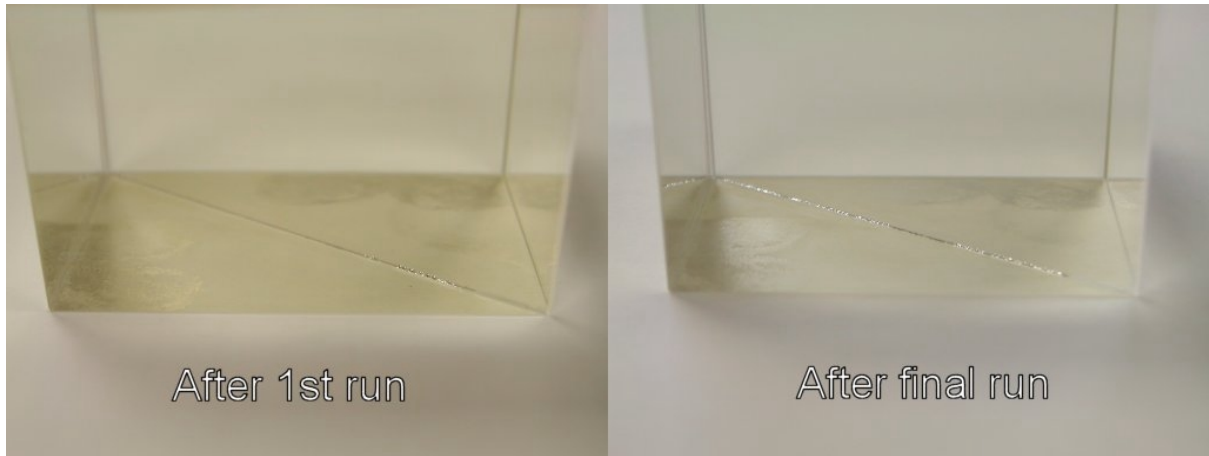


Figure 1: BK7 Cube Beamsplitter After 1st and 10th Run

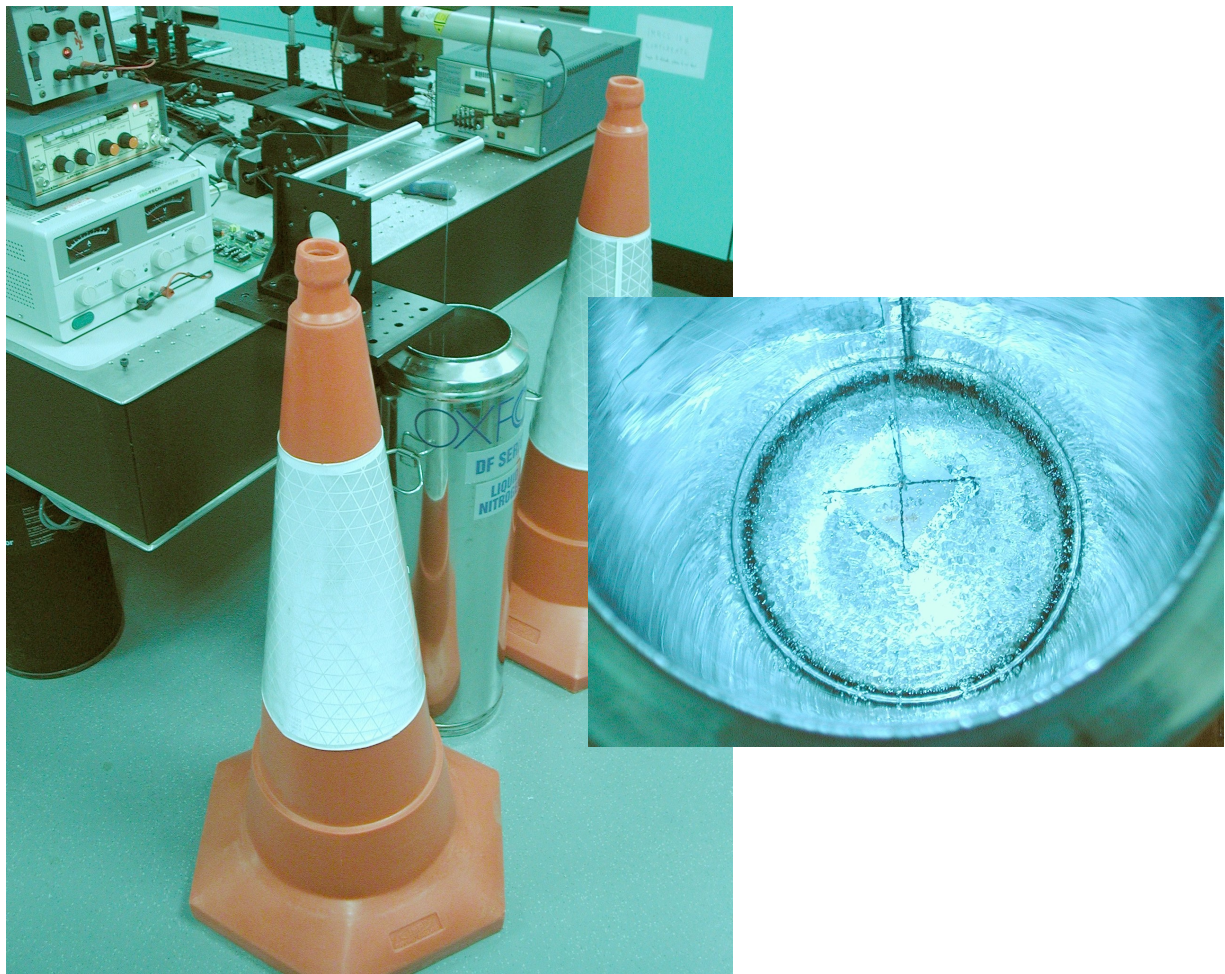


Figure 2: Cube Beamsplitter Qualification Test

25 Appendix 12: LOCS/AG Alignment Analysis (Richard Bingham)

VISTA Low Order Curvature Sensor (LOCS) Shifts of the LOCS parallel to the science focal plane

R. G. Bingham 1 March 2004

I carried out trials in which the whole LOCS assembly with its CCDs was moved in different directions parallel to the science focal plane. For different positions of the assembly, I ray-traced it to five field points in the LOCS field (corners and centre) and four field points in the Autoguider field (the corners). As the assembly is moved, these nine field points are moved with it, and so for example, they become further off-axis in the telescope for a shift in the minus Y direction. I determined the wavefront aberrations at 800 nm, referring the aberrations to the image centroids. This note reports the largest observed changes in the peak-to-valley aberration at the various field points. The results are not dominated by focus or tilt of the CCD.

The coordinate system is shown in Figures 1 and 2 overleaf.

The results are shown in Table I.

Table I
Change in aberrations if LOCS is moved

	Effect of shift on p-v wavefront aberration at the most affected field point Wavelengths at 800 nm	
	LOCS	Autoguider
	X + 1 mm	+0.01
X - 1 mm	+0.01	+0.03
X + 5 mm	+0.06	-0.16
X - 5 mm	+0.06	+0.16
Y + 1 mm	-0.07	-0.05
Y - 1 mm	+0.01	+0.04
Y + 5 mm	-0.30	-0.17
Y - 5 mm	+0.29	+0.22

Doc. Number:	VIS-DES-UOD-06042-0001
Date:	8 th March 2004
Issue:	3.0
Page:	Page 140 of 140
Author:	Paul Clark

Comments

1. The largest p-v aberration before introducing shifts was 1.78 waves at 800 nm in the LOCS and 2.12 waves in the Autoguider.
2. It is not the case that an error in the +Y direction is desirable (to reduce aberrations). The LOCS is close to the point where the edge of its first mirror clips rays that lead to the extreme edge of the science field.
3. Possible tolerances would be in the region of +/- one to three mm, except that (a) Y is best tolerated plus zero to avoid clipping the science field, and (b) the tighter end of such tolerances might be used if there is no cost implication.
4. Presumably the LOCS is fixed in position once calibrated.

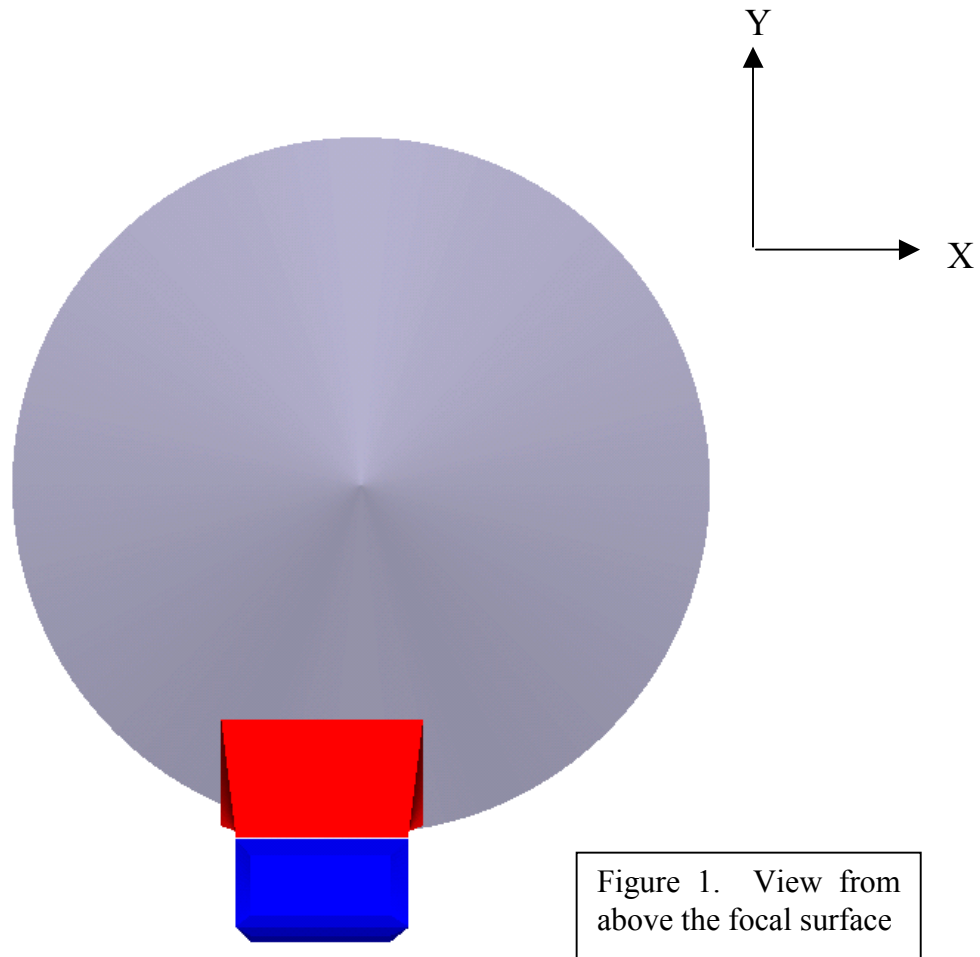


Figure 1. View from above the focal surface

Doc. Number:	VIS-DES-UOD-06042-0001
Date:	8 th March 2004
Issue:	3.0
Page:	Page 141 of 141
Author:	Paul Clark

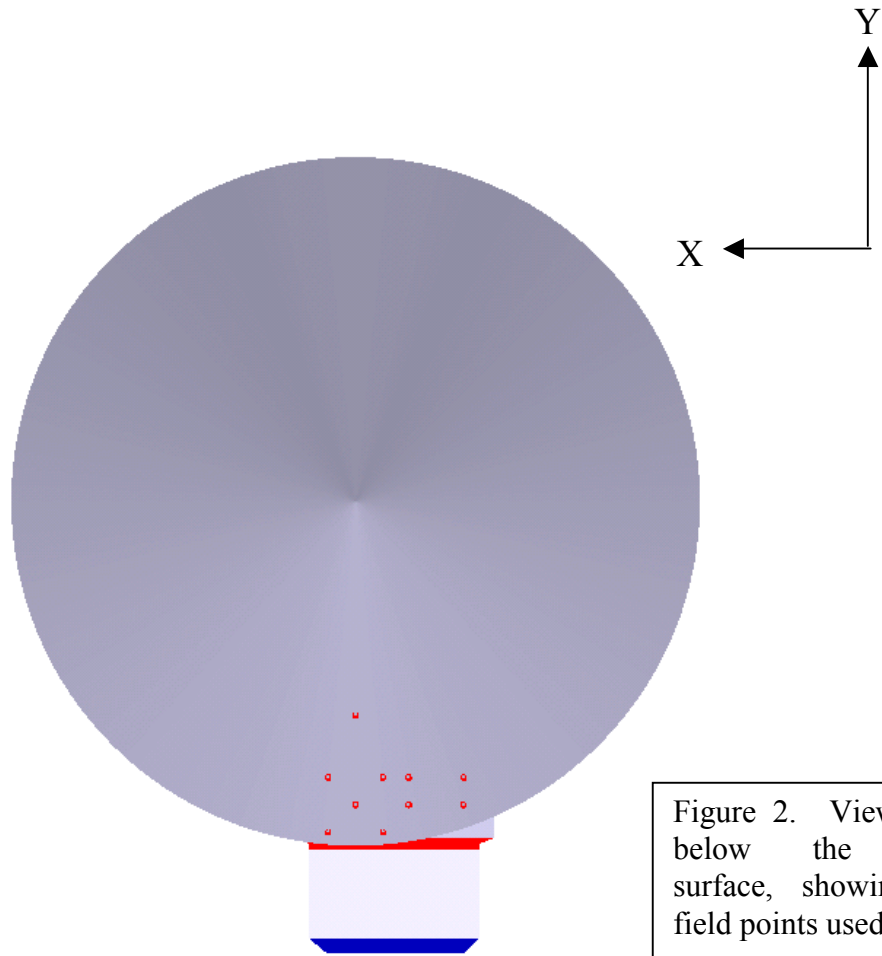


Figure 2. View from below the focal surface, showing the field points used.

Doc. Number:	VIS-DES-UOD-06042-0001
Date:	8 th March 2004
Issue:	3.0
Page:	Page 142 of 142
Author:	Paul Clark

26 Appendix 13: Sky Coverage Calculations

In this section we present the calculations to: validate the LOCS and AG fields of view; evaluate possible operation of the AG after sunset; and validate HOCS star availability.

Rather than calculate the required star magnitude and hence probability of availability, we have instead calculated the star magnitude providing 99% probability and calculated the resulting signal to noise ratio from the use of that star brightness.

26.1 Autoguider Field of View Validation

Wavelength	
Sensor Wavelength Coverage	50% Cut-On 730nm 50% Cut-Off 910nm pseudo-I
Telescope Properties	
Telescope Diameter (m)	3.705
Telescope Central Obscuration Diameter (m)	1.635
Effective Collecting Area (m ²)	8.68
f/#	3.26
Focal Length (mm)	12072.00
Plate Scale (arcsec/mm)	17.09
Throughput	
Primary Reflectance	0.97
Secondary Reflectance	0.97
Camera Window,L1,L2,L3 Throughput	0.85
Pick-Off Mirror Reflectance	0.97
RG9 Filter Transmittance	0.92
Short Pass Filter Transmittance	0.85
Autoguider Beamsplitter Transmittance	0.9
CCD QE in I-Band	0.85
Autoguider Total Throughput	0.46
Detector & Sky Properties	
I-Band $\Delta\lambda/\lambda$	0.19
1 μ Jy (photons/second)	24.91

0th Magnitude in I-Band (μJy)	2.55E+09
CCD Pixel Size (mm)	1.35E-02
Pixel Area (m^2)	1.8225E-10
Pixel Width (arcsec)	0.23066
Pixel Area (arcsec^2)	0.05321
Combined Autoguider Area on Sky 2040x2040 Pixels (arcmin^2)	61.51
Autoguider Equivalent Radius on Sky (arcsec)	265.48
FWHM including seeing (arcsec)	1
Autoguider Star Image Area (pixels)	59.05
Worst case sky brightness I-Band, full moon 10° away ($\text{mag}/\text{arcsec}^2$) R 17.2 - R-I 0.5	16.7
Background Flux ($\mu\text{Jy}/\text{arcsec}^2$)	532.77
Background Flux ($\text{photons}/\text{sec}/\text{arcsec}^2$)	13270.04
Background Flux At Autoguider ($\text{e}/\text{sec}/\text{arcsec}^2$)	6158.49
Background flux at autoguider ($\text{e}/\text{sec}/\text{pixel}$)	327.67
CCD Read Noise at 1MHz (e -)	8
CCD Dark Signal at 190K ($\text{e}/\text{pixel}/\text{second}$)	1

Autoguider Properties	
Autoguider Exposure Time (seconds)	0.09
I-Band Guide Star Magnitude 99% Probability at Equivalent Radius near Pole R 15.6 - R-I 0.5	15.2
Guide Star Flux (μ Jy)	2121.00
Guide Star Flux (photons/sec)	52828.98
Guide Star Signal including Throughput (e-/sec)	24517.41
Autoguider Signal/Noise Ratio	25.09

26.2 LOCS Field of View Validation

Wavelength	
Sensor Wavelength Coverage	50% Cut-On 730nm 50% Cut-Off 910nm pseudo-I
Telescope Properties	
Telescope Diameter (m)	3.705
Telescope Central Obscuration Diameter (m)	1.635
Effective Collecting Area (m ²)	8.68
f/#	3.26
Focal Length (mm)	12072.00
Plate Scale (arcsec/mm)	17.09
Throughput	
Primary Reflectance	0.97
Secondary Reflectance	0.97
Camera Window,L1,L2,L3 Throughput	0.85
Pick-Off Mirror Reflectance	0.97
RG9 Filter Transmittance	0.92
Short Pass Filter Transmittance	0.85
Curvature Sensor Beamsplitter Transmittance	0.45
CCD QE in I-Band	0.85
Curvature Sensor Total Throughput	0.23
Detector & Sky Properties	
I-Band $\Delta\lambda/\lambda$	0.19
1 μ Jy (photons/second)	24.91

0th Magnitude in I-Band (μJy)	2.55E+09
CCD Pixel Size (mm)	1.35E-02
Pixel Area (m^2)	1.8225E-10
Pixel Width (arcsec)	0.23066
Pixel Area (arcsec^2)	0.05321
Curvature Sensor Area on Sky 2008x1968 Pixels (arcmin^2)	58.40
Curvature Sensor Equivalent Radius on Sky (arcsec)	258.70
FWHM including seeing (arcsec)	1
Worst case sky brightness I-Band, full moon 10° away ($\text{mag}/\text{arcsec}^2$) R 17.2 - R-I 0.5	16.7
Background Flux ($\mu\text{Jy}/\text{arcsec}^2$)	532.77
Background Flux ($\text{photons}/\text{sec}/\text{arcsec}^2$)	13270.04
Background Flux At Curvature Sensor ($\text{e}/\text{sec}/\text{arcsec}^2$)	3079.25
Background Flux At Curvature Sensor ($\text{e}/\text{sec}/\text{pixel}$)	163.83
CCD Read Noise at 1MHz ($\text{e}-$)	8
CCD Dark Signal at 190K ($\text{e}/\text{pixel}/\text{second}$)	1
LOCS Properties	
Curvature Sensor Defocus (mm)	1

Doc. Number:	VIS-DES-UOD-06042-0001
Date:	8 th March 2004
Issue:	3.0
Page:	Page 148 of 148
Author:	Paul Clark

Curvature Sensor Image Diameter Including Seeing (pixels)	31.39
Curvature Sensor Image Area (pixels)	774.01
Curvature Sensor Exposure Time (seconds)	30
I-Band Guide Star Magnitude 99% Probability at Equivalent Radius near Pole R 15.7 - R-I 0.5	15.4
Curvature Sensor Star Flux (μ Jy)	1764.17
Curvature Sensor Star Flux (photons/sec)	43941.23
Curvature Sensor Signal including Throughput (e-/sec)	10196.35
LOCS Signal/Noise Ratio	149.56

26.3 Autoguider Operation After Sunset

Wavelength	
Sensor Wavelength Coverage	50% Cut-On 730nm 50% Cut-Off 910nm pseudo-I
Telescope Properties	
Telescope Diameter (m)	3.705
Telescope Central Obscuration Diameter (m)	1.635
Effective Collecting Area (m ²)	8.68
f/#	3.26
Focal Length (mm)	12072.00
Plate Scale (arcsec/mm)	17.09
Throughput	
Primary Reflectance	0.97
Secondary Reflectance	0.97
Camera Window,L1,L2,L3 Throughput	0.85
Pick-Off Mirror Reflectance	0.97
RG9 Filter Transmittance	0.92
Short Pass Filter Transmittance	0.85
Autoguider Beamsplitter Transmittance	0.9
CCD QE in I-Band	0.85
Autoguider Total Throughput	0.46
Detector & Sky Properties	
I-Band $\Delta\lambda/\lambda$	0.19
1 μ Jy (photons/second)	24.91

0th Magnitude in I-Band (μJy)	2.55E+09
CCD Pixel Size (mm)	1.35E-02
Pixel Area (m^2)	1.8225E-10
Pixel Width (arcsec)	0.23066
Pixel Area (arcsec^2)	0.05321
Combined Autoguider Area on Sky 2040x2040 Pixels (arcmin^2)	61.51
Autoguider Equivalent Radius on Sky (arcsec)	265.48
FWHM including seeing (arcsec)	1
Autoguider Star Image Area (pixels)	59.05
Worst case sky brightness ($\text{mag}/\text{arcsec}^2$) (adjust until S/N is 7)	3
Background Flux ($\mu\text{Jy}/\text{arcsec}^2$)	160894122.84
Background Flux (photons/sec/ arcsec^2)	4007487833.46
Background Flux At Autoguider ($\text{e}/\text{sec}/\text{arcsec}^2$)	1859835483.37
Background flux at autoguider ($\text{e}/\text{sec}/\text{pixel}$)	98954305.47
CCD Read Noise at 1MHz ($\text{e}-$)	8
CCD Dark Signal at 190K ($\text{e}/\text{pixel}/\text{second}$)	1
Autoguider Properties	

Doc. Number:	VIS-DES-UOD-06042-0001
Date:	8 th March 2004
Issue:	3.0
Page:	Page 151 of 151
Author:	Paul Clark

Autoguider Exposure Time (seconds)	0.01
I-Band Guide Star Magnitude (as bright as required) (adjust until Total e- is 60,000)	9.23
Guide Star Flux (μ Jy)	518251.04
Guide Star Flux (photons/sec)	12908393.99
Guide Star Signal including Throughput (e-/sec)	5990658.03
Total e- (assume in one pixel to avoid saturation) Limit 60,000 e-	59906.58
Autoguider Signal/Noise Ratio Limit 7	7.83

26.4 HOCS Star Availability

Wavelength	
Sensor Wavelength Coverage	50% Cut-On 1160nm 50% Cut-Off 1340nm J
Telescope Properties	
Telescope Diameter (m)	3.705
Telescope Central Obscuration Diameter (m)	1.635
Effective Collecting Area (m ²)	8.68
f/#	3.26
Focal Length (mm)	12072.00
Plate Scale (arcsec/mm)	17.09
Throughput	
Primary Reflectance	0.97
Secondary Reflectance	0.97
Camera Window,L1,L2,L3 Throughput	0.85
Filter Transmittance	0.8
Beamsplitter Transmittance (Worst case - multiple reflection)	0.01
Detector QE	0.8
Curvature Sensor Total Throughput	0.01
Detector & Sky Properties	
J-Band $\Delta\lambda/\lambda$	0.16
1 μ Jy (photons/second)	20.97
0th Magnitude in J-Band (μ Jy)	1.60E+09

CCD Pixel Size (mm)	2.00E-02
Pixel Area (m ²)	4E-10
Pixel Width (arcsec)	0.34172
Pixel Area (arcsec ²)	0.11678
FWHM including seeing (arcsec)	1
Worst case sky brightness J-Band, full moon 10° away (mag/arcsec ²) R 17.2 - R-I 1.3	15.9
Background Flux (μJy/arcsec ²)	699.73
Background Flux (photons/sec/arcsec ²)	14676.82
Background Flux At Curvature Sensor (e-/sec/arcsec ²)	75.12
Background Flux At Curvature Sensor (e-/sec/pixel)	8.77
Detector Read Noise (e-)	15
CCD Dark Signal at 190K (e-/pixel/second)	1
HOCS Properties	
Curvature Sensor Defocus (mm)	1
Curvature Sensor Image Diameter Including Seeing (pixels)	21.19
Curvature Sensor Image Area (pixels)	352.66
Curvature Sensor Exposure Time (seconds)	60

J-Band Guide Star Magnitude 99% Probability at 0.5° radius from Pole R 9.9 - R-I 1.5	8.4
Curvature Sensor Star Flux (μJy)	699734.88
Curvature Sensor Star Flux (photons/sec)	14676818.92
Curvature Sensor Signal including Throughput (e-/sec)	75123.24
HOCS Signal/Noise Ratio	2058.72

Doc. Number:	VIS-DES-UOD-06042-0001
Date:	8 th March 2004
Issue:	3.0
Page:	Page 155 of 155
Author:	Paul Clark

27 Appendix 14: LOCS Aberrations (Richard Bingham)

VISTA Wavefront Sensors Aberrations with and without the LOCS beamsplitter Richard G. Bingham 8 March 2004

Table I shows Zernike aberrations up to Z11 for the field centre of the LOCS at a wavelength of 0.8 microns. In Table II, the beamsplitter is removed and moving the CCD detector refocuses the instrument. Figures 1 and 2 overleaf show the aberrations in the form of spot diagrams. In this case, three wavelengths are shown, 750 nm, 800 nm and 850 nm. In each case a series of spot diagrams is shown to illustrate the effect of changing the focus position, in steps of 40 microns.

Table I

Listing of Zernike Standard Coefficient Data
With beamsplitter

Field : 0.0000, -0.7229 deg
Wavelength : 0.8000 microns

Z	1	0.086931	:	1	
Z	2	-0.000000	:	$4^{(1/2)}$	$(p) * \text{COS}(A)$
Z	3	-0.072023	:	$4^{(1/2)}$	$(p) * \text{SIN}(A)$
Z	4	0.034197	:	$3^{(1/2)}$	$(2p^2 - 1)$
Z	5	-0.000000	:	$6^{(1/2)}$	$(p^2) * \text{SIN}(2A)$
Z	6	0.048702	:	$6^{(1/2)}$	$(p^2) * \text{COS}(2A)$
Z	7	0.003418	:	$8^{(1/2)}$	$(3p^3 - 2p) * \text{SIN}(A)$
Z	8	-0.000000	:	$8^{(1/2)}$	$(3p^3 - 2p) * \text{COS}(A)$
Z	9	0.107308	:	$8^{(1/2)}$	$(p^3) * \text{SIN}(3A)$
Z	10	0.000000	:	$8^{(1/2)}$	$(p^3) * \text{COS}(3A)$
Z	11	-0.019264	:	$5^{(1/2)}$	$(6p^4 - 6p^2 + 1)$

Table II

Listing of Zernike Standard Coefficient Data
Without beamsplitter

Z	1	-0.692653	:	1	
Z	2	-0.000000	:	$4^{(1/2)}$	$(p) * \text{COS}(A)$
Z	3	-0.360540	:	$4^{(1/2)}$	$(p) * \text{SIN}(A)$
Z	4	-0.277335	:	$3^{(1/2)}$	$(2p^2 - 1)$
Z	5	-0.000000	:	$6^{(1/2)}$	$(p^2) * \text{SIN}(2A)$
Z	6	0.020370	:	$6^{(1/2)}$	$(p^2) * \text{COS}(2A)$
Z	7	-0.094390	:	$8^{(1/2)}$	$(3p^3 - 2p) * \text{SIN}(A)$
Z	8	0.000000	:	$8^{(1/2)}$	$(3p^3 - 2p) * \text{COS}(A)$
Z	9	0.105932	:	$8^{(1/2)}$	$(p^3) * \text{SIN}(3A)$
Z	10	-0.000000	:	$8^{(1/2)}$	$(p^3) * \text{COS}(3A)$
Z	11	0.085421	:	$5^{(1/2)}$	$(6p^4 - 6p^2 + 1)$

Doc. Number:	VIS-DES-UOD-06042-0001
Date:	8 th March 2004
Issue:	3.0
Page:	Page 157 of 157
Author:	Paul Clark

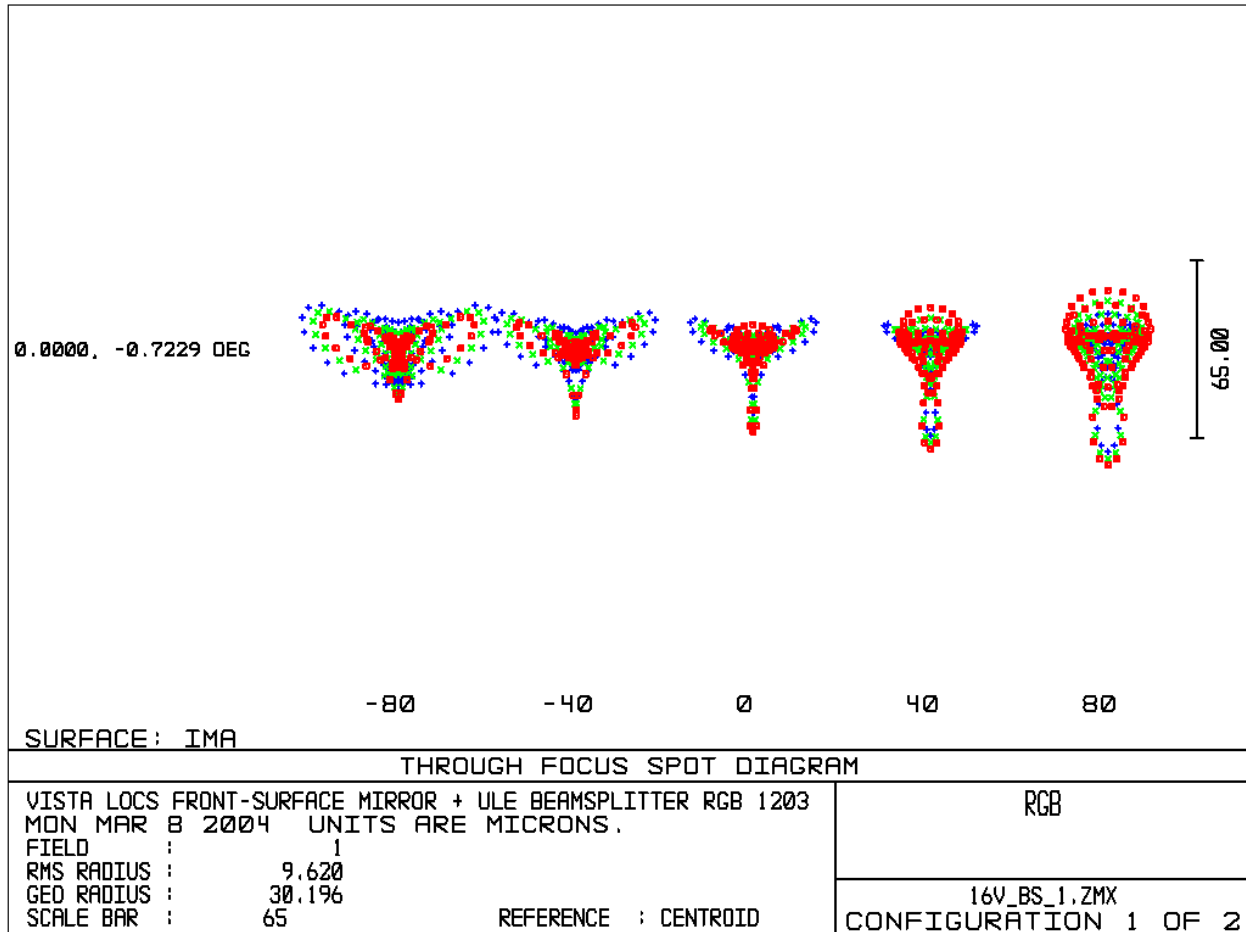


Figure 1. Through-focus LOCS spot diagrams with the beamsplitter. Wavelengths are 750, 800 and 850 nm (blue, green and red). The focus step is 40 microns. The field point used is the centre of the LOCS field. The scale bar spans 65 microns.

Doc. Number:	VIS-DES-UOD-06042-0001
Date:	8 th March 2004
Issue:	3.0
Page:	Page 158 of 158
Author:	Paul Clark

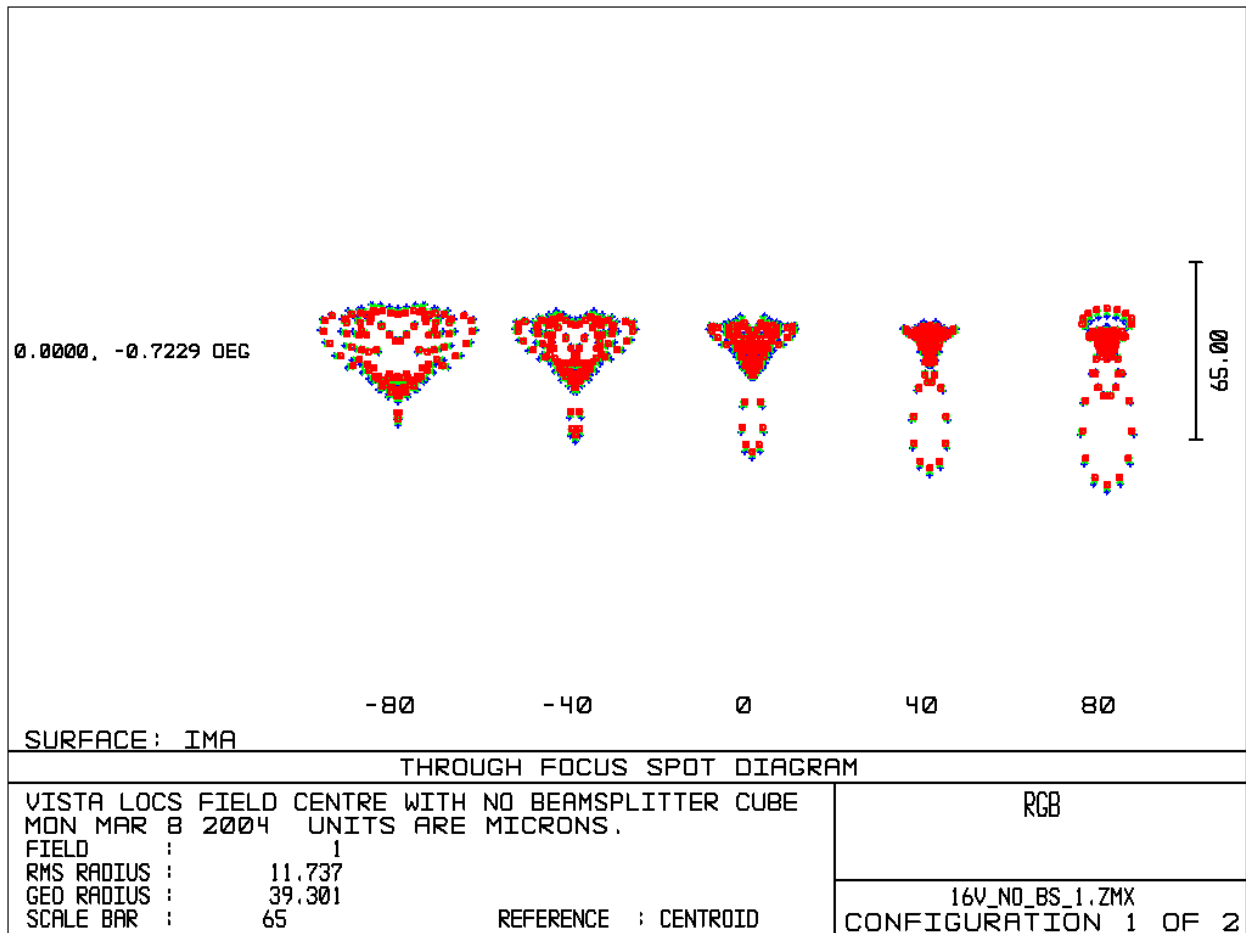


Figure 2. Through-focus LOCS spot diagrams without the beamsplitter. Details as for Figure 1.

__oOo__